COMMUNICATIONS

Martin Bereta - Michal Cifra - Katerina Cervinkova - Ladislav Janousek - Jan Barabas *

HYDROXYL RADICAL INDUCED ULTRA-WEAK PHOTON EMISSION FROM TYROSINE SOLUTIONS

This paper deals with ultra-weak photon emission (UPE) from aqueous tyrosine solutions induced by hydroxyl radical. The physical nature of this specific phenomenon is presented and the proposed mechanism of its origin during oxidation of tyrosine is described. The experimental part of the work is focused on the measurements of intensity of ultra-weak photon emission from different solutions of tyrosine. The emission from solutions with and without presence of hydroxyl radical is analyzed. The results confirm the assumption that the highest intensity is detected from the solution of tyrosine, hydrogen peroxide and ferrous sulphate heptahydrate, likely due the Fenton reaction originated hydroxyl radical, which causes oxidation of tyrosine, formation of high-energy intermediates and electron excited species. Since hydroxyl radical induced ultra-weak photon emission from tyrosine has not been analyzed before in the available literature, our results could be the beneficial contribution to this field of research.

Keywords: *Ultra-weak photon emission, reactive oxygen species, tyrosine, hydroxyl radical.*

1. Introduction

The emission of light, originated from chemical processes in organisms is an externally detectable manifestation of the metabolic activity of living cells. One of the most commonly used terms for this kind of light emission is ultra-weak photon emission (UPE). Due to its non-invasive, low-operation-cost and label-free application, it can be used in many fields of biomedicine, such as dermatology, neuroscience or oncology [1].

Ultra-weak photon emission originates during relaxation of electronically excited species, which are generated chemically by oxidative reactions of reactive oxygen species (ROS) with bio-molecules. The formation of ROS is caused by physical, chemical and biological stimuli [2]. ROS can be distinguished in two main groups – radical ROS and non-radical ROS. Molecules of radical ROS have one or more unpaired electrons, and therefore they are highly reactive. Non-radical ROS have no unpaired electron, but they still exhibit rather high reactivity. ROS oxidize bio-molecules and these reactions can further lead to the formation of intermediate chemical species which decay to form electronically excited species. The transition of these species to the ground state is accompanied by the photon emission in near UVA (350 - 400 nm), visible (400 - 750 nm) and near IR (750 - 1300 nm) regions of the electromagnetic spectrum [1].

ROS have an important role in biochemical reactions in living cells. They have a great significance in intracellular signaling [3] and intercellular communication [4]. On the other hand, there is also an extensive evidence for harmful effects of excessive ROS levels in organisms [5]. It is known that reactions of radical species can be affected by magnetic field. There are many scientific works dealing with magnetic field effects on free radical reactions and radical pair mechanism [6 - 11]. Besides these works, numerous experimental works have shown that magnetic field can affect metabolic processes of cells [12 - 14]. Therefore it could be beneficial to find a connection between the mechanism of magnetic field effects on radical reactions and the evaluation of its influence on cell metabolism by the UPE detection.

UPE can be considered as a product of biochemical processes in living organisms, which involves oxidation of bio-molecules [15].The subject matter of this paper is focused on ultra-weak photon emission derived from oxidation of amino-acid tyrosine mediated by hydroxyl radical. Tyrosine is aromatic nonessential amino-acid formed in organism from phenylalanine. Tyrosine is a building block for several important neurotransmitters, such as epinephrine or dopamine. It also underlies production of melanin, the pigment responsible for hair and skin color [16]. In this paper, it is shown that chemically produced hydroxyl radical is responsible for oxidation of tyrosine; and there are presented

* [1]Martin Bereta, [2]Michal Cifra, [2]Katerina Cervinkova, [1]Ladislav Janousek, [3]Jan Barabas
[1]Department of Electromagnetic and Biomedical Engineering, Faculty of Electrical Engineering, University of Zilina, Slovakia
[2]Institute of Photonics and Electronics, Czech Academy of Sciences, Prague, Czech Republic
[3]University Science Park of the University of Zilina, Slovakia
E-mail: martin.bereta@fel.uniza.sk

experimental results of detection of ultra-weak photon emission from tyrosine aqueous solution.

2. Mechanism of ultra-weak photon emission from tyrosine

It is known that the oxidation of amino-acids and proteins is also associated with ultra-weak photon emission [17 and 18]. Tyrosine is one of the residues which are most prone to oxidation by hydroxyl radical (*i.e.* tyrosine has a relatively low reduction potential [19]) in proteins and its oxidation can be monitored by detection of ultra-weak photon emission. Oxidation of tyrosine mediated by hydroxyl radical involves a one-electron oxidation to form the tyrosyl radicals. It is known that hydroxyl radical originates from hydrogen peroxide by Fenton reaction:

$$Fe^{2+} + H_2O_2 \rightarrow Fe^{3+} + {}^{\cdot}OH + OH^{-}. \quad (1)$$

The interaction of hydroxyl radical with tyrosine initiates oxidative reactions. Tyrosine molecule contains an aromatic ring. The computational study of Mujika *et al.* [20] analyzed oxidation of some aromatic amino-acids including tyrosine. They considered two reaction pathways by the oxidation process: addition of hydroxyl radical to the aromatic ring and hydrogen abstraction from all of the possible side-chain atoms. The energy barriers for hydrogen abstraction from aromatic ring are slightly larger and thermodynamically less favorable than for addition processes. However, hydrogen abstraction from the beta-carbon (C_7) or from the O_8 atom show similar energy barriers as the addition processes and both these abstraction processes are thermodynamically favored. Hydrogen abstraction from the O_8 atom (Fig. 1) would be sterically favorable compared to from the beta-carbon.

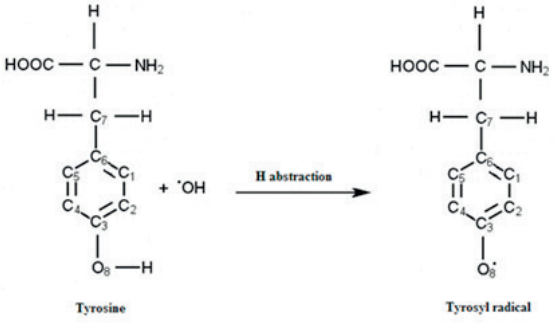

Fig. 1 The most energetically and thermodynamically favored hydroxyl radical attack on tyrosine molecule

Summarizing the Mujika computational results it seems that hydrogen abstraction from the O_8 atom is the most favorable hydroxyl radical attack on tyrosine molecule. Next favored attack is the H abstraction from beta-carbon and then the addition of OH radicals to the aromatic ring (C_1-C_6). The least favorable reactions are H abstraction from C_1, C_2, C_4 and C_5 atoms. Following the aim of the paper to try to propose possible mechanism leading to the formation of electronically excited species, hydrogen abstraction from O_8 atom is one of the expected reactions that could initiate this process. It is generally considered that reaction pathway resulting to the excited species origin involves the formation of intermediates tetroxide (ROOOOR) or dioxetane (ROOR) [1 and 2]. In the case of tyrosine oxidation by hydroxyl radical, tetroxide could be formed by the recombination of two tyrosyl radicals (on O_8) and addition of molecular oxygen. Since the formation of dioxetane requires the cyclization of peroxyl radicals (ROO•) molecules or cycloaddition of singlet oxygen ($^1O_2$) [2], its origin in this oxidation process (hydrogen abstraction from O_8) seems to be lowly probable, though not absolutely excluded. It is expected that the decomposition of tetroxide would be then followed by the formation of excited triplet carbonyl or singlet oxygen and ground state carbonyl [1]. However, we are not able to distinguish from the current data which pathway is dominant or if there is an additional unknown reaction pathway taking place.

The transition of the excited triplet carbonyl to the ground state can be accompanied by ultra-weak photon emission. Besides this, energy of the excited carbonyl could be transferred to the molecular oxygen and lead to the formation of singlet oxygen that subsequently can also emit a photon. Dimol emission of singlet oxygen lies in the visible region of the spectra. The reaction pathway of the dioxetane decomposition would be identical besides the possibility of the direct singlet oxygen formation [2]. The proposed principal mechanism of the origin of UPE during tyrosine oxidation by hydroxyl radical, following the results of Mujika computational study is shown in Fig. 2.

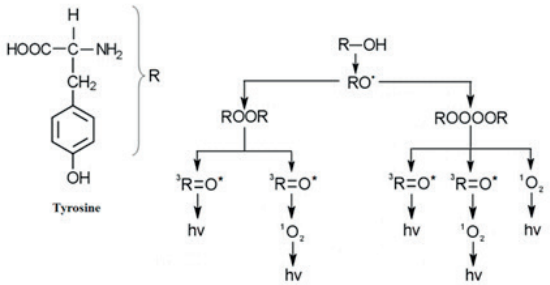

Fig. 2 Proposed mechanism of the origin of photon emission from tyrosine involves radical reactions, formation of intermediates and electron excited species (adopted from [2])

3. Materials and methods

The experimental part of the paper is focused on the detection of ultra-weak photon emission from different solutions of amino-acid tyrosine. In the experiments these compounds are used:

tyrosine (P-Lab, CZ, purity 99 %), 30 % hydrogen peroxide (Penta, CZ, p.a.), ferrous sulphate heptahydrate (Penta, CZ, purity 99 %). Four different solutions of tyrosine are prepared. The first solution is composed of tyrosine with molecular concentration 0.38 mM. The second solution contains tyrosine (0.38 mM) and hydrogen peroxide (166.7 mM). The third solution consists of tyrosine (0.38 mM) and ferrous sulphate heptahydrate, where the concentration of iron is 0.27 mM. The fourth solution is composed of tyrosine (0.38 mM) with presence of hydrogen peroxide (166.7 mM) and ferrous sulphate heptahydrate ($FeSO_4.7H_2O$), with the same concentration of iron as in previous case. All the mentioned concentrations of individual components represent their final concentrations in the measured solution. Purified water and solution of hydrogen peroxide (166.7 mM) and ferrous sulphate heptahydrate (0.27 mM of iron) are used as control samples.

Photomultiplier tube H7360-01, selected type (Hamamatsu Photonics K. K.) with a spectral sensitivity in the range 300 - 650 nm is used to detect photon emission. Typical dark count (noise) of the photomultiplier (PMT) is 15 counts per second. Measurement of the samples takes place in a light-tight chamber (standard black box, Institute of Photonics and Electronics, CZ) specially designed for the purposes of UPE measurements. The photomultiplier is mounted on the top of the chamber viewing a sample inside the chamber. Measurement equipment can be seen in Fig. 3.

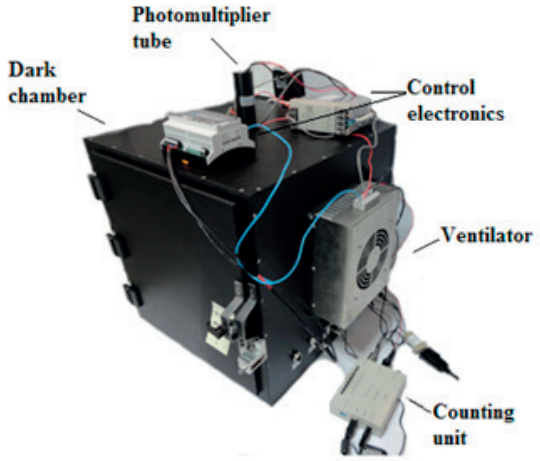

Fig. 3 Measurement equipment consists of the dark chamber, photomultiplier tube, control electronics, ventilator and counting unit

The temperature in laboratory is about 21°C in all the measurements. The duration of every measurement is one hour. The volume of measured samples is 9 ml in all cases. Every experiment is performed in triplicate.

4. Results and discussion

The results of ultra-weak photon emission measurement are presented in the following figures. Figure 4 shows results of the intensity of ultra-weak photon emission from water, solution of tyrosine, solution of tyrosine with presence of hydrogen peroxide and with presence of ferrous ions and solution of hydrogen peroxide and ferrous sulphate. The results represent the mean intensity of UPE, calculated from mean values of three repetitions of every experiment. The error bars constitute the standard deviation of the mean values. It can be seen that the intensity of UPE is very similar for both solutions water and tyrosine and not distinguishable from the PMT dark count. No detectable photon emission arises in these cases. In the case of the solution of tyrosine and hydrogen peroxide (H_2O_2), an increase of the UPE intensity can be seen. Although hydroxyl radicals are not formed in the solution, some molecules of tyrosine are probably oxidized by molecular oxygen or by products of the autooxidation of hydrogen peroxide. Electronically excited species are then formed from oxidation products of these reactions. An increase of intensity of UPE is observed also from control solution of hydrogen peroxide and ferrous sulphate. Hydroxyl radical originated by the Fenton reaction could likely oxidize some molecules of air in chamber, which could lead to the formation of excited species and photon emission.

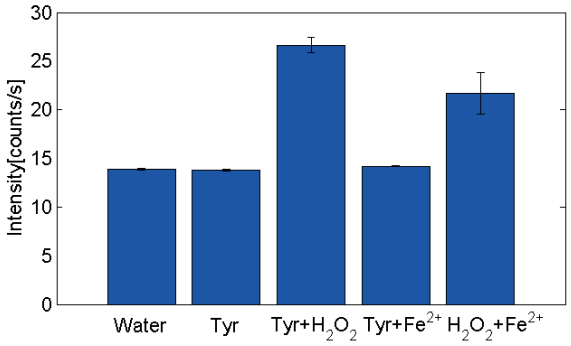

Fig. 4 Averaged intensity of ultra-weak photon emission from different solutions of tyrosine and control solutions

After the addition of ferrous sulphate to the solution of tyrosine and hydrogen peroxide and following Fenton reaction, the notable increase of photon emission is detected. The results of UPE for three repetitions of the experiment are shown in Fig. 5. The first peak in the UPE kinetics is likely caused by a fast oxidation of tyrosine molecules by hydroxyl radical. Total final shape of UPE intensity is likely due to the multiple reaction pathways as described in Fig. 2.

The observed results confirm the key role of hydroxyl radical in oxidation processes leading to the photon emission from tyrosine. Although any exact mechanism of UPE from tyrosine is not actually known, the presented reaction scheme (Fig. 2) could

be expected as one of the pathway of origin of light emission from tyrosine.

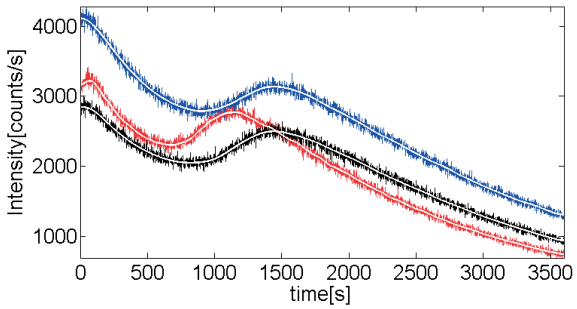

Fig. 5 Ultra-weak photon emission solution of tyrosine, hydrogen peroxide and ferrous sulphate manifests high intensity compared to control samples.

5. Conclusion

The detection of ultra-weak photon emission from different solutions of tyrosine was presented in this paper. The results confirmed the assumption that the highest intensity of UPE is detected from solution of tyrosine with the presence of hydrogen peroxide and ferrous sulphate, likely due to the hydroxyl radical mediated oxidation of tyrosine. The kinetics of UPE intensity from tyrosine without presence of hydrogen peroxide and from purified water was not distinguishable from dark count (noise) of photomultiplier. As it was noted above, UPE can be detected also from living cells and can be likely affected by magnetic field. Possible differences in kinetics of UPE from cells exposed to magnetic field and from unexposed cells could indicate the changes in biochemical reactions during cell metabolism. Our next research will be focused on evaluation of magnetic field effects on cells using UPE detection.

Acknowledgement

The research presented in the paper has been financially supported by the Czech Science Foundation, grant no. GP13-29294S and by the following project: University Science Park of the University of Zilina (ITMS: 26220220184) supported by the Research&Development Operational Program funded by the European Regional Development Fund. The research was carried out during Short Term Scientific Mission 21626 of the COST Action BM1309. Jiri Prusa is acknowledged for helpful comments and Michaela Poplova for help with results processing.

References

[1] CIFRA, M., POSPISIL, P.: Ultra-weak Photon Emission from Biological Samples: Definition, Mechanisms, Properties, Detection and Applications. *J. of Photochemistry and Photobiology B: Biology,* vol. 139, pp. 2-10, 2014.

[2] POSPISIL, P., et al.: Role of Reactive Oxygen Species in Ultra-weak Photon Emission in Biological Systems. *J. of Photochemistry and Photobiology B: Biology,* vol. 139, pp. 11-23, 2014.

[3] LANDER, H. M.: An Essential Role for Free Radicals and Derived Species in Signal Transduction. *The FASEB J.,* vol. 11, No. 2, pp. 118-124, 1997.

[4] THANNICKAL, V. J. FANBURG, B. L.: Reactive Oxygen Species in Cell Signaling. *American J. of Physiology,* vol. 279, no. 6, pp. 1005-1028, 2000.

[5] WARIS, G., ASHAN, H.: Reactive Oxygen Species: Role in the Development of Cancer and Various Chronic Conditions. *J. of Carcinogenesis,* vol. 5, No. 14, 2006.

[6] ENGSTROM, S.: Magnetic Field Effects on Free Radical Reactions in Biology. *Bioengineering and Biophysical Aspects of Electromagnetic Fields,* 3rd ed., CRC Press: Boca Raton _ Fla, 2007. ISBN: 978-0-8493-9539-0

[7] BARNES, F.S. GREENEBAUM, B.: The Effects of Weak Magnetic Fields on Radical Pairs. *Bioelectromagnetics,* vol. 36, pp. 45-54, 2015.

[8] WOODWARD, J.R.: Radical Pairs in Solution. *Progress in Reaction Kinetics and Mechanism,* vol. 27, pp. 165-207, 2002.

[9] TIMMEL, C. R. et al.: Effects of Weak Magnetic Fields on Free Radical Recombination Reactions. *Molecular Physics,* vol. 95, No. 1, pp. 71 – 89, 1998.

[10] OKANO, H.: Effects of Static Magnetic Fields in Biology: Role of Free Radicals. *Frontiers in Bioscience,* vol. 13, pp. 6106-6125, 2008.

[11] STEINER, U.E., ULRICH, T.: Magnetic Field Effects in Chemical Kinetics and Related Phenomena. *Chemical Reviews,* vol. 89, pp. 51-147, 1989.

[12] BARABAS, J., RADIL, R.: Evidence of S. Cerevisiae Proliferation Rate via Exogenous Low Frequency Electromagnetic Field. *Information Technologies in Biomedicine,* vol. 7339, pp. 295-303, 2012.

[13] AKAN, Z., et al.: Extremely Low-frequency Electromagnetic Fields Affect the Immune Response of Monocyte-derived Macrophages to Pathogens. *Bioelectromagnetics,* vol. 31, pp.603-612, 2010.
[14] AKDAG, M.Z., *et al.*: Alteration of Nitric Oxide Production in Rats Exposed to a Prolonged, Extremely Low-frequency Magnetic Field. *Electromagnetic Biology and Medicine,* vol. 26, pp. 99-106, 2007.
[15] KHABIRI, F., *et al.*: Non-invasive Monitoring of Oxidative Skin Stress by Ultraweak Photon Emission (UPE)-measurement. I: Mechanisms of UPE of Biological Materials. *Skin Research and Technology,* vol. 14, pp. 103-111, 2008.
[16] Tyrosine. [online][cit. 2015-03-10] <http://umm.edu/health/medical/altmed/supplement/tyrosine>
[17] BARNARD, M. L., et al.: Protein and Amino Acid Oxidation is Associated with Increased Chemiluminescence. *Archives of Biochemistry and Biophysics,* vol. 300, No. 2, pp. 651-656, 1993.
[18] FEDOROVA, G. F. et al.: Peroxy-radical-mediated Chemiluminescence: Mechanistic Diversity and Fundamentals for Antioxidant Assay. *Arkivoc*, pp. 163-215, 2007.
[19] MILLIGAN, J. R., et al. Repair of Oxidative DNA Damage by Amino Acids. *Nucleic Acids Research,* vol. 31, pp.6258-6263, 2003.
[20] MUJIKA, J. I., et al.: Computational Study on the Attack of ·OH Radicals on Aromatic Amino-acids. *Chemistry-A European J.,* vol. 19, pp. 6862-73, 2013.

Miroslav Kvassay - Jozef Kostolny *

EVALUATION OF ALGORITHMS FOR IDENTIFICATION OF MINIMAL CUT VECTORS AND MINIMAL PATH VECTORS IN MULTI-STATE SYSTEMS

Minimal Cut Vectors (MCVs) and Minimal Path Vectors (MPVs) are one of the key concepts of reliability analysis. They allow us to estimate system availability or to analyze influence of individual system components on the entire system. However, the main problem of their use, especially in reliability analysis of complex systems, lies in their identification. Several algorithms have been proposed to solve this task. Some of the most universal ones are based on logical differential calculus. These algorithms use integrated direct partial logic derivatives to find situations that can correspond to the MCVs (MPVs) and a special type of logic conjunction to select only those situations that really agree with the MCVs (MPVs). In this paper, we summarize the ideas behind these algorithms in more formal way and present results of some experiments performed to study their time complexity.

Keywords: *Reliability, multi-state system, minimal cut vector, minimal path vector, direct partial logic derivative, integrated direct partial logic derivative.*

1. Introduction

Reliability has been considered as an important characteristic of many systems [1 - 6]. One of the current issues of reliability engineering is the analysis of complex systems [7]. These systems are characterized by the fact that they consist of many elements (components) with very different behavior. Typical instances of such systems are healthcare systems [5] or gas distribution networks [6]. A healthcare system consists of very variable components that can be identified as hardware, software, organizational, and human, while a gas network is composed of many different hardware components, such as pipelines with various capacities, compressor stations, and supply and demand centers. This variability implies that such systems can operate at several performance levels. However, many approaches of reliability engineering are based on the assumption that the system and all its components can be either functioning or failed [8]. This indicates that many methods of reliability analysis have originally been developed for so-called Binary-State Systems (BSSs) and, therefore, they are not very appropriate for the analysis of complex systems operating at several performance levels. Furthermore, classical approaches of reliability analysis assume that the system and all its components have very similar behavior and, therefore, they are not very suitable for the analysis of complex systems consisting of components with various natures. Because of that, new methods have to be developed for the analysis of such systems. One of the possible ways is application of models that allow defining more than two states in system/components performance. These models are known as Multi-State Systems (MSSs) [7, 9 and 10].

One of the most important tasks of reliability analysis based on BSSs is finding minimal scenarios that result in system failure or minimal scenarios ensuring that the system will be working. In case of MSSs, this task can be generalized as identification of minimal scenarios whose occurrence causes that the system performance decreases below a given level or minimal scenarios ensuring that the system achieves its mission. Special instances of these scenarios are Minimal Cut Vectors (MCVs) and Minimal Path Vectors (MPVs). A MCV represents a situation in which an improvement (in case of MSSs) or repair (in case of BSSs) of any non-perfectly functioning component results in improvement/repair of the system. Similarly, a MPV agrees with a situation in which a degradation (in case of MSSs) or failure (in case of BSSs) of any working component causes system degradation/failure. Knowledge of the MCVs and MPVs can be used to estimate system availability [8 and 9] or to find components with the greatest influence on the system [11 and 12]. However, the main issue is their detection.

* **Miroslav Kvassay, Jozef Kostolny**
Department of Informatics, Faculty of Management Science and Informatics, University of Zilina, Slovakia
E-mail: Miroslav.Kvassay@fri.uniza.sk

There exist a lot of algorithms for finding the MCVs and MPVs or their equivalents known as minimal cut sets and minimal path sets in case of BSSs [13 - 18]. Several algorithms have also been proposed for identification of the MCVs or MPVs in a MSS [19 - 21]. However, these algorithms have been developed specially for network systems and, therefore, there can be some complications to apply them to other types of MSSs. Because of that, new methods for identification of the MCVs and MPVs of a MSS have been considered in [12, 22 and 23]. These methods are based on the investigation of system structure using logical differential calculus [24]. However, time complexity of these algorithms has not been studied in [12, 22 and 23] and, therefore, we decided to perform some experiments whose results are presented in this paper.

2. Mathematical Background

Reliability analysis of a system requires creation of its model. Every system consists of one or more components (elements that are assumed to be indivisible into smaller parts). This implies that one of the principal information that has to be carried by the model is dependency between system state and states of its components. This dependency is usually expressed using a special mapping that is known as structure function. For a general MSS consisting of n components, this function has the following form [9 and 12]:

$$\phi(x) = \phi(x_1, x_2, ..., x_n) : \{0, 1, ..., m_1 - 1\} \times ... \times \{0, 1, ..., m_n - 1\} \rightarrow \{0, 1, ..., m - 1\}, \quad (1)$$

where m is a number of possible states of the system (state m -1 corresponds to perfectly functioning while state 0 agrees with the complete failure of the system), m_i, for i = 1,2,...,n, represents number of states of the i-th system component (state m_i -1 means that component i is perfectly functioning while state 0 means that it completely failed), x_i is a variable denoting state of the i-th system component, and $\boldsymbol{x} = (x_1, x_2, ..., x_n)$ is a vector of components states (state vector). Specially, if all system components have the same number of states as the system, i.e. $m_1 = m_2 = ... = m_n = m$, then the system is recognized as a homogeneous [9 and 10]. Using this notation, a BSS, which allows defining only two states in the system/components performance, can be viewed as a homogeneous system in which m = 2.

Two classes of systems can be recognized depending on the properties of the structure function – coherent and noncoherent. The coherent systems are characterized by the fact that their structure function is monotone [8 - 10], which means that there exist no circumstances under which a failure/degradation (repair/improvement) of any system component can cause system repair/improvement (failure/degradation). Although real examples of noncoherent systems exist, e.g. logic networks studied in [4], most of the systems that are investigated by reliability engineers are coherent. Furthermore, MCVs and MPVs, which are studied in this paper, have been defined in terms of coherency and, therefore, only coherent systems will be considered in what follows.

The structure function defines system topology. Its analysis can reveal conditions under which a failure (repair) of a binary-state component or degradation (improvement) of a multi-state component results in a failure (repair) of the BSS or in degradation (improvement) of the MSS. Because of that, it is useful in the qualitative analysis of BSSs and MSSs. However, only its knowledge is not sufficient for quantitative analysis for which the probabilities of individual states of individual system components have to be known:

$$p_{i,s} = \Pr\{x_i = s\}, \sum_{s=0}^{m-1} p_i = 1, \quad i = 1, 2, ..., n, s = 0, 1..., m_i - 1. \quad (2)$$

The knowledge of these probabilities allows us to calculate the system availability (unavailability) defined as the probability that the system can (cannot) satisfy a demand requiring at least level j of system performance [9 and 10], or to analyze importance of individual system components or their states for system activity. This investigation is done using some special measures, such as Birnbaum's, criticality, or Fussell-Vesely's importance [11, 12, 25 and 26]. Computation of some of these measures, e.g. the Fussell-Vesely's importance, requires knowledge of MCVs or MPVs [12].

2.1. Minimal Cut Vectors and Minimal Path Vectors

A MCV for system state j (for j = 1,2,..., m -1) is defined as a state vector $\boldsymbol{x}$ such that $\phi(\boldsymbol{x}) < j$ and $\phi(\boldsymbol{y}) \geq j$ for any $\boldsymbol{y} > \boldsymbol{x}$ where notation $\boldsymbol{y} > \boldsymbol{x}$ between state vectors $\boldsymbol{x} = (x_1, x_2, ..., x_n)$ and $\boldsymbol{y} = (y_1, y_2, ..., y_n)$ expresses that $y_i \geq x_i$ for i = 1,2,..., n and there exists at least one i such that $y_i > x_i$ [9 and 10], This definition implies that a MCV for a given system state corresponds to such situation in which a minor improvement (i.e. improvement by one state) of any non-perfectly working component causes that the system achieves at least state j. (Please note that component i is non-perfectly working if it is in a state that is less than m_i -1.)

Similarly, a MPV for state j (for j = 1,2,..., m -1) of a MSS is defined as a state vector $\boldsymbol{x}$ such that $\phi(\boldsymbol{x}) \geq j$ and $\phi(\boldsymbol{y}) < j$ for any $\boldsymbol{y} < \boldsymbol{x}$ [9 and 10]. Using this definition, it can be shown easily that a MPV for a given system state represents such situation in which a minor degradation (i.e. degradation by one state) of any working component (i.e. component that is not in state 0) causes that the system state decreases below value j.

2.2. Logical Differential Calculus and Integrated Direct Partial Logic Derivatives

Logical differential calculus has been developed for analysis of dynamic properties of Boolean and Multiple-Valued Logic (MVL) functions. Direct Partial Logic Derivatives (DPLDs) are a special part of this tool. They allow finding situations in which a change of a value of a Boolean (MVL) variable results in a change of the analyzed Boolean (MVL) function [24].

The use of DPLDs in reliability analysis of BSSs and MSSs has been considered in several works. In [25], DPLDs have been used in the analysis of BSSs to detect situations in which a failure of a component results in system failure. In [26], the use of DPLDs to investigate circumstances under which a degradation of a multi-state component causes degradation of a MSS has been considered. These two works have primarily focused on homogeneous systems because the structure function of such systems can be recognized as a Boolean function (in the case of BSSs) or as a MVL function (in the case of MSSs). Other works, such as [12, 23 and 27], have considered application of DPLDs in the analysis of non-homogeneous systems. Based on these works, a DPLD investigating the structure function of a non-homogeneous system should be defined in the following way:

$$\frac{\partial \phi(j \to h)}{\partial x_i(s \to r)} = \begin{cases} 1 & \text{if } \phi(s_i, \boldsymbol{x}) = j \text{ and } \phi(r_i, \boldsymbol{x}) = h, \\ 0 & \text{otherwise,} \end{cases} \quad (3)$$

$$s, r \in \{0, 1..., m_i - 1\}, s \neq r; j, h \in \{0, 1..., m - 1\}, j \neq h.$$

Clearly, the nonzero elements of this derivative identify situations in which change of component i from state s to r causes change of the system state from value j to h. Since only coherent systems are studied in this paper, only DPLDs in which $j > h$ and $s > r$ or DPLDs in which $j < h$ and $s < r$ can be nonzero. The former can be used to find correlation between degradation of component i and system degradation while the latter can reveal circumstances under which the improvement of component i results in system improvement. This fact and the interpretation of MCVs and MPVs indicate that DPLDs $\partial \phi(j \to h)/\partial x_i(s \to s+1)$ where $j < h$ could be used to detect the MCVs and DPLDs $\partial \phi(j \to h)/\partial x_i(s \to s-1)$ in which $j > h$ to find the MPVs. This idea has been considered for homogeneous MSSs in [22] and for non-homogeneous systems in [12 and 23]. In these papers, it has been shown that direct use of DPLDs to identify MCVs or MPVs can be quite complicated and, therefore, new types of DPLDs have been introduced:

$$\frac{\partial_e \phi(h_{<j} \to h_{\geq j})}{\partial_e x_i(s \to r)} = \begin{cases} 1 & \text{if } x_i = s \text{ and } \phi(s_i, \boldsymbol{x}) < j \text{ and } \phi(r_i, \boldsymbol{x}) \geq j, \\ 0 & \text{if } x_i = s \text{ and } (\phi(s_i, x) \geq j \text{ or } \phi(r_i, x) < j), \\ * & \text{if } x_i \neq s, \end{cases} \quad (4)$$

$$\frac{\partial_e \phi(h_{\geq j} \to h_{<j})}{\partial_e x_i(s \to r)} = \begin{cases} 1 & \text{if } x_i = s \text{ and } \phi(s_i, \boldsymbol{x}) \geq j \text{ and } \phi(r_i, \boldsymbol{x}) < j, \\ 0 & \text{if } x_i = s \text{ and } (\phi(s_i, x) < j \text{ or } \phi(r_i, x) \geq j), \\ * & \text{if } x_i \neq s, \end{cases} \quad (5)$$

$$s, r \in \{0, 1, ..., m_i - 1\}, s \neq r; j \in \{1, 2, ..., m - 1\},$$

where notation $h_{<j}$ expresses that all system states that are less than j are investigated while notation $h_{\geq j}$ implies that we take into account all situations in which the structure function has at least value j. These derivatives will be referred to as expanded Integrated Direct Partial Logic Derivatives (IDPLDs) because (a) they expand classical DPLDs using value "*", and (b) it can be shown that they combine (integrate) several DPLDs together.

3. Algorithms for Identification of Minimal Cut Vectors and Minimal Path Vectors based on Integrated Direct Partial Logic Derivatives

The definition of expanded IDPLD (4) introduced in the previous section implies that value "1" of this IDPLD detects situations in which change of the i-th system component from state s to r causes that the system achieves at least state j, value "0" agrees with situations in which the considered change of component state does not result in achieving at least system state j, and value "*" implies that the component cannot change from state s to r because it is not in state s. It has been shown in [12 and 22] that if we compute expanded IDPLDs of the form of $\partial_e \phi(h_{<j} \to h_{\geq j})/\partial_e x_i(s \to s+1)$ for all possible values of i and s, i.e. for i = 1,2,..., n and for s = 0,1,..., m_i -2, and then calculate some form of their conjunction, i.e. Π-conjunction defined in Table 1-a, then we can identify all situations in which a minor improvement of any non-perfectly working component causes that the system achieves at least state j. This agrees with the interpretation of a MCV for system state j and, therefore, the MCVs for system state j can be computed using the algorithm presented in Fig. 1. If we repeat this algorithm for all possible system states, i.e. for j = 1,2,..., m-1, then all MCVs of the MSS can be found. Using IDPLDs (5) and Π-conjunction shown in Table 1-b, the similar algorithm can be derived for identification of the MPVs (Fig. 2).

4. Experimental Investigation of Algorithms Performance

The aforementioned algorithms for identification of the MCVs and MPVs are very similar. In fact, the only difference is that the algorithm for finding the MCVs uses expanded IDPLDs of the form of $\partial_e \phi(h_{<j} \to h_{\geq j})/\partial_e x_i(s \to s+1)$, while the algorithm for computation of the MPVs uses expanded IDPLDs

Π-conjunction of two expanded IDPLDs

Table 1

Table 1-a		$\frac{\partial_e \phi(h_{<j} \to h_{\geq j})}{\partial_e x_k(s_k \to r_k)}$		
		*	0	1
$\frac{\partial_e \phi(h_{<j} \to h_{\geq j})}{\partial_e x_i(s_i \to r_i)}$	*	*	0	1
	0	0	0	0
	1	1	0	1

Table 1-b		$\frac{\partial_e \phi(h_{\geq j} \to h_{<j})}{\partial_e x_k(s_k \to r_k)}$		
		*	0	1
$\frac{\partial_e \phi(h_{\geq j} \to h_{<j})}{\partial_e x_i(s_i \to r_i)}$	*	*	0	1
	0	0	0	0
	1	1	0	1

1. Repeat the next two steps for all system components:
   1.1. Compute expanded IDPLDs $\partial_e \phi(h_{<j} \to h_{\geq j})/\partial_e x_i(s \to s+1)$ for $s = 0,1,\dots,m_i - 2$.
   1.2. Calculate Π-conjunction $\Pi_{s=0}^{m_i-2} \partial_e \phi(h_{<j} \to h_{\geq j})/\partial_e x_i(s \to s+1)$ of the expanded IDPLDs computed in the previous step.
2. Calculate Π-conjunction of the Π-conjunctions computed in step 1 and identify state vectors for which it has value 1. These vectors correspond to the MCVs for system state j.

Fig. 1 Algorithm for finding all MCVs for state j of a MSS

1. Repeat the next two steps for all system components:
   1.1. Compute expanded IDPLDs $\partial_e \phi(h_{\geq j} \to h_{<j})/\partial_e x_i(s \to s-1)$ for $s = 1,2,\dots,m_i - 1$.
   1.2. Calculate Π-conjunction $\Pi_{s=1}^{m_i-1} \partial_e \phi(h_{\geq j} \to h_{<j})/\partial_e x_i(s \to s-1)$ of the expanded IDPLDs computed in the previous step.
2. Calculate Π-conjunction of the Π-conjunctions computed in step 1 and identify state vectors for which it takes value 1. These vectors correspond to the MPVs for system state j.

Fig. 2 Algorithm for finding all MPVs for state j of a MSS

of the form of $\partial_e \phi(h_{\geq j} \to h_{<j})/\partial x_i(s \to s-1)$. However, based on (4) and (5), there is no significant difference in their computation and, therefore, the algorithm for computation of the MPVs has the similar properties as the algorithm for finding the MCVs. Because of that, we investigated only the algorithm for identification of the MCVs. The study was done by performing some experiments on a computer with CPU Intel Core i5 (2.5 GHz), 4 GB RAM and Windows 7 OS. The algorithm was implemented in C++ programing language, and we analyzed its time complexity depending on the number of system components and depending on the number of all system MCVs. (For simplicity, we considered only homogeneous systems.) Firstly, the dependency of the computation time on the number of all system MCVs was studied. For such analysis, we generated systems with the same number of components but with the variable count of the MCVs. Typical examples of such systems are *k*-out-of-*n* homogeneous *m*-state systems that are defined as follows [28]:

- if at least *k* components are in state *m* -1, then the system is in state *m* -1;
- else if at least *k* components are in state *m* -2 or better, then the system is in state *m* -2;
- ...
- else if at least *k* components are in state 1 or better, then the system is in state 1;
- else the system is in state 0.

The results of these experiments for 3- and 4-state homogeneous systems are presented in Figs. 3 and 4. Based on these figures, we can state that the running time of the algorithm does not depend on the number of the MCVs. On the other

hand, these figures indicate that the running time increases exponentially with the increasing number of system components. This is clearer in Fig. 5, in which the dependency of the running time on the number of system components for systems with the similar numbers of the MCVs is presented. This figure also implies that the algorithm depends exponentially on the number of components states and, therefore, it is not very appropriate for systems with a lot of components or systems containing components that have many states.

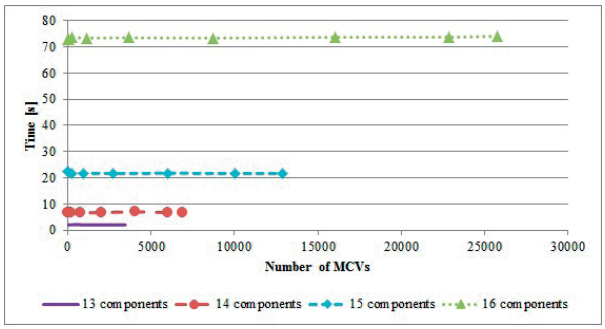

Fig. 3 Dependency of computation time on the number of the MCVs for homogeneous 3-state systems

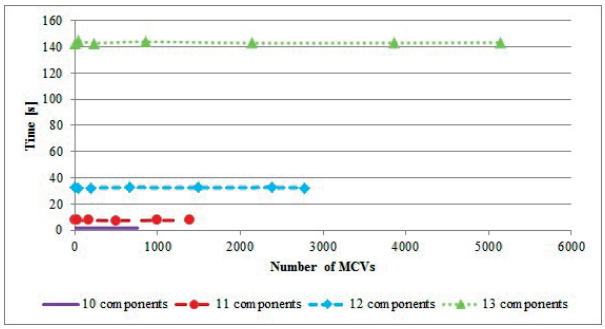

Fig. 4 Dependency of computation time on the number of the MCVs for homogeneous 4-state systems

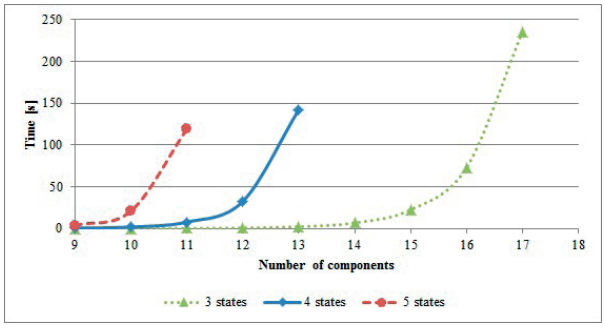

Fig. 5 Dependency of computation time on the number of system states for homogeneous multi-state systems with the similar numbers of the MCVs

5. Conclusion

MCVs and MPVs are one of the key concepts of reliability analysis. In the case of BSSs, a MCV represents such situation in which a repair of any failed component results in system repair, while a MPV corresponds to such situation in which a failure of any working component causes the system failure. In the case of MSSs, the MCVs for a given system state describe circumstances under which a minor improvement of any non-perfectly working component causes that the system achieves at least the considered state, while the MPVs for system state j agree with situations in which a minor degradation of any working component results in decrease in system state below value j.

MCVs and MPVs are very useful in reliability analysis. They can be used to estimate system availability or to analyze influence of individual system components on the system activity. Methods based on MCVs and MPVs could be used to analyze a large scale of systems, such as healthcare systems considered in [5 and 23], distribution networks presented in [6], or medical and temporal database systems studied in [29 and 30]. However, one of the main issues of use of these methods is identification of the MCVs and MPVs. For BSSs, many algorithms have been proposed for detection of the MCVs and MPVs or their equivalents known as minimal cut sets and minimal path sets. In the case of MSSs, some algorithms have also been designed. However, these algorithms are based on the assumption that the considered system is a network. Because of that, new algorithms that can be applied to a system of any type have been considered in [12, 22 and 23]. The mathematics behind these algorithms was summarized in this paper. Furthermore, some experiments estimating their time complexity were also done. The experiments showed that the running time of the algorithms does not depend on the number of system MCVs (MPVs) and, therefore, they are very suitable for the analysis of systems with a complicated structure, i.e. systems with a huge amount of the MCVs or MPVs. On the other hand, the experiments also showed that the running time depends exponentially on the number of system components and the number of components states and, therefore, the further research should focus on solving this issue.

References

[1] EISENBERG, N. A., SAGAR, B.: Importance Measures for Nuclear Waste Repositories, *Reliability Engineering & System Safety*, vol. 70, No. 3, pp. 217-239, 2000.

[2] RADOS, I., SCHWARTZ, L.: The Worst Availability as a Parameter for Designing and Reporting on the Network Performances, *Communications - Scientific Letters of the University of Zilina*, vol. 13, No. 1, pp. 60-66, 2011.

[3] BRIS, R.: Assessment of the Availability of an Offshore Installation by Stochastic Petri Net Modeling, *Communications - Scientific Letters of the University of Zilina*, vol. 16, No. 1, pp. 90-96, 2014.

[4] ZAITSEVA, E., KVASSAY, M., LEVASHENKO, V., KOSTOLNY, J.: Reliability Analysis of Logic Network with Multiple Outputs, *Communications - Scientific Letters of the University of Zilina*, vol. 17, No. 1A, pp. 44-50, 2015.

[5] ZAITSEVA, E., LEVASHENKO, V., RUSIN, M.: *Reliability Analysis of Healthcare System*, 2011 Federated Conference on Computer Science and Information Systems, FedCSIS 2011, 2011, pp. 169-175.

[6] PRAKS, P., KOPUSTINSKAS, V.: *Monte-Carlo Based Reliability Modelling of a Gas Network Using Graph Theory Approach,* Ninth Intern. Conference on Availability, Reliability and Security, 2014, pp. 380-386.

[7] ZIO, E.: Reliability Engineering: Old Problems and New Challenges, *Reliability Engineering & System Safety*, vol. 94, No. 2, pp. 125-141, 2009.

[8] RAUSAND M., HOYLAND, A.: *System Reliability Theory*, 2nd ed., Haboken: John Wiley & Sons, 2004.

[9] LISNIANSKI, A., FRENKEL, I., DING, Y.: *Multi-state System Reliability Analysis and Optimization for Engineers and Industrial Managers.* London : Springer-Verlag, 2010.

[10] NATVIG, B.: *Multistate Systems Reliability Theory with Applications*. Chichester : John Wiley & Sons 2011.

[11] KUO, W., ZHU, X.: *Importance Measures in Reliability, Risk, and Optimization: Principles and Applications*. Chichester : Wiley, 2012.

[12] KVASSAY, M., ZAITSEVA, E., LEVASHENKO, V.: Minimal Cut Sets and Direct Partial Logic Derivatives in Reliability Analysis, *Safety and Reliability: Methodology and Applications, Proc. of the European Safety and Reliability Conference, ESREL 2014*, 2015, pp. 241-248.

[13] VATN, J.: Finding Minimal Cut Sets in a Fault Tree, *Reliability Engineering & System Safety*, vol. 36, No. 1, pp. 59-62, 1992.

[14] RAUZY, A.: New Algorithms for Fault Trees Analysis, *Reliability Engineering & System Safety*, vol. 40, No. 3, pp. 203-211, 1993.

[15] SINNAMON R. M., ANDREWS, J. D.: New Approaches to Evaluating Fault Trees, *Reliability Engineering & System Safety*, vol. 58, No. 2, pp. 89-96, 1997.

[16] SHEN, Y.: A New Simple Algorithm for Enumerating All Minimal Paths and Cuts of a Graph, *Microelectronics Reliability*, vol. 35, No. 6, pp. 973-976, 1995.

[17] YEH, W.-C.: Search for all MCs in Networks with Unreliable Nodes and Arcs, *Reliability Engineering & System Safety*, vol. 79, No. 1, pp. 95-101, 2003.

[18] EMADI, A., AFRAKHTE, H.: A Novel and Fast Algorithm for Locating Minimal Cuts up to Second Order of Undirected Graphs with Multiple Sources and Sinks, *Intern. J. of Electrical Power & Energy Systems*, vol. 62, pp. 95-102, 2014.

[19] YEH, W.-C.: A New Approach to the d-MC Problem, *Reliability Engineering & System Safety*, vol. 77, No. 2, pp. 201-206, 2002.

[20] YEH, W.-C.: The Extension of Universal Generating Function Method to Search for All One-to-Many d-Minimal Paths of Acyclic Multi-State-Arc Flow-Conservation Networks, *IEEE Transactions on Reliability*, vol. 57, No. 1, pp. 94-102, 2008.

[21] YEH, W.-C.: A Fast Algorithm for Searching All Multi-state Minimal Cuts, *IEEE Transactions on Reliability*, vol. 57, No. 4, pp. 581-588, 2008.

[22] KVASSAY, M., ZAITSEVA, E., LEVASHENKO, V., KOSTOLNY, J.: *Minimal Cut Vectors and Logical Differential Calculus*, 2014 IEEE 44th Intern. Symposium on Multiple-Valued Logic, 2014, pp. 167-172.

[23] KVASSAY, M., ZAITSEVA, E.: *Construction of Healthcare System Structure for Reliability Analysis,* 2014 Federated Conference on Computer Science and Information Systems, FedCSIS 2014, 2014, vol. 2, pp. 191-199.

[24] YANUSHKEVICH, S. N., MILLER, D. M., SHMERKO, V. P., STANKOVIC, R. S.: *Decision Diagram Techniques for Micro- and Nanoelectronic Design Handbook*, vol. 2, Boca Raton: CRC Press, 2005.

[25] ZAITSEVA, E. N., LEVASHENKO, V. G.: Importance Analysis by Logical Differential Calculus, *Automation and Remote Control*, vol. 74, No. 2, pp. 171-182, 2013.

[26] ZAITSEVA, E., LEVASHENKO, V.: Multiple-valued Logic Mathematical Approaches for Multi-state System Reliability Analysis, *J. of Applied Logic*, vol. 11, No. 3, pp. 350-362, 2013.

[27] ZAITSEVA, E., LEVASHENKO, V.: Multi-state System Analysis based on Multiple-valued Decision Diagram, *J. of Reliability and Statistical Studies*, vol. 5, No. Special, pp. 107-118, 2012.

[28] BOEDIGHEIMER, R. A., KAPUR, K. C.: Customer-driven Reliability Models for Multistate Coherent Systems, *IEEE Transactions on Reliability*, vol. 43, No. 1, pp. 46-50, 1994.

[29] KVET, M., VAJSOVA, M., MATIASKO, K.: Complex Data Management in MRI Results Processing, in *Applications of Computational Intelligence in Biomedical Technology*, BRIS, R., MAJERNIK, J., PANCERZ, K., ZAITSEVA, E., Eds. Springer International Publishing, 2016, pp. 119-141.

[30] KVET, M., MATIASKO, K.: Column Level Uni-temporal Data, *Communications - Scientific Letters of the University of Zilina*, vol. 16, No. 1, pp. 97-104, 2014.

Zuzana Stankovicova - Vladimir Dekys - Leszek Radziszewski - Milan Uhricik - Milan Sapieta *

COMPARISON OF EXPERIMENTAL RESULTS WITH NUMERICAL SOLUTION OF THERMAL STRESS ANALYSIS

This paper presents experimental measurement of the first stress invariant on the plate with hole at fatigue testing machine due to adiabatic elastic deformation. The theoretical part is concentrated on the theory of thermal stress analysis focusing on thermoelastic analysis. The experimental part is dedicated to the postprocessing of the measured data including analytical and numerical solutions for the plate with hole using finite element method (FEM).

Keywords: *Thermoelastic, thermal stress analysis, infrared camera, first stress invariant, temperature.*

1. Introduction

The determination of stress and strain fields can be made in many ways. It can be used, for example, classical strain gauges [1], optical methods based on correlation of the image [2] but also on the base of detection of infrared radiation.

The deformation of structural materials is followed by thermal effects. We recognize thermoelastic or thermoplastic stress analysis, depending on whether the load creates elastic or plastic strains. Thermoelastic stress analysis describes the relation between stress changes and temperature changes of a body in specimens. When the tensile deformation is in the elastic field specimen's temperature increases, on the other hand when there is a pressure load it decreases. The thermoplastic effect quantifies the heat generated by plastic deformation. In the elastic part it is possible under adiabatic conditions to determine the value of the first stress invariant on the material surface by measuring changes of the surface temperature. Adiabatic conditions are ensured by frequency higher than 2Hz for steel specimens and more than 20Hz for aluminum specimens (aluminum sample was used in experiment by Estrada [3]). In plastic zone it is possible only to estimate the trace of stress tensor, because there is not a total conversion of mechanical energy into heat.

Surface temperature in thermal stress analysis was previously measured using thermocouples. The development of new technologies brought a new contactless method for measuring the temperature with greater sensitivity by using thermography. Infrared thermography is a unique technology which allows using an infrared cooled detector to measure the surface temperature of an object. It is possible to determine the temperature changes on the surface of the measured object from the thermogram [4]. Rajic describes the development and validation of a novel thermoelastic stress analysis system based on a low cost microbolometer device [5].

Most of applications of thermal stress analysis concern FEM comparison, fatigue testing and vibration analysis in automotive industry, naval, aircraft and steel industry [6].

2. Thermal stress analysis

Thermoelastic and thermoplastic effect are summarized in a 3 – dimensional heat equation together with the effect of heat conduction [7 and 8]:

$$\rho C_\varepsilon \frac{\partial T}{\partial t} = k\left(\frac{\partial^2 T}{\partial x^2} + \frac{\partial^2 T}{\partial y^2} + \frac{\partial^2 T}{\partial z^2}\right) + \\ + T_0 \sum \frac{\partial \sigma_{ij}}{\partial T} \dot{\varepsilon}_{IJ}^{\ e} + \alpha_p \sigma_{ij} \dot{\varepsilon}_{ij}^{\ p} \quad , \tag{1}$$

where ρ is the material density, C_ε is specific heat capacity at constant deformation, T is absolute temperature, t is time, k thermal conductivity, x, y and z are spatial coordinates, T_0 is the initial temperature, σ_{ij} stress tensor, $\dot{\varepsilon}_{IJ}^{\ e}$ is the rate of change of elastic deformation, α_p is the ratio of plastic deformation, which is converted to total heat of plastic deformation, $\dot{\varepsilon}_{IJ}^{\ P}$ is the irreversible part of deformation tensor [7].

* [1]Zuzana Stankovicova, [1]Vladimir Dekys, [2]Leszek Radziszewski, [1]Milan Uhricik, [1]Milan Sapieta
[1]Department of Applied Mechanics, Faculty of Mechanical Engineering, University of Zilina, Slovakia
[2]Kielce University of Technology, Faculty of Mechatronics and Machine Design, Kielce, Poland
E-mail: zuzana.stankovicova@fstroj.uniza.sk

2.1. Thermoelastic effect

Thermoelastic effect is known as the conversion between mechanical forms of energy and heat. This transformation occurs when stress changes within a material element alter its volume. Density of energy generated in an object is transformed into local temperature changes. If specific heat of metal is high this phenomenon is insignificant in terms of temperature change. Roughly 1 MPa change in stress state causes a temperature change of 1mK in steel [6].

The equation of thermoelasticity is derived from heat equation ignoring thermoplastic effect [9]:

$$\rho C_\varepsilon \frac{\partial T}{\partial t} = k\left(\frac{\partial^2 T}{\partial x^2} + \frac{\partial^2 T}{\partial y^2} + \frac{\partial^2 T}{\partial z^2}\right) + T_0 \sum \frac{\partial \sigma_{ij}}{\partial T} \dot{\varepsilon}^e_{IJ}. \quad (2)$$

To evoke the thermoelastic effect it is standard to load object cyclically so that no heat conduction takes place. Therefore the first term on the right side of (2) can be neglected. Time integration of (2) ignoring heat transfer leads to the following equation:

$$\rho C_\varepsilon \Delta T = T_0 \sum \frac{\partial \sigma_{ij}}{\partial T} \varepsilon^e_{ij} \; pre\; i,j = 1,2,3. \quad (3)$$

Using Hooke´s law and simple mathematical operations we obtain an expression that relates the trace of stress tensor (first stress invariant) σ_{ii} and temperature changes ΔT

$$\sum_{i=1,2} \sigma_{ii} = -\frac{\Delta T}{\alpha}\left[\frac{\rho C_\varepsilon}{T_0} - \frac{2\alpha^2 T_0}{1-\nu}\right]. \quad (4)$$

where ν - Poisson´s ration *(-)*
α - linear coefficient of thermal expansion *(K^{-1})*.

Equation (4) can be simplified by using the relationship between heat capacity at constant deformation C_ε and heat capacity at constant pressure C_p [9]:

$$C_\varepsilon = C_p - \frac{2E\alpha^2 T_0}{\rho(1-\nu)}, \quad (5)$$

where *E* - Young´s modulus *(Pa)*.

Substituting (5) to (4) we obtain

$$\Delta T = -\frac{\alpha}{pC_p} T_0 \sum_{i=1,2} \sigma_{ii}. \quad (6)$$

The term $\frac{\alpha}{pC_p}$ is a proportionality constant known as thermoelastic constant *K*. Therefore (6) can be rewritten as:

$$\Delta T = -KT_0(\sigma_1 + \sigma_2 + \sigma_3), \quad (7)$$

where, $\sigma_1, \sigma_2, \sigma_3$, are changes in the principal stresses. The sum of principal stresses is known as the first invariant of stress or trace of stress tensor. Equation (7) says that the sum of the principal stresses is related to the dilatational component of deformation. Tensile load causes a decrease of temperature and vice versa.

3. Experimental part

The experimental part consists of measuring the temperature change by using an infrared camera in elastic field during cyclic tension – compression load. The measurement was carried out at the Department of material engineering, which has a frequency Zwick Roel pulsator. The sample was loaded by dynamic amplitude of 1kN with a frequency of 104 Hz. The measurement was performed on a plate with a hole. On the specimen a black emissivity spray (for LWIR) was applied to prevent the partial reflection of the surrounding surfaces. The emissivity spray for MWIR was not used, this problem is difficult and complex [10].

3.1. Measurement preparation

To measure the temperature change an infrared camera with a cooled detector FLIR SC7000 was used (Fig. 1). Three software were used to evaluate the measured data: Research IR MAX, ALTAIR LI, ALTAIR. The software ALTAIR LI provides thermograms of stress fields using thermoelastic effect, which is based on a linear relationship between the temperature changes induced mechanical load and stress at the surface of the material. ALTAIR LI software is associated with the Lock In method that is used to extract the signal from noise and for synchronization signal load to signal measured data.

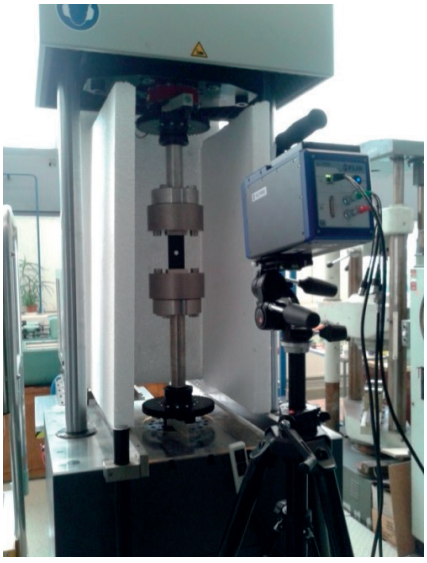

Fig. 1 Measuring the temperature changes using infrared camera FLIR SC7000 and frequency pulsator

The sample used in the experiment was a steel plate with dimensions 50 x 111 mm with a thickness of 1 mm. In the middle of the plate a hole was drilled with a diameter of 12 mm (Fig. 2). The specimen material is steel S355J with properties:

- Young´s modulus E=200 GPa,
- Poisson´s ratio μ=0.3,
- density ρ=7800.

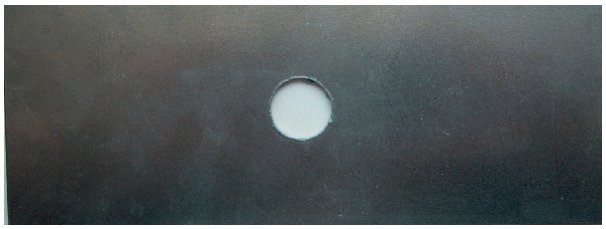

Fig. 2 Steel plate with hole

3.2. Analytical solution

In plane stress problems during the applied loading of plate with hole results in stress concentration at the edge of the hole. For an infinite plate the stress is equal to three times the stress in full cross section. For finite plate (cantilevered on one side), the value is slightly higher. The maximum stress in place of stress concentrator is analytically calculated by the stress concentration factor K_t:

$$\sigma_{\max} = K_t \cdot \sigma_{nom}. \tag{8}$$

The stress concentration factor is determined from the graph in Fig. 3. Nominal stress is stress in cross section at half the length of the bar:

$$\sigma_{nom} = \frac{P}{(D-2r)\cdot thickness'} \tag{9}$$

where P is loading force in N and dimensions are given according to Fig. 2.

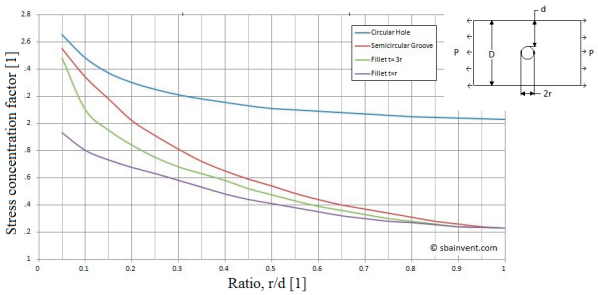

Fig. 3 Stress concentration factor (http://engineering-references.sbainvent.com/strength_of_materials/stress-concentrations.php#.VglAK5cl-VM)

If the sample is loaded with force 1kN, the nominal stress is calculated:

$$\sigma_{nom} = \frac{P}{(H-2r)\cdot thickness} = \\ = \frac{1000}{(50-12)\cdot 1} = 26.3\ MPa \tag{10}$$

and the stress in the field of stress concentration:

$$\sigma_{\max} = 2,425 \cdot 26,3 = 63.8\ MPa \tag{11}$$

In full cross section stress evoked by loading force of 1kN is 20 MPa. In the place of stress concentration it is 64 MPa after rounding.

4. Measurement results

Figure 4 shows thermograms of stress fields under tension (Fig. 4a) and compression loading (Fig. 4b). Here we can see that the maximum stress is at the edge of the hole as we assumed in the analytical solution.

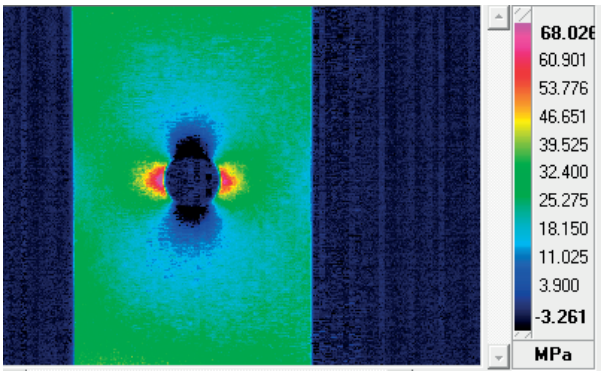

a)

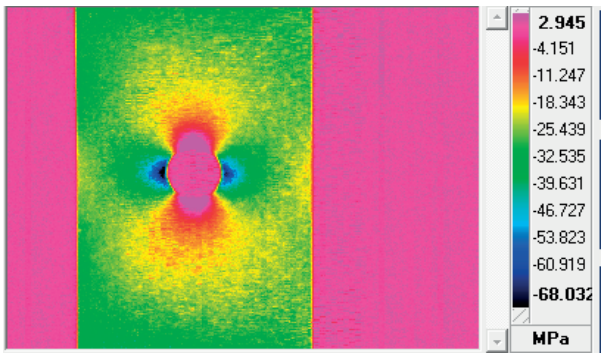

b)

Fig. 4 Measured results for a) tension loading, b) compression loading

Further processing of the results was carried out in ALTAIR software, which provides the user greater comfort with

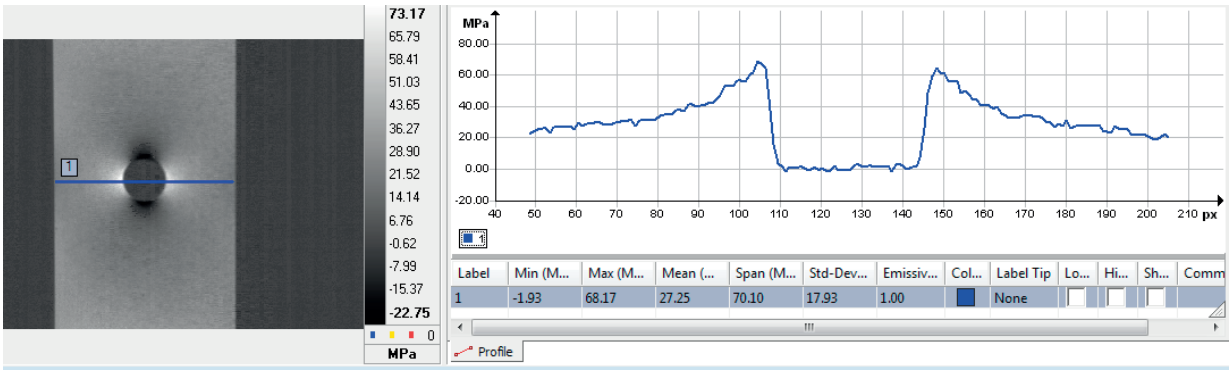

Fig. 5 Measured results for tension loading

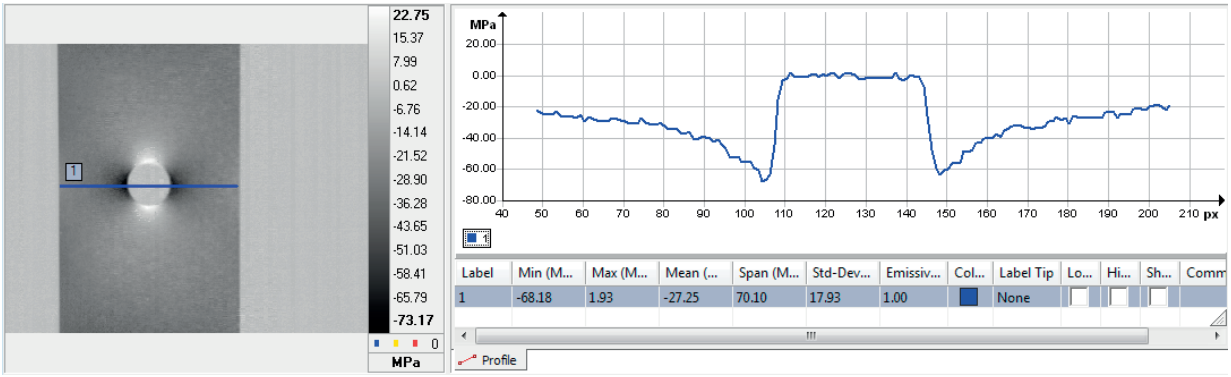

Fig. 6 Measured results for compression loading

processing of measured data. For a sample in tension loading (Fig. 5) and compression loading (Fig. 6) was chosen transverse line and plotted curve of the first stress invariant in each pixel (px). In Fig. 5 you can see that maximum first invariant stress is on the edge of the hole and its value is 68.17 MPa. The maximum value during compression loading is -68.18 MPa.

5. Numerical solutions

Numerical solution was performed by finite element method in two software: ANSYS and ABAQUS. Structural analyses were created to find out stress field of the specimen during cyclic loading tension – compression. We present results during tension loading. The applied material and boundary conditions were defined according to the experiment. In both of software mesh was generated by 4 node element which is used for modeling plane stress. The result of the structural analysis in software ANSYS for tensile loading is presented in Fig. 7. Here we can see that maximum first stress invariant is 65.2MPa.

Numerical solution performed in software ABAQUS is in Fig. 8. Here we can see that that maximum first invariant stress is on the edge of the hole and its value is 65.3 MPa.

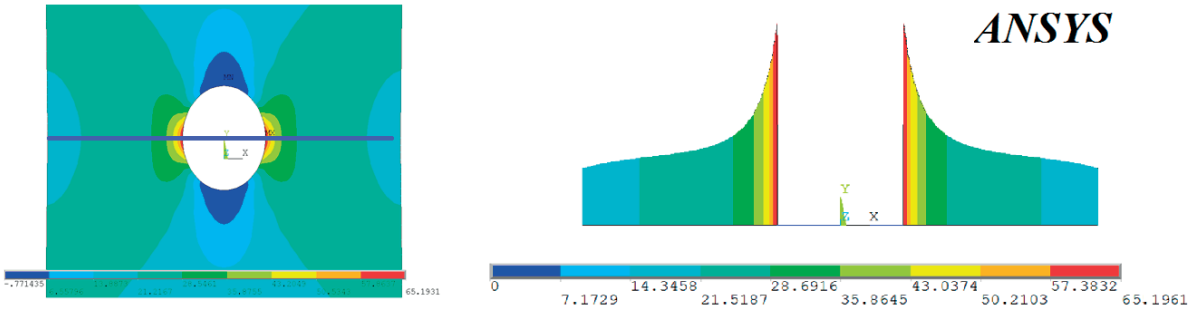

Fig. 7 Numerical solutions for tensile loading in ANSYS software in MPa

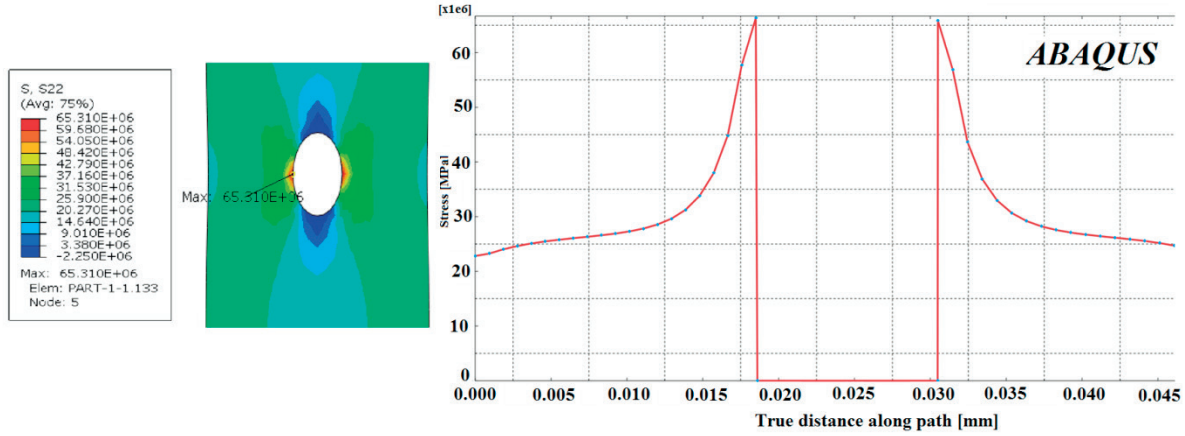

Fig. 8 Numerical solutions for a tensile loading in ABAQUS software in MPa

Measured data comparison with numerical and analytical solutions — Table 1

	Experiment	Analytical solution	Numerical solution	
			ANSYS	ABAQUS
Maximum first stress invariant in tension loading [MPa]	68.17	63.8	65.2	65.3

6. Conclusion

The paper deals with thermal stress analysis focusing on the thermoelastic analysis. The introduction provides an overview of the theory of thermal stress analysis. The experimental part is preceded by the preparation of the measurement including analytical solution for the plate with a hole. Measured data are compared with numerical solution using the finite element method.

In this paper we compare measured data with analytical and numerical solutions (Table 1). The specimen used for measurement was selected due to better comparison of results. During solution of plane stress of plate with hole stress concentration at the edge of the hole occurs. The error in measurements is less than 5 % compared to numerical solutions under tension loading.

Very interesting area for further measurements based on infrared thermography is determining the stress fields in the composite material [11, 12 and 13].

Acknowledgement

This work was supported by the Slovak Research and Development Agency under the contract No. APVV-0736-12.

References

[1] DEKYS, V., BRONCEK, J.: *Communications - Scientific Letters of the University of Zilina,* 14, 2, 2012.

[2] ZMINDAK, M., NOVAK, P.: *Communications - Scientific Letters of the University of Zilina,* 14, 4A, 2012, p. 85.

[3] ESTRADA, J. R., PATTERSON, E. A.: Path Dependency in Thermoelastic Stress Analysis. *Experimental mechanics*, vol. 44, No. 6, 2004, pp. 567-573.

[4] EISENLOHR, A.: *Adiabatic Temperature Increase Associated with Deformation Winning and Dislocation Plasticity*. [online]. 2012. Available online at www.sciencedirect.com, 2012.

[5] RAJIC, N., ROWLANDS, D.: Thermoelastic Stress Analysis with a Compact Low Cost Microbolometer System. *Quantitative Infrared Thermography*, vol. 10, No. 2, 2013, pp. 135-158.

[6] BREMOND, P.: *New Developments in ThermoElastic Stress Analysis by Infrared Thermography.* [online]. 2007. Available online at: < *http://www.ndt.net/article/panndt2007/papers/138.pdf* >.

[7] PLUM, R. et al.: *Extended Thermoelastic Stress Analysis Applied to Carbon Steel and CFRP*. [online]. 1999. Available online at: < *http://ebookbrowsee.net/we5a3-pdf-d75918406* >.

[8] WANG, G. et al.: *Thermographic Studies of Temperature Evolutions in Bulk Metallic Glasses: An overview.* Intermetallics. [online]. 2012. Available online at: <www.sciencedirect.com>. ISSN: 0966-9795.

[9] BARTON, J.: *Introduction to Thermoelastic Stress Analysis.* Strain [online]. 1999. Available online at: < http://onlinelibrary.wiley.com/doi/10.1111/j.1475-1305.1999.tb01123.x/abstract >. ISSN: 0039-2103

[10] HONNER M., HONNEROVA, P.: *Survey of Emissivity Measurement by Radiometric Methods*. Applied Optics, vol. 54, 2015, 2015, pp. 669-683. < http://dx.doi.org/10.1364/AO.54.000669 >.

[11] ZMINDAK, M., NOVAK, P.: *Communications - Scientific Letters of the University of Zilina,* 14, 3A, 2012, p. 73.

[12] NOVAK, P., ZMINDAK, M., PELAGIC, Z.: *Applied Mechanics and Materials,* 486, 2014, p. 181.

[13] RIECKY, D., ZMINDAK, M., PELAGIC, Z.: *Communications - Scientific Letters of the University of Zilina,* 14, 3A, 2012, p. 142.

Jan Zamecnik - Juraj Jagelcak *

EVALUATION OF WAGON IMPACT TESTS BY VARIOUS MEASURING EQUIPMENT AND INFLUENCE OF IMPACTS ON CARGO STABILITY

This article deals with impact tests of wagons, evaluation of impacts from various measuring equipment and influence of impacts on cargo motion in the wagons when various manners of cargo securing were used. The accelerations generated during impacts were observed also by monitoring units designed for monitoring of transport and by recordings from cameras GoPro Hero. Instead of observing the influence of impacts on the cargo loaded in impacting wagons, the function of the monitoring units in a closed building with not very good GPS signal was also observed.

Keywords: *Impact tests, wagon, acceleration, lashings, damages in railway transport.*

1. Introduction and description of measuring equipment

One of the most significant risks in railway transport is the risk of damages on transported cargo due to impacts, which are generated mainly during fly or gravity shunting. Damages on cargo can be caused e.g., by its stroke on wagon´s sidewalls, by drop or by shaving between pieces of cargo, between cargo and floor or sidewalls as a result of undesirable cargo movement. This risk is most significant for consignments of one or several wagons, which are not transported as block trains, because during long-haul transports these wagons can be repetitively shunted in railway hubs with cargo inside them.

UIC Loading Guidelines state that in railway transport is needed to take into account occurrence of accelerations up to 4 g in longitudinal direction when cargo is rigidly secured, up to 1 g in longitudinal direction when cargo can slide lengthways in the wagon. Accelerations up to 1 g in longitudinal direction should also be taken into account for wagons in block trains or those used for intermodal transport. Accelerations up to 0.5 g in transverse direction and up to 0.3 g in vertical direction are also defined in these guidelines. Such accelerations occur mainly during shunting and their duration is in general about 100 ms [1].

Experience from research done by Mariterm AB advert to a fact that number and intensity of accelerations actuating on cargo loaded in wagons are strongly influenced by type of wagons used (construction of running gear and buffers). It was found out that occurrence of accelerations exceeding trig values (0.9 g in longitudinal axis, 0.5 g in transverse and vertical axis) was rapidly different among five wagons of various types, which were transported together. During testing transport and impact tests vertical accelerations between 0.5 – 0.8 g (in few cases even up to 1 g) were often measured in commonly used types of wagons with no special adjustments of either running gear or buffers [2]. We also tested wagons of common construction, which are often used in Central European Railways.

According to Table 4 of UIC Loading Guidelines the purpose of impact tests is to check whether the loading methods used and loose fastenings stand up to the longitudinal stresses exerted during railway operation. In compliance with the testing method, the wagons to be used should be fully-loaded. There should be done 2 impacts in the same direction, (1st impact at 5-7 km/h and 2nd impact at 8-9 km/h) followed, without any adjustment of the load fastenings, by counter-shock (impact in opposite direction) at 8-9 km/h with these wagons, fly or gravity shunted [1].

This article deals with the impact tests of wagons, evaluation of impacts by various measuring devices, and influence of impacts on cargo motion in the wagons with three various manners of cargo securing. For these purposes 10 impact tests were performed, for which the following wagons loaded with coils of steel wire were used (Table 1):

* **Jan Zamecnik, Juraj Jagelcak**
Department of Road and Urban Transport, Faculty of Operation and Economics of Transport and Communications, University of Zilina, Slovakia
E-mail: zamecnik@fpedas.uniza.sk

Description of wagons used for the impact tests Table 1

Wagon type	Loading length (m)	Length including buffers (m)	Wagon weight (kg)	Cargo weight (kg)	Total weight (kg)	Floor	Buffers
Impact wagon							
Eas	12.8	14.04	22 500	52 000	74 500		cat. A
Tested (impacting) wagons							
Res	18.5	19.9	24 100	31 740	55 840	wooden, damp	cat. A
Rils	18.53	19.9	24 000	44 284	68 284	wooden, dry	cat. A

Buffers with 105 mm stroke are, in accordance with UIC 526-1, divided into 3 groups, where for category A energy absorption of at least 30 kJ is required, for category B at least 50 kJ and for category C at least 70 kJ.

Following equipment was used for measuring of acceleration in these tests:

- device Saver 9X of the University of Zilina, placed in the middle of the tested wagon, using sample rate 1 000 Hz;
- device MoniLog EnDal Curve of CD Cargo placed in the middle of the tested wagon;
- monitoring units A1 and A2 equipped with tri-axial accelerometers, fixed on the wagon by magnetic plates, both placed close to one another on the side of impact of the impacting wagon in the same height as buffers. These units can be used for the tracking and tracing of transport (including intermodal transport) and can automatically detect the accident situations;
- monitoring units X1 and X2 equipped with tri-axial accelerometers, fixed on the wagons by magnets (magnets are their integral part). Unit X1 was placed on the impact wagon and X2 on the testing wagon on the side of impact. These units are other type of monitoring units used for the tracking and tracing of transport (including intermodal transport) and also can automatically detect the accident situations;
- 6-axis MotionTracking device (next as MT6) equipped with a tri-axial accelerometer and tri-axial gyroscope, the accelerometer was set to range +/- 8g for purposes of these tests. The real sample rate was around 65 +/-3 Hz;
- 2 cameras GoPro HD Hero 3. Recordings from them were processed by the Tracker software and then we calculated acceleration in longitudinal axis x from its results. We used frame rate 120 frames per second.

All the wagons were during the impact tests loaded by coils of wire weighing about 2 000 kg/coil. Ten impact tests were done in three series with different wagons and cargo loading:

- in the first series the wagon Res was used as tested (impacting) wagon. This series consisted of 2 impact tests in front direction (next as Res F01 and Res F02) and one test in reverse direction (Res R03);
- the Res wagon was also used in the second series, but the way of cargo securing was different. This series consisted of 2 impact tests in front direction (next as Res F04 and Res F05) and one test in reverse direction (Res R06);
- in the third series the wagon Rils was used as a tested wagon. This series consisted of 2 impact tests in front direction (Rils F07 and Rils F08) and 2 in reverse direction (Rils R09 and Rils R10), because of the low speed before shock in the test Rils R09.

The tests were done in a closed hall where the temperature was from 5 to 7 °C.

2. Impact tests and their influence on loaded cargo

The maximum recorded accelerations in the longitudinal axis x by particular equipment are stated in Table 2 (instead of GoPro cameras from which the average accelerations in the impact duration of 0.06 to 0.125 s are stated). Particular series of impact tests are highlighted by different colours.

In the first series of impact tests the Res wagon with 16 coils was used as an impacting wagon. 15 coils were loaded on the floor, one coil was placed in the upper layer in the saddle between the 8th and 9th coil from the front. There was a space of 60 cm between these coils. The coil in the upper layer was fixed with each of neighbouring coils by a polyester lashing strap with the lashing capacity of 3 000 daN (Fig. 1 on the left). No blocking of the cargo was used in transverse direction. It was supposed that the friction between coils and wagon floor and an effect of pushing the windings of particular neighbouring coils one into another will be satisfying for fixation of coils in transverse direction.

After the first impact (Res F01) the coil in upper layer skipped up and all the coils moved frontwards (closer to the impact wagon). The space under the coil in the upper layer was shortened from 60 cm to only 5 cm and in the rear part of wagon the 40 cm long space was created. After the second impact the same situation was repeated and the coils in the front part of wagon pushed more one onto another while the space in the rear part of wagon was lengthened to 50 cm. The third impact was done in reverse direction. The coil in the upper layer skipped up again and all the coils moved frontwards (in direction to the impact wagon). 40 cm long space was created between the last coil in the rear and the wagon rear wall. The space under the coil in the upper layer lengthened from 5 to 15 cm. This manner of

Accelerations in the x-axis recorded in particular impact tests. All the values of accelerations are stated in g Table 2

Impact test	Speed before impact [km/h]	In the place of impact				On the floor in the middle of impacting wagon			
		A1	A2	X1	X2	MT6	Saver 9X	EnDal Curve	GoPro Hero 3
Res F01	5.76	1.56	1.68	1.01	1.34	1.48	2.24 to -2.01	N/A	1.57
Res F02	8.67	2.12	2.04	1.54	1.76	2.48	N/A	N/A	1.69
Res R03	8.89	2.06	2.08	1.21	1.31	1.41	3.30 to -2.08	1.82	1.92
Res F04	6.67	1.60	1.48	1.17	1.18	2.44	2.14 to -1.12	N/A	1.42
Res F05	11.08	0.20[3]	0.20[3]	1.40	1.23	2.06	N/A	N/A	1.84
Res R06	10.14	2.32	2.00	1.39	1.78	2.02	N/A	2.32	3.13/2.18[1]
Rils F07	6.99	1.44	1.56	1.11	1.09	1.60	0.82 to -0.71	N/A	1.37
Rils F08	8.00	1.72	1.88	1.45	0.57	1.16	2.01 to -4.33	N/A	1.61
Rils R09	5.33	1.16	1.08	N/A	0.93	0.95	0.81 to -0.72	N/A	1.67/0.81[2]
Rils R10	10.14	2.16	2.20	1.25	1.22	1.39	1.01 to -0.83	N/A	2.99

cargo securing cannot be considered as satisfying because of the cargo movement after all the shocks, when in the rear part of wagon the coils can move not only in longitudinal direction but there is also a risk of their movement in transverse direction (the coils can move frontwards and rearwards, so their windings do not fit one into another and do not block particular coils against movement in transverse direction). The coil in the upper layer does not fulfil crowding-out effect.

The second series of impact tests was done with the same wagon and cargo loading distribution, but the way of securing the upper coil was different. The upper coil was secured by a loop lashing by two straps to lashing points of the wagon. After the first impact (F04) the cargo did not move. After the second impact a 5 cm long free space was created in the rear part of wagon and the space under the upper coil was shortened by the same length. The speed before impact was in this case higher than UIC Loading Guidelines recommend for impact tests. After the reverse impact R06 whole cargo moved frontwards to the place where had been the space created after previous impact. The space of the same length was created in the rear part of the wagon. The biggest acceleration in the longitudinal axis x was measured in this reverse impact by most of devices which were used (see Table 2). High peak values of acceleration were recorded also in vertical axis z.

In the third series of impact tests the wagon Rils was used. The wagon was loaded by 22 coils, 15 of which on the floor and 7 in the upper layer. The coils 1 to 3 and 5 to 7 were fixed always

Fig. 1 Securing of the coil in the upper layer in the first series of impact tests (on the left) and in the second series of impact tests (on the right)

[1] Higher value was found out in duration of 0.075 s, the lower one in duration of 0.125 s. The impact wagon moved after this impact.

[2] Higher value was found out in duration of 0.075 s, it is also possible to evaluate the deceleration as 0.81 g in duration of 0.2 s.

[3] In these cases the monitoring units evaluated other shock instead of the shock during the impact. This shock actuated mainly in the vertical (z) axis and occured immediately before the impact, when the impacting wagon passed through an obstacle on the track.

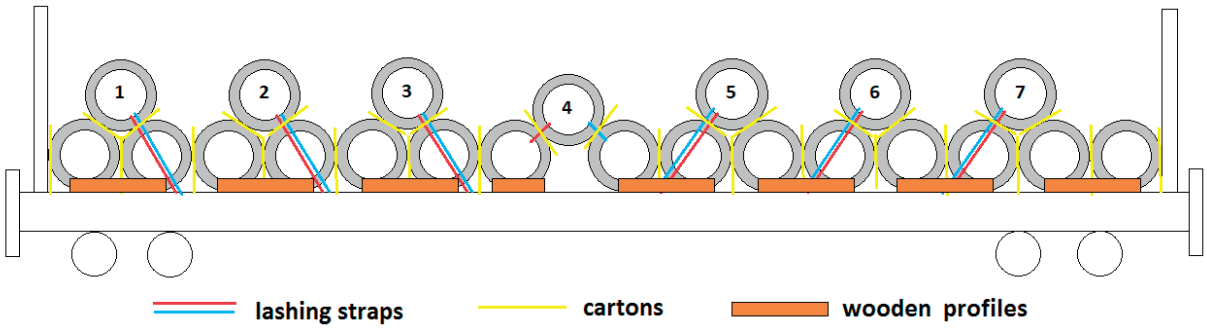

Fig. 2 Cargo loading on the wagon Rils in the third series of impact tests

by a loop lashing with two lashing straps to the lashing points of the wagon (see Figs. 2 and 3), whilst the middle-placed coil no. 4 was lashed by lashing straps only with the neighbouring coils placed on the floor and there was 60 cm long space under it. The neighbouring coils were separated by 5 mm thick cartons. The cargo was blocked against transverse movement by wooden profiles. After the first impact (F07) the coils in the upper layer skipped up but no movement of cargo was detected. The forces in lashings in the front part of the impacting wagon increased, but lashing straps in the rear part of the wagon became looser. After the second impact (F08) the 5 cm long space was created in the rear part of the wagon. This space was created because the coils pushed one into another and the space under coil no. 4 was not shortened. The measuring devices MT6 and Saver 9X placed in the middle of the wagon, measured high acceleration in the vertical axis in this impact (1.08 g by MT6). The speed of impacting wagon before the third impact in reverse direction (R09) was very low, so the reverse impact test was repeated. In the repeated reverse impact test R10 the cargo moved frontwards and 5 cm long space was created in the rear part of the wagon. Loose lashing straps in the front part of wagon (which had been its rear part in F07 and F08) became tightened and the straps in the rear part of the wagon became looser.

Fig. 3 Lashing on the wagon Rils in the third series of impact tests

The accelerations in the place of impact were measured by four monitoring units which are used for the monitoring of road, railway or intermodal transport and are also equipped with accelerometers with a function of accident situations detection. Units marked as A1 and A2 were placed in the same height as wagon buffers and in general these units recorded higher values of acceleration than units called X1 and X2 placed about 75 cm higher. Average values of accelerations in the axes x, y and z from all the measuring devices, except GoPro Hero 3 cameras (the data analysis does not allow to determine the accelerations in the axes y and z) and device Saver 9X (unsuitable data structure), are given in Table 3. Incorrect data from monitoring units A1 and A2 at impact test Res F05 are also not included to the average values. The last column states maximum values of acceleration in the vertical axis measured by MT6 (this device allowed to analyse runs of accelerations in all three axes during and after impacts). These maximum values occurred with time shift of 50 – 80 ms from occurrence of maximum values of accelerations in the longitudinal axis, as is visible in Figs. 5 and 6.

The highest accelerations were reached in the longitudinal axis x. In several cases the impacted wagon moved after the impact, mostly in the tests Res F01, Res F02, Res F05, Res F06 and Rils F08. Average values of accelerations in the y-axis and the z-axis were recorded as about 25 % and 43 %, respectively, of the average value of acceleration in the x-axis. Transverse acceleration in the y-axis in the three cases lightly exceeded 0.5 g which is the value considered for cargo securing to prevent the movement sidewards in railway transport. In general, results from these tests indicate that transverse accelerations reach higher values in the impact tests in front direction when there is no space near the frontwall of the wagon. Accelerations actuating in the vertical axis z in their peak values mostly exceeded 0.3 g, as is stated in UIC Loading Guidelines, but their peak values actuated only for short-term. The device MT6 placed in the middle of tested wagons measured very high peak values of vertical acceleration in most cases, whereas in some cases it recorded two peaks, mainly in such cases when the coils skipped. Peak values in the vertical axis actuated for shorter time than that in the longitudinal axis (see Fig. 6). The problem for

Accelerations in three axes in particular impact tests as average from various measuring equipment Table 3

Impact test	Average accelerations			Maximum values of vertical (z) acceleration measured by MT6
	longitudinal (x)	transverse (y)	vertical (z)	
Res F01	1.44	0.59	0.88	1.52
Res F02	2.17	0.53	0.80	1.20
Res R03	1.64	0.26	0.58	0.60
Res F04	1.90	0.48	0.62	0.95
Res F05	1.69	0.49	1.14	1.70
Res R06	2.02	0.44	1.00	2.01
Rils F07	1.45	0.45	0.59	0.80
Rils F08	1.28	0.51	0.64	1.08
Rils R09	1.01	0.07	0.28	0.25
Rils R10	1.55	0.19	0.37	0.30
Average	1.61	0.40	0.69	1.04

Values of speed before impact and acceleration in x-axis during impact calculated from analysis of video recordings from GoPro Hero 3 cameras Table 4

Impact test	Referential speed found out by stopwatch [km/h]	Speed - cal. dist. 1 [km/h]	Speed – cal. dist. 2 [km/h]	Acceleration in x-axis – cal. dist. 1 [g]	Acceleration in x-axis – cal. dist. 2 [g]	Duration of acceleration [s]
Res F01	5.76	5.70	5.55	1.06	1.04	0.15
Res F02	8.67	8.06	8.50	1.65	1.74	0.108
Res R03	8.89	8.32	7.64	2.01	1.84	0.109
Res F04	6.67	6.27	6.46	1.40	1.44	0.084
Res F05	11.08	8.94	9.28	1.80	1.87	0.092
Res R06	10.14	9.83	10.31	3.05/2.12	3.20/2.23	0.075/0.125
Rils F07	6.99	7.00	7.24	1.35	1.39	0.091
Rils F08	8.00	8.04	7.76	1.64	1.58	0.125
Rils R09	5.33	5.17	4.99	1.70/0.82	1.64/0.80	0.075/0.200
Rils R10	10.14	8.87	8.30	3.09	2.89	0.059

evaluating accelerations in the z-axis can arise due to time shift between peaks of acceleration in the x-axis and in the z-axis. Therefore, it is not correct to evaluate the maximum values of accelerations in particular axes only from the point where the maximum total acceleration was reached (which occurs mostly when the peak value of longitudinal acceleration was reached).

Monitoring units A1 and A2 placed in the height of buffers recorded high values of vertical acceleration mainly in impacts Res F01 (measured values were 0.80 and 1.36 g respectively), Res F02 (0.88 and 0.60 g respectively) and Res R06 (1.16 and 0.76 g respectively). High acceleration in the vertical axis was recorded also in impact Res F05 by monitoring units X1 and X2 (its peak value was 0.66 and 1.06 g respectively). Device MT6 in the middle of the wagon also detected strong vertical acceleration with two short-term peaks 1.70 and 1.47 g at this impact.

3. Evaluation of parameters of impact from video analysis

If the video analysis is used for evaluation of impact or braking parameters, there is important to take into account that correctness of acquired data depends on correct setting of calibration distance (referential distance according to which the software can count the video recording distances to real distances). It is also necessary to remove fish-eye effect. We used calibration distance of 1 meter, which was marked on the

impacting wagon (Fig. 4). We also used referential point which was marked on the wagon and had contrastive colour. Tracker software using the function of Autotrack traced this referential point and recorded values of calculated speed and distance. The calibration distance is located in different place at the beginning and at the end of video recording and is recorded under different angle due to movement of observed wagon. So there are some differences in the measured values between using calibration distance in place at the beginning of video recording (cal. dist. 1, about 20 m before the place of impact) and calibration distance in the place at the end of recording (cal. dist. 2, at place of impact) due to distortion of video. Therefore, there are two data results. For purposes of comparison with other measuring equipment we used the average value of both results. Runs of speed and accelerations are similar when using both results (see Figs. 5 and 6), only calculated numerical values are different. Result values from video analysis are stated in Table 4.

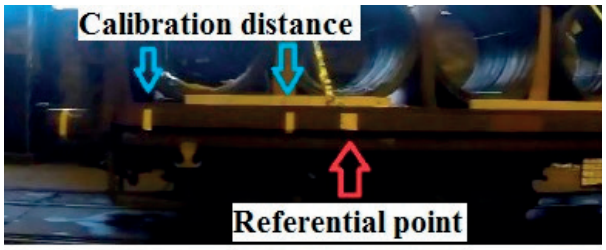

Fig. 4 Illustration of calibration distance and referential point on the wagon. Source: [3]

4. Functionality of monitoring units during the impact tests

The monitoring units which were used allow also recording the position and sending the automatic reports about detected accident situations. For purposes of these impact tests they were set to such initial level of acceleration for accident detection that all the impact tests should be evaluated as crashes. Monitoring unit A1 recorded all 10 impacts and 8 of them correctly evaluated and sent to the provider`s information system. Some other smaller acceleration had occurred few seconds before both impacts which were not correctly evaluated. Unit A2 evaluated all 10 impacts as crashes, but in one case (Res F05) it also probably recorded other acceleration caused by an obstacle on the track which the wagon passed through. Unit X1 placed on the impact wagon recorded 9 of 10 observed impacts (only impact Rils R09 with low speed before impact missed) but only 5 of them were sent to the provider`s information system as crashes. Unit X2 recorded all 10 impacts and 7 of them evaluated as crashes. The impact tests were done at a closed hall, therefore the positions of impacts were not recorded very exact. Differences between determined positions and real positions of impacts were from 50 to 200 m in almost all the cases. Also the ride direction before the shock was in several cases recorded incorrectly or not recorded at all.

5. Evaluation of runs of accelerations from device equipped with accelerometer and from video analysis

In Figures 5 and 6 are stated runs of acceleration at two impacts as they were recorded by the device MT6 equipped with a tri-axial accelerometer and with video analysis of recordings from GoPro cameras. The time shift between peak values of longitudinal and vertical acceleration is visible in runs from MT6 device. Accessible data from monitoring units are not suitable for purpose of evaluating the run of acceleration, because they contain only the highest evaluated values and simplified runs of acceleration with interval of 0.1 – 0.3 s, which means too small frequency for evaluating such short-term actions as wagon impact tests are. In both figures is visible that runs of acceleration acquired from the video analysis are very irregular.

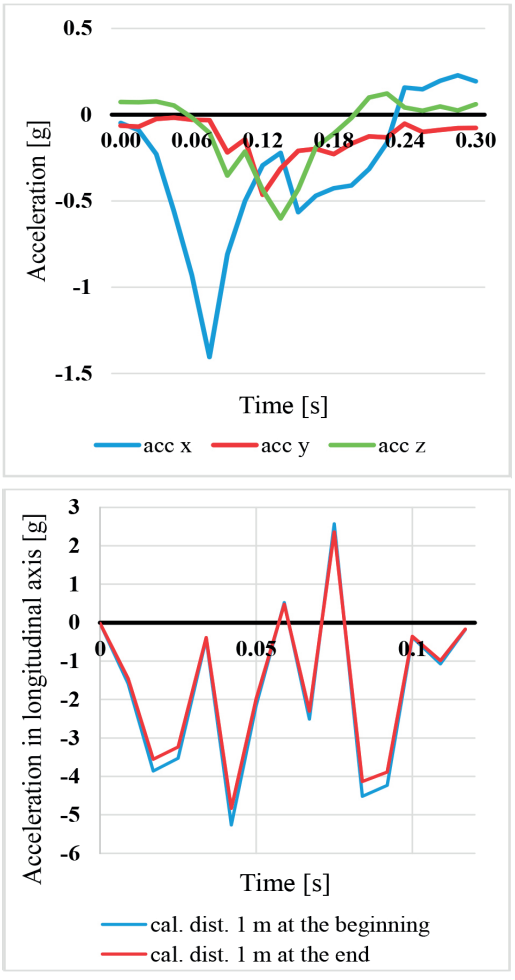

Fig. 5 Runs of accelerations in impact Res R03 acquired from data from device MT6 (up) and from video analysis (down)

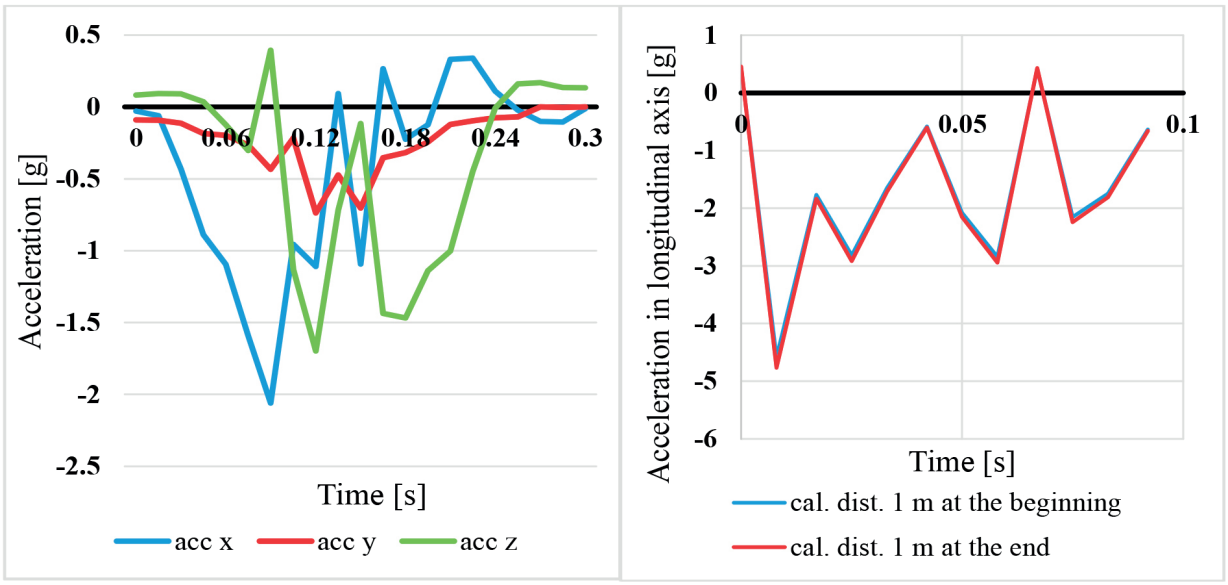

Fig. 6 Runs of accelerations in impact Res F05 acquired from data from device MT6 (on the left) and from video analysis (on the right)

6. Conclusions

In these impact tests the influence of wagon impacts on secured cargo consisting of coils of wire was observed. The securing of cargo only with the neighbouring coils caused that the cargo moved, the manner of securing used in the first series of impact tests was considered improper because the coil in the upper layer did not fulfil the crowding-out effect. Securing the coils in the upper layer to lashing points on the wagon can be considered as more proper way. Higher accelerations in the longitudinal axis were measured by measuring devices placed in the level of buffers than by devices placed higher on the wagon. Monitoring units intended for tracking and tracing of transport and detection of accidents were also used in these impact tests. The monitoring units did not reach such accuracy of position determination as it is usual when they are used on the roads or railways due to measuring in a closed building, probably not very well-covered with GPS signal. The majority of shocks during the impacts were detected correctly. However, not all shocks were evaluated as accidents including the accident message in provider`s information system. The reliability of accident evaluation was about 75 %.

It is necessary to take into account that in some cases relatively high accelerations occur also in the vertical axis in commonly used wagons during shunting. These accelerations may reach about 1 g. Such values of accelerations can be rarely reached also in the transverse axis. The construction of running gear and buffers of wagons strongly affects the accelerations actuating on cargo inside the wagons during shunting. Long stroke buffers capable to compress can rapidly reduce the accelerations actuating on cargo during impacts. Such buffers are capable to reduce the action of accelerations in the longitudinal axis on cargo even to 0.5 - 0.8 g for impacts at speed up to 10 km/h. When the speed before impact is higher, their dampening effect is lowered [2].

References

[1] International Union of Railways, RIV Appendix II, Loading Guidelines, Section 1, Principles, Paris, 2013

[2] ANDERSSON, P. et al.: *Transport Quality on Railway Regarding Breakage,* MariTerm AB: Hoganas, Sweden, 2006. Accessible at: *http://www.mariterm.se/Download/BREAKAGE/ BREAKAGE.pdf*

[3] MISKOV, M.: *Possibilities of Using Software for Video Analysis in Selected Tests Related with Cargo Securing (in Slovak)*, Diploma thesis (consultant J. Jagelcak), University of Zilina, 2015.

Michal Smalo - Libor Izvolt *

ASSESSMENT OF TRACK QUALITY IN TRIAL TEST SECTIONS BY SPOT AND CONTINUOUS METHOD

Abstract. The quality of track alignment and track geometry is an essential precondition of safe and economical operation of railway track. The paper provides an analysis of diagnostics of relative track geometry parameters and evaluation of measurement deviations carried out by the spot and continuous method in sections of the ballasted track, transition areas and sections with the slab track structure.

Keywords: *Railway track, ballasted track, ballastless track, slab track, track geometry, diagnostics.*

1. Introduction

The ballasted track has been proven for many decades. From the structural point of view, the ballasted track is referred to as a railway track whose track skeleton is stored in railway ballast. In the case of high line tonnage and axle load and increasing track speeds, it appears that such a structure has its operational and economical limits [1]. The ballasted track is characterized by "floating" placement of track skeleton which causes the growth of dynamic forces during each passage of a train. This can be and usually is the cause of gradual degradation of the track geometry. The need of elimination of irregularities in the track geometry forces the operator to regularly remove the diagnosed track deficiencies by time-consuming and costly maintenance works. This phenomenon grows with increasing track speed and thus increases the maintenance costs and the share of track possessions. In this way the attractiveness of the track for passengers can be reduced. It is sufficient, however, to only replace the weakest structural element of the ballasted track - the track ballast by another more suitable structural element which shows no plastic behavior. The term slab track, as defined in [2], refers to such a structure of railway superstructure in which a spread function of railway ballast is replaced by reinforced materials, and which is placed on a concrete or asphalt substructure (slab). The slab track structure consists of (top-down):

- track superstructure
  - rails and fastenings of the rails to the rail support,
  - rail support (sleepers, single supporting points, pre-fabricated or monolithic slab),
  - concrete foundation layer (*CFL*) or asphalt foundation layer (*AFL*),
  - hydraulically bonded foundation layer (*HBL*);
- track substructure (if the slab track construction is built on earthworks)
  - frost protective layer (FPL),
  - subsoil layers (consolidated or improved material of earthworks),
  - consolidated soil or bedrock.

2. Experimental section parameters

The experimental sections are situated on the modernized double-track railway line *Nove Mesto nad Vahom - Puchov* and are located in the areas of the portals of the tunnel *Turecky vrch*. The track speed in both tracks is 160 $km.h^{-1}$, which ranks the railway line to the category of velocity range No. 4 (*RP4*). The superstructure of each section is constructed as a construction with ballast bed and the slab track *RHEDA 2000®* (in tunnel, on bridges and on earthwork). The construction of the superstructure in transition areas is constructed as improved ballast placed in the concrete trough.

The monitoring of the track geometry aims to determine the condition of the parts of the track structure and the entire track. This kind of monitoring is one of the basic diagnostic activities by which also the traffic and climatic load and the effects of maintenance on track skeleton are monitored.

The experimental track sections are labeled as [3]:

- section 1.1 (track No. 1, south portal of the tunnel *Turecky vrch*) and 2.1 (track No. 2, south portal; both sectors of length 175 m; km 102.360 000 – km 102.535 000):

* **Michal Smalo, Libor Izvolt**
Department of Railway Engineering and Track Management, Faculty of Civil Engineering, University of Zilina, Slovakia
E-mail: michal.smalo@fstav.uniza.sk

- km 102.360 000 – km 102.460 500 structure with ballast bed,
- km 102.460 500 – km 102.480 500 structure with ballast bed in the concrete trough,
- km 102.480 500 – km 102.535 000 slab track;

• section 1.2 (track No. 1, north portal of the tunnel *Turecky vrch*) and 2.2 (track No. 2, north portal); both sectors of length 640 m; km 104.200 000 – km 104.840 000):
  - km 104.200 000 – km 104.720 500 slab track,
  - km 104.720 500 – km 102.480 500 structure with ballast bed in the concrete trough,
  - km 104.740 500 – km 104.840 000 structure with ballast bed.

3. Diagnostic methods and equipment

The diagnostics of the track alignment design and track geometry by the spot method is realized by gauge-checkers *ROBEL* (Fig. 1) and *GEISMAR*. The spot method is used to control deviations of gauge *ΔRK* (mm) and cant *PK* (mm) and monitoring is performed at each fastening point of the rail support [4].

For the sake of comprehensive diagnostics, each section No. 1.1 and No. 2.1 is represented by 288 samples (fixation points) and each section No. 1.2 and No. 2.2 is represented by 1 009 samples (fixation points) [5].

Fig. 1 Gauge checker ROBEL

The comprehensive diagnostics of the track alignment design and track geometry by continuous method is carried out by continuously measuring trolley *KRAB™-Light* (Fig. 2). The measurement is referred to as continuous, but in fact, the data is recorded with the measuring step of 250 mm [5] and [6]:

- gauge deviation *RK* (after calculating the change of gauge *ZR* is also recorded),
- alignment of right rail *SR* (after calculating the alignment of left rail *SL* is also recorded),
- rail top level of right rail st*VR* (after calculating the rail top level of left rail *VL* is also recorded),
- cant *PK*,
- quasi-twist on a short base (calculated to a quasi-twist on a base of 1.8 m long – *ZK 1.8*, on a base of 6.0 m long – *ZK 6.0* and on a base of 12.0 m long – *ZK 12.0*),
- track distance.

For the sake of comprehensive diagnostics, each of the sections No. 1.1 and No. 2.1 is represented by 701 samples, each of the sections No. 1.2 and No. 2.2 is represented by 2 561 samples.

Fig. 2 Continuously measuring trolley KRAB™-Light (on the up) and computer Nomad (on the down)

4. Assessment of results of track alignment design and track geometry diagnostics

The assessment of results of the track alignment design and track geometry is carried out according to the valid technical standards and regulations [5]. The diagnostics of structure layout and track geometry of the track section:

- measurements before putting sections into operation (*MSO*) were made in 10.07. – 11.7.2012, 2.10. – 3.10.2012,
- first operational measurement (*PO*1) 09.04. – 10.04.2013, 21.04 – 22.04.2013,

The deviations of the relative geometric parameters of the track for RP4 [5] Table 1

Measured parameter	Limit input deviations		Operational deviations		Limit operational deviations		Note
***RK* (mm)**	-2	2	-3	5	-5	10	–
***ZR* (mm/m)**	2		3		4		–
***PK* (mm)**	-3	3	-6	6	-8	8	–
Measured parameter	Limit value		Operational value		Limit operational value		Note
***ZK* (1:*n*) (mm / base)**	1:250 (7.2; 4.0)		1:250 (7.2; 4.0)		1:167 (10.8; 5.99)		on measuring base 1.8 m
	1:832 (7.2; 1.20)		not evaluated		1:250 (24.0; 4.0)		on measuring base 6.0 m
	not evaluated		not evaluated		1:333 (36.0; 3.0)		on measuring base 12.0 m
Measured parameter	**Limit input relative deviations**		**Relative operational deviations**		Limit operational relative deviations		Note
***VL*, *VP* (mm)**	-3	3	-6	6	-8	8	–
***SL*, *SP* (mm)**	-3	3	-6	6	-8	8	–

- second operational measurement (*PO*2) 08.10. – 09.10.2013, 21.10. – 22.10.2013,
- third operational measurement (*PO*3) 25.5.2014 and 28.5.2014,
- fourth operational measurement (*PO*4) 29.10.2014.

The measured parameters were evaluated according to the limit input deviations for acceptance of works with the use of new material (*MSO*) and according to the operational deviations and limit operational deviations (*PO*1, *PO*2, *PO*3 and *PO*4) in Table 1 [7].

The results of measurement before putting sections into operation (*MSO*) obtained by the spot method have been compared to operational measurements (*PO*1, *PO*2, *PO*3 and *PO*4) and the differences are shown in Table 2 - measurement of gauge deviations *ΔRK* and Table 3 - measurement of cant deviations *PK* [8] and [4].

The sections with the lowest quality shown by evaluation are the section of track No. 1 in the area of the southern portal and the section of track No. 2 in the area of the northern portal, where incidence of local errors is the highest. There is expected

Differences of measurement of ΔRK – operational measurement (PO1, PO2, PO3, PO4) and measurement before putting sections into operation (MSO) Table 2

Track / section	**Differences of measurement *ΔRK* (mm)**							
	PO1-MSO		***PO2-MSO***		***PO3-MSO***		***PO4-MSO***	
	max.	min.	max.	min.	max.	min.	max.	min.
Track No. 1 / Section No. 1	1.2	-1.0	0.7	-1.0	2.1	-0.9	1.1	-1.0
Track No. 1 / Section No. 2	1.4	-1.0	0.7	-1.5	0.6	-1.8	0.9	-1.7
Track No. 2 / Section No. 1	0.8	-2.7	0.5	-2.5	0.5	-2.8	0.4	-1.5
Track No. 2 / Section No. 2	1.3	-1.3	2.0	-3.1	1.0	-3.6	1.2	-2.9

Differences of measurement of PK – operational measurement (PO1, PO2, PO3, PO4) and measurement before putting sections into operation (MSO) Table 3

Track / section	**Differences of measurement *PK* (mm)**							
	PO1-MSO		PO2-MSO		***PO3-MSO***		***PO4-MSO***	
	max.	min.	max.	min.	max.	min.	max.	min.
Track No. 1 / Section No. 1	0.6	-4.2	-1.1	-4.6	0.8	-3.1	-0.6	-4.7
Track No. 1 / Section No. 2	1.8	-2.0	1.1	-3.8	3.3	-4.4	1.4	-4.1
Track No. 2 / Section No. 1	1.6	-2.2	1.9	-3.2	1.7	-2.8	1.3	-3.4
Track No. 2 / Section No. 2	2.0	-4.5	2.2	-4.4	2.3	-4.9	1.2	-2.9

improvement of the quality of all sections after their maintenance [9] and [10].

The continuous method used for overall superevaluation of the test sections (so called "section evaluation") is, in accordance with [2], given by the quality number of the section evaluated (*QN*), and the quality mark (*QM*) of *SR* parameters (*SL*), *RK*, *PK* and *VR* (*VL*).

The evaluation of the section by the number of quality (*QN*), calculated according to the equation:

$$QN = \sqrt{0,57 \cdot SDV_{RK}^2 + 1,6 \cdot SDV_{SR,SL}^2 + 1,6 \cdot SDV_{VR,VL}^2} \quad (1)$$

where: SDV_{RK} - Standard deviation of variable of track gauge,
$SDV_{SR,\,SL}$ - Standard deviation of variable of direction of the track,
SDV_{PK} - Standard deviation of variable of cant,
$SDV_{VR,\,VL}$ - Standard deviation of variable of longitudinal track height.

where $SDV = \sqrt{\frac{1}{n-1}\sum_{i=1}^{n} x_i^2}$ (mm) (2)

expresses irregular course of the track geometry parameter in the section evaluated, where:

n - number of points measured after 0.25 m,
i - marking measuring point,
x_i - dynamic component of the relevant quantity of track geometry (deviation from the center line in the wavelength range 1 m to 25 m).

The evaluation of section according to quality marks shall be carried out according to the equation:

$$QM = \frac{\ln \frac{SDV}{b}}{m} \quad (3)$$

where b and m are numerical constants determined on the basis of the SDV statistics of relevant parameter and speed zone.

Considering the Railways of the Slovak Republic, the results of the quality section evaluation of the track according to quality marks are indicative and additional and are not binding for the evaluation of *RK* state. The measures which are set for individual intervals of quality marks are recommendatory according to Table 4.

The scale of quality marks (QM) according to quality section evaluation [6] Table 4

Interval of quality marks	Verbal assessment of the section according to the quality mark	Color of the quality mark in printed output
$0 < QM \leq 2$	the state of track geometry is satisfactory in the section evaluated	no color marking
$2 < QM \leq 3$	it is recommended to design the repair of track geometry in the section evaluated into the maintenance work plan	green color
$3 < QM < 4$	it is recommended to perform the repair of the track geometry in the section evaluated before the nearest inspection	violet color
$4 \leq QM \leq 6$	it is recommended to perform immediate measures in the section evaluated to ensure the safety of operation	red color

Quality in section No. 1 in track No. 1 Table 5

Stationing (km)	Railway superstructure	Quality mark	MSO			PO1			PO2			PO3			PO4		
			Local errors	*QM*	*QN*	Local errors	*QM*	*QN*	Local errors	*QM*	*QN*	Local errors	*QM*	*QN*	Local errors	*QM*	*QN*
102.360 000	BT	QM_{SK}	**10**	**2.07**	1.19	0	**2.67**	1.88	0	**2.25**	1.89	0	1.88	1.96	0	**3.12**	2.36
102.460 500		QM_{RK}		1.73		0	1.73		**2**	1.73		**4**	1.74		**4**	1.70	
102.480 500	TA	QM_{PK}	0	1.88			2.00			**2.03**			**2.03**			**2.05**	
102.535 000	ST	QM_{VK}	0	**2.50**		0	**3.21**		**1**	**3.37**		0	**3.49**		0	**3.50**	

Quality in section No. 2 in track No. 1 Table 6

Stationing (km)	Railway superstructure	Quality mark	MSO			PO1			PO2			PO3			PO4		
			Local errors	*QM*	*QN*	Local errors	*QM*	*QN*	Local errors	*QM*	*QN*	Local errors	*QM*	*QN*	Local errors	*QM*	*QN*
102.360 000	BT	QM_{SK}	0	**2.38**	1.09	0	**2.37**	1.12	0	**2.36**	1.14	0	**2.40**	1.23	0	**2.40**	1.22
102.460 500		QM_{RK}		1.53			1.51			1.52			1.52			1.52	
102.480 500	TA	QM_{PK}	0	1.68		0	1.76		0	1.80		0	1.86		0	1.82	
102.535 000	ST	QM_{VK}	**1**	**2.06**		0	**2.13**		0	**2.19**		0	**2.34**		0	**2.35**	

Quality in section No. 1 in track No. 2 Table 7

Stationing (km)	Railway superstructure	Quality mark	MSO			PO1			PO2			PO3			PO4		
			Local errors	*QM*	*QN*	Local errors	*QM*	*QN*	Local errors	*QM*	*QN*	Local errors	*QM*	*QN*	Local errors	QM	QN
102.360 000	BT	QM_{SK}	**13**	**2.26**	1.03	0	**2.80**	1.46	0	**2.76**	1.54	0	**2.78**	1.67	0	**3.05**	1.86
102.460 500		QM_{RK}		1.78			1.78			1.75			1.77			1.76	
102.480 500	TA	QM_{PK}	**1**	1.70		0	1.56		0	1.60		0	1.63		0	1.72	
102.535 000	ST	QM_{VK}	0	1.97		0	**2.49**		0	**2.71**		0	**2.91**		0	**2.94**	

Quality in section No. 2 in track No. 2 Table 8

Stationing (km)	Railway superstructure	Quality mark	MSO			PO1			PO2			PO3			PO4		
			Local errors	*QM*	*QN*	Local errors	*QM*	*QN*	Local errors	*QM*	*QN*	Local errors	*QM*	*QN*	Local errors	*QM*	QN
102.360 000	BT	QM_{SK}	**9**	**2.50**	1.31	0	**2.50**	1.20	0	**2.50**	1.21	0	**2.49**	1.23	0	**2.50**	1.24
102.460 500		QM_{RK}		1.72			1.60			1.58			1.58			1.58	
102.480 500	TA	QM_{PK}	0	1.90		0	1.63		0	1.61		0	1.61		0	1.62	
102.535 000	ST	QM_{VK}	**7**	**2.39**		0	**2.24**		0	**2.29**		0	**2.34**		0	**2.36**	

The development of the track alignment design and track geometry of monitored sections is shown in Tables 5 - 8.

The evaluation of deviations of the track alignment design and track geometry in velocity zone RP 4 according to [7 and 6] is calculated separately for sections with the ballasted track (*BT*), for transition areas (*TA*) and sections with the slab track structure (*ST*).

From the overview of the track section quality it is clear that local errors noticed before putting sections into operation were eliminated by maintenance interventions carried out after input measurements. The section with the lowest quality shown by evaluation is the section of track No. 1 in the area of the southern portal, where occurence of local errors is the highest. This section also is of the lowest quality mark and number of quality. There is expected improvement of the track section quality after maintenance interventions.

5. Conclusions

The comparison of the results of diagnostics obtained by spot method and also by continuous method in the experimental sections shows direct connection. The section with the lowest quality shown by evaluation by both methods is the section No. 1 in the area of the southern portal.

The output of diagnostics is a set of information about the railway track quality. By using it, it is possible to predict further progress of the structure and then plan maintenance interventions.

The essential preconditions for the competitiveness of rail transport are sustainability and reliability of railway line operation. Only the development of various diagnostic methods and assessment of track alignment and track geometry can ensure the quality of the track geometry parameters, reduce maintenance costs, extend the service life of the structure and increase the competitiveness and attractiveness of railway lines in long- term perspective.

Acknowledgement

The paper contains partial results of the grant VEGA 1/0597/14”Analysis of methods used to measure the unconventional railway track construction from the point of view of accuracy and reliability”.

References

[1] IZVOLT, L., SMALO, M.: Historical Development and Applications of Unconventional Structure of Railway Superstructure of the Railway Infrastructure of the Slovak Republic. *Civil and Environmental Engineering,* vol. 10, No. 2, 2014, pp. 79-94. EDIS: University of Zilina. ISSN 1336-5835.

[2] ZSR SR 103-8 (S): General requirements for the design, construction, repair, maintenance and acceptance of construction repair and maintenance works on the slab track construction (in Slovak). 2012, Bratislava: GR ZSR.

[3] IZVOLTOVA, J., PISCA, P., VILLIM, A., MANCOVIC, M.: Precision Analysis of Height Measurements Realized on Ballastless Track. *Communications - Scientific Letters of the University of Zilina,* vol. 16, No. 4, 2014, p. 63-74. EDIS: University of Zilina. ISSN 1335-4205.

[4] SMALO, M., IZVOLT, L.: *Assessment of Track Superstructure Quality - Spot and Method.* Proc. of 11th European Conference of Young Researchers and Scientists, TRANSCOM 2015, Zilina, June 2015, pp. 291-296. University of Zilina, 2015, ISBN 978-80-554-1049-4.

[5] SESTAKOVA, J.: Quality of Slab Track Construction - Track Alignment Design and Track Geometry. *Civil and Environmental Engineering,* vol. 11, No. 1, 2015, pp. 2-9. EDIS: University of Zilina. ISSN 1336-5835.

[6] ZSR SR 103-7 (S): *Measurement and Evaluation of Track Geometry by Measuring Trolley KRAB (in Slovak).* 2008. Bratislava: GR ZSR.

[7] STN 73 6360: 1999. *Track Alignment Design and Track Geometry of Normal-gauge Tracks* and *Amendment - part 1 (in Slovak).* Bratislava: SUTN.

[8] IZVOLT, L. et al.: *Monitoring of Sections of Non-conventional Constructions of the Railway Superstructure and the Transition Areas - 5th and 6th Stage. ZSR Modernization of Railway Track Nove Mesto nad Vahom - Puchov, km 100.500 to 159.100, part 24-32-01 Nove Mesto - Trencianske Bohuslavice (in Slovak),* 2014. Department of Railway Engineering and Track Management: Faculty of Civil Engineering : University of Zilina.

[9] IZVOLTOVA, J., SESTAKOVA, J.: *Analysis of the Impact of Traffic Load on the Slab Track Construction (in Slovak).* Proc. of XII intern. conference Geodezia a kartografia v doprave. Praha : Cesky svaz geodetu a kartografu, 2014, pp. 168-176. ISBN 978-80-12-02553-5.

[10] PLASEK, O., HRUZIKOVA, M., SVOBODA, R., BILEK, J.: Under Sleeper Pads in Railway Track. *Communications - Scientific Letters of the University of Zilina,* vol. 16, No. 4, 2014, p. 27-35. EDIS : University of Zilina ISSN 1335-4205.

Jozef Micieta - Jiri Hajek - Jozef Jandacka *

SIMPLE MODEL OF PELLET COMBUSTION IN RETORT BURNER

Combustion of the solid fuel in the burner is an important issue when discussing the CFD simulation of combustion in automatic boiler. In the present work is employed a simplified method for modeling the fuel bed, which is based on mass and heat balances in order to simplify the simulation of combustion in pellet boiler. The model for solid fuel combustion in a burner is created for the purpose of automatic boiler simulations. Such approach does not require a detailed bed model of fired solid fuel. A simple model of the bed can be very useful for designers and engineers of automatic boilers. The described approach to modeling the combustion process in a burner helps to shorten the calculation time and simplify the model of pellet combustion in various types of automatic boilers for households.

Keywords: *Simulation, CFD, combustion, biomass, pellet, boiler.*

1. Introduction

CFD simulations may help to increase understanding and provide detailed prediction of combustion taking place in a boiler. However, modeling of combustion is more complex in biomass boilers than in gas or oil-fired boilers, due to the complexity of the heterogeneous reactions in the bed, the turbulent reactive flow in the freeboard and the very strong coupling between those two regions. However, it is usually not required to describe in depth and in every detail all phenomena that occur in a combustion system. Instead, CFD calculations should give an approximate view of system behavior, help in troubleshooting and provide insights necessary to fine-tune the system's operation, as well as give assistance when dealing with new designs [1].

From an engineer point of view a detailed model of combustion process in a burner is too complicated to be useful, as it requires great amount of time and effort to set it up, run, and analyze its results. Therefore it can be useful to introduce some assumptions in order to simplify a boiler simulation. From an overall point of view on a boiler as a unit, only integral factors like heat and mass transfer in the bed and the boiler are relevant. A simplified method of bed modeling based on thermal and mass balances was employed in this work to describe pellet combustion process in the simulation of an experimental 20 kW boiler. The predictions from CFD simulation were compared with the analytic results from thermal and mass analysis of the combustion process. The model employed in this work may be readily adapted for the modeling of other solid fuel burners and boiler designs. Several combustion parameters need to be defined in order to a practicable model would be achieved.

1.1. Combustion process in a retort burner

The analyzed boiler (Fig. 1) is equipped with a retort burner, which works on underfeeding principle. Fuel (e.g. pellets) is fed from a fuel tank through a horizontal pipe by a feeding screw. The burner elbow changes the direction of movement and pellets are slowly pushed from the bottom into the mouth of the burner, where the combustion process starts. From long-time viewpoint, the pellet boiler operation is a steady process. In fact, the pellet supply to the burner is discontinuous, because the feeder is in operation for tens of seconds and then certain time in rest during the next pellet batch is fired. The primary air is usually blown into the feeder, but also directly to the fired pellets through slits in the burner mouth. The fuel is gradually fed to the bed, where it is heated and gradually releases volatile gases [2]. Depending on the specific fuel, volatile gases start to be released already from 150 – 200 °C. Gases then pass through the hot upper layer of bed, which leads to their ignition and subsequent burning in the combustion chamber [3]. The upper layer of bed consists mainly of fixed carbon and non-combustible inorganic material, with inter-particle space filled by gases.

* [1]**Jozef Micieta,** [2]**Jiri Hajek,** [1]**Jozef Jandacka**
[1]Department of Power Engineering, Faculty of Mechanical Engineering, University of Zilina, Zilina, Slovakia
[2]Department of Process and Environmental Engineering, Faculty of Mechanical Engineering, Brno University of Technology, Brno, Czech Republic
E-mail: jozef.micieta@fstroj.uniza.sk

Small part of the combustible gases burns in the bed, but the main combustion process takes place in the combustion chamber above the burner (freeboard). Burned pellets, or their parts are pushed away from the bed surface and then to burner edge, where they gradually burn out. The edge of the retort burner is usually made of cast iron, which resists well the hot environment and accumulates heat, so it creates favorable conditions for fuel gasification. Oxygen in the primary air, which is not used for the char combustion, is preheated so that there is no problem with incomplete oxidation of combustible gases in the combustion chamber [4]. Residues (ash and unburnt fuel) are either (in the case of fine particles) blown away by the combustion air or (heavier particles) are gradually pushed out of the burner to the ashtray. Secondary air is introduced into the combustion chamber at a certain height above the burner through nozzles in the intermediate wall, which leads to the burnout of remaining combustible gases. Before secondary air blows into the combustion chamber, it is heated in the distribution channel, pipes and intermediate wall.

1.2. Biomass fuel

Ultimate and proximate analysis of the fuel that is used in the model is shown in Table 1. More physical and chemical properties of various biomass fuels could be found in databases, which are quoted in [5] or e.g. [6] and in similar work [7]. Parameters of fuel like moisture, ash content, ratio of char and volatile combustible compounds, and calorific value are obtained in proximate analysis, which is performed experimentally. From the point of view of energy content it is more practical and useful as the ultimate analysis of fuel and it defines fuel parameters necessary as input for CFD simulations.

Proximate analysis is in this work directly used to define composition of gases entering the combustion chamber. As noted above, primary air is supplied together with fuel to the bed. Gaseous products of fuel drying and devolatilization are thus mixed with primary air. This defines the composition of gas entering the combustion chamber.

2. CFD model description

The present CFD model was set up within commercial code Ansys Fluent, but it would be the same in other software as well. The modeling of biomass boiler includes two main areas of interest: 1) combustion process of biomass in the bed and 2) homogeneous reactions and heat transfer in the combustion chamber (freeboard). These two processes are strongly coupled, as freeboard reactions depend on the gases leaving the bed, and as the radiative heat flux emitted by flames above the bed drives the processes inside the bed [1].

Combustible gases in reality begin to be released at the so-called devolatilization temperature, which according to the Ion`s work [8] is about 330 °C (about 600 K). With further increase of temperature, the composition of the released gases changes.

Thus, there is apparent that devolatilization process is strongly coupled to the temperature in combustion chamber, which in turn depends on the amount and composition of the released volatile gases. Therefore, in the present simplified model it is necessary to select a reference temperature, which is key to determining the composition of released gases [7]. There was chosen a temperature level of 600 K (about 330 °C) to estimate the composition of introduced volatile gases, adopting the individual mass fractions according to Ion [8] or Thunman [9]. For simplification, the model assumes devolatilization like an instantaneous phenomenon of thermal transformation of fuel. Volatile gases are represented by CO, CO_2, H_2, H_2O, plus CH_4 representing light hydrocarbons, and finally C_6H_6 representing heavy hydrocarbons (tar), optionally also NH_3.

The amount of nitrogen in a majority of biomass fuels is below 1 %, (although some phytomass fuels may contain up to 4 %). It reacts by endothermic reaction (the energy gain is negative). The reaction can be neglected, because the relative energy gain is very small. Some authors have defined the biomass by a substitutive substance with the chemical formula $C_6H_aO_b$. It replaces biomass in dry, ash-free state, where *a* and *b* are coefficients [5 and 10]. For this substance are defined physical parameters similar to the real for biomass. The devolatilization model of biomass is then described by the following reaction (1).

Approximate composition and properties of the employed fuel — Table 1

Ultimate analysis		Proximate analysis		Bed and particle parameters	
Carbon	52.0 wt%	Moisture	8.5 wt%	Particle diameter	6 mm
Hydrogen	6.8 wt%	Ash	0.6 wt%	Average pellet length	12 mm
Oxygen	41.0 wt%	Fixed carbon	16.2 wt%	Void fraction	0.4
Nitrogen	0.2 wt%	Volatile	74.7 wt%	Net calorific value	18.3 MJ/kg

$$C_6H_aO_b = x_{char,ashfree}C + x_2CO_2 + x_3H_2 + \\ + x_4H_2O + x_5CH_4 + x_6C_6H_6 \quad (1)$$

where x_i is the number of moles of a given species involved in the process. After gasification, only a solid substance remains in the bed. This charcoal can be considered for wood pellets as pure carbon, because the ash content is usually below 1 %. Sulphur content is at trace level, so it is neglected as well. Char combustion is a complex process that is affected by the fuel composition, particle shape and boiler conditions. A simplified model is used by Porteiro [11], which considers a heterogeneous reaction of char to form CO and CO_2 (2), where the ratio of the CO/CO_2 formation rate depends on the temperature (3). A representative char combustion temperature of 1373 K (about 1100 °C) is employed in this work to estimate the composition of the char combustion products [7].

$$\eta C + O_2 \rightarrow 2(\eta - 1)CO + (2 - \eta)CO_2 \quad (2)$$

$$\eta = \frac{2\left(1 + 4 \cdot 3e^{(-3390/T)}\right)}{\left(2 + 4 \cdot 3e^{(-3390/T)}\right)} \quad (3)$$

The present work simulates combustion at nominal power of the boiler, as the most representative operating condition. In the long-term point of view, the combustion can be considered as continuous steady process. Adopting this assumption implies that the various zones in the boiler, where certain processes dominate (such as heating, drying, gasification, combustion of volatile gases and char combustion...) are fixed in space. Then the overall combustion process can be considered as steady. Main boundary conditions of the model then include mass flow inlet defined at the fuel and air inlet (burner), secondary air inlet and flue gas outlet to the chimney (pressure outlet).

2.1. Model of fuel conversion - bed model

As noted above, it is evident that the most complicated processes occur in the burner. The top layer of burner volume that contains burning pellets is called the bed. Within the bed take place several phenomena, from the initial heating of fuel, through its drying, devolatilization, gas combustion and fixed carbon burnout. Reactants, which include the primary combustion air and the solid fuel, are fed to this bed layer. In the computational model devised in this work, the bed is a part of the computational domain and there is no separate bed model to define the boundary conditions, similarly as in [1].

If boiler is considered as a device for transformation of chemically stored energy into heat carried by hot utility water, then burner is a device for fuel transformation to combustible gases and consequently to flue gases, while the thermal energy is released. The subsequent combustion of devolatilized fuel takes place in the freeboard (combustion chamber). As detailed description of the processes occurring in the burner is not required in this work, the burner may be considered as the source (inlet) of flammable gases, thermal energy and primary combustion air, the oxygen in which is already partially consumed. Gas leaves the bed at a certain temperature, which is higher than the devolatilization temperature. If the gas species were inserted into the computational domain through mass sources, the FLUENT software would provide no option to specify their inlet temperature. This problem can be eliminated by assumption that the volatile gases enter the domain through the inlet boundary. The inlet however may not be located at the interface of the bed and the freeboard, as in that case the bed would behave as a reflective surface (diffuse or specular). Thus it is better to place the inlet below the porous fuel bed.

A substitution for the heterogeneous char oxidation in the bed (2) is one of major simplifications, which can be adopted only for automatic boilers. This reaction was replaced by volatile compounds (CO and CO_2) and a heat source in the bed. The number of moles of gaseous species and the released energy during reaction were calculated externally, according to equations (2) and (3) [1 and 7]. Volatile compounds produced during the heterogeneous char reaction were incorporated into the mass flow inlet of species and the energy generated by char oxidation reaction was considered as the heat source in the bed. The simplified model then considered only homogeneous gas reactions.

One role of the bed was to distribute fluid flow on the interface with freeboard evenly across the burner. Furthermore, the bed provided space and time to heat up the gas. These two effects of the bed are closely coupled. The pellets fill up the bed volume and they had the shape of cylinders with known properties. With this assumption, it was possible to replace the bed volume by a porous zone. There was necessary to specify parameters of the porous zone to generate a correct pressure loss in the gas passing through the pellets.

Different flow regimes were expected in the boiler due to its complex geometry. The gases were practically still in some regions and, on the contrary, high gas velocities and fully turbulent flow were expected in areas such as the flame or secondary air injections. Beneath the bed was primary air inlet and various thermo-chemical processes take place in the bed, thus there was also expected turbulent flow. The realizable k-ε model was employed to account for the effect of turbulence due to its proven effectiveness in industrial applications [12 and 13].

In this work the modeling of a packed bed was performed without considering channeling effect. In turbulent flows, packed beds were modeled using both permeability α (a viscous resistance coefficient is $1/\alpha$) and an inertial loss coefficient C_2. One technique for deriving the appropriate values of the porous properties involves the use of the Ergun equation [14]. It is a semi-empirical correlation applicable over a wide range of Reynolds numbers and for many types of packing.

The effect of the bed porosity on the gas flow was introduced by the addition of a source term S_i, calculated by the formula (4), into the momentum equation. Three parameters were needed in the CFD code to evaluate the source term: permeability α, inertial losses coefficient C_2 and porosity ε. The source term was composed of two parts: a viscous loss term (Darcy`s, the first term in equation (4)), and an inertial loss term (the second term in the same equation (4)) [15]. To cover the present case of simple homogeneous and isotropic porous media, it was sufficient to use the same porous properties in the whole bed volume.

$$\nabla p = S_i = -\left(\frac{\mu}{\alpha} v_1 + C_2 \frac{1}{2} \rho_p |v| v_i\right) \quad \left(kg \cdot m^{-2} \cdot s^{-2}\right) \tag{4}$$

Where S_i is the source term for the i th (x, y, or z) momentum equation, $|v|$ is the magnitude of the velocity, μ is the viscosity. In equations (5) and (6) that define permeability and inertial loss coefficient, d_{eq} is the equivalent particle diameter and ε is the void fraction, defined as the volume of voids divided by the volume of the packed bed region. Comparing Darcy`s equation and equation for inertial loss in the porous media with Ergun equation, the permeability and inertial loss coefficient in each component direction may have been identified as:

$$\alpha = \left(\frac{\Psi^2 d_{eq}^2}{150} \frac{\varepsilon^3}{(1-\varepsilon)^2}\right) \quad (m^2), \tag{5}$$

$$C_2 = \frac{3,5}{\Psi d_{eq}} \frac{(1-\varepsilon)}{\varepsilon^3} \quad (m^{-1}). \tag{6}$$

Permeability (5) and inertial loss coefficients (6) were estimated by the Ergun equation using the mean diameter D_p of the fuel particles [15]. The sphericity Ψ and the spherical equivalent diameter d_{eq} were calculated from fuel parameters shown in Table 1 using formulas (7) and (8):

$$\Psi = \frac{\pi^{1/3} (6V_p)^{2/3}}{A_p} \quad (-), \tag{7}$$

$$d_{eq} = D_p \left(\frac{3L_p}{2D_p}\right)^{1/3} \quad (m^2). \tag{8}$$

The fuel in the burner was modeled by 4 layers with different porosity and total height 20 mm, which were discretized by several layers of hexahedra. Mesh of bed should be sufficiently fine in order to cover fluid flow changes (Fig. 2).

The computational model used the symmetry of the boiler, and therefore it modelled only 1/4 of the boiler. The boundaries of the model in the radial direction were defined as symmetry planes,

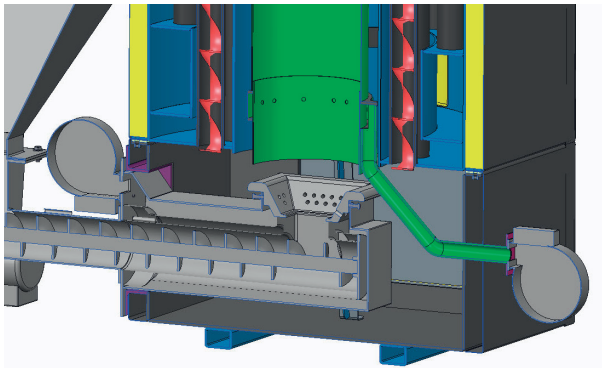

Fig. 1 3D geometry of the burner and the freeboard

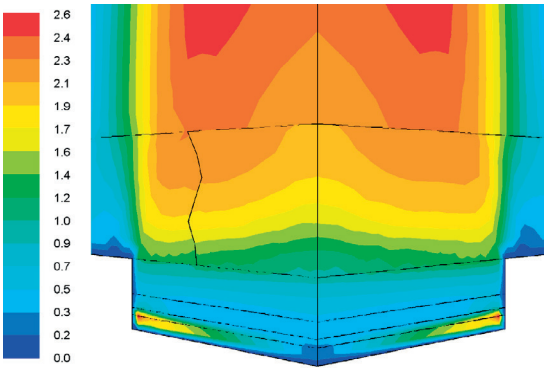

Fig. 2 Velocity (m/s) in the bed

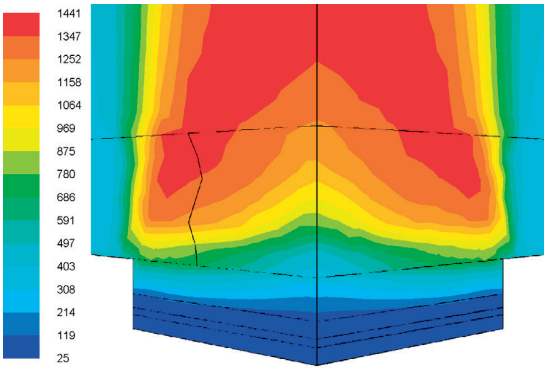

Fig. 3 Temperature (°C) in bed, without radiation

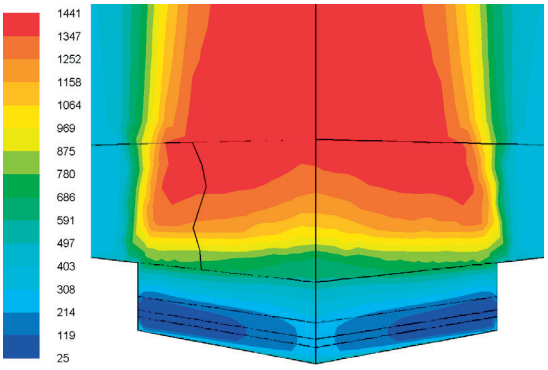

Fig. 4. Temperature (°C) in bed, with radiation

as there was no tangential flow. The wall of the burner, which was in contact with the bed, was considered adiabatic.

A significant effect on the temperature of combustion chamber had the radiative heat transfer in the fuel bed. Radiation increased the temperature inside the bed, as shown by the temperature fields on the symmetry planes in Figs. 3 and 4.

In the model set-up, there was important to set the absorption coefficient of the burner walls equal to unity (black body). Otherwise, all radiative flux would be reflected back. During the model development it was also found as very important to carefully design the porous fuel volume and the primary air inlet, because the area of the input boundary leads to radiation losses. Therefore the inlet area should be small and shielded from the direct radiative flux of the combustion chamber. It also had to ensure uniform velocity and mass flux distribution on the bed-freeboard interface. In simulations, several design alternatives for the supply of reactants were tested. The most appropriate method in this particular burner was from placing the inlets on the burner perimeter. The inlet had the shape of a narrow slit in under the porous bed. The space under the bed was open to horizontal flow, which helped to distribute the fluid flow. This solution ensured almost uniform flow in the layer above it.

3. Conclusion

The described model is substitution of combustion process and it greatly simplifies the modeling approach for pellet combustion and also it is simple and easy to apply for a user of CFD software. This model can be used for simulation in a relatively simple way and it is able to predict the general behavior of solid fuel-fired boilers. In developing the model, it is necessary to consider the impact of the assumptions which may vary depending on the design of the burner and boiler.

The limitations of the bed model include the assumption that the reactants are well mixed with each other and that the heterogeneous combustion process is also uniform in space. Another important limitation of the model is that it considers constant temperatures of devolatilization and of char combustion. Perhaps the main simplifying assumption is that the production of volatiles in the bed is independent of the conditions in the combustion chamber. An advantage is that the model bed is set up directly in the CFD model and does not require programming of external libraries.

The present model does not substitute more advanced models and tools that can be used to design biomass combustion systems, such as three dimensional bed, transient modeling, solid to gas conversion or bed particles feeding. These all are however quite complex tasks, which require the implementation of external libraries. The work introduces the model that may provide the useful tool in the design of small automatic boilers, where fuel consists of well-defined pellets, the fixed bed is small relative to the combustion chamber, and where high development costs preclude the application of more sophisticated tools. Although the described model was developed for the retort burner, the model can be applied also on wide range of various pellet burners and boiler.

Acknowledgement

This article has been prepared within the framework of the project R&D – APVV-0458-11 “Solving issues with low-melting ash during the biomass combustion“. The author JH gratefully acknowledges financial support of the Ministry of Education, Youth and Sports within the programme ”National Sustainability Programme I“, project NETME CENTRE PLUS (LO1202).

References

[1] COLLAZO, J. et al.: Numerical Simulation of a Small-scale Biomass Boiler. *Energy Conversion and Management,* 2012, vol. 64, pp. 87-96.

[2] NOSEK, R. et al.: *The Measurement of Emission during Biomass Combustion in a Small Heat Source (in Slovak).* 32. stretnutie katedier mechaniky tekutín a termomechaniky, VysokeTatry : Tatranska Lomnica : Zilinska univerzita, 2013, pp. 205-208.

[3] KOLONICNY, J. et al.: *Progress of Proper Heating (in Czech).* Ostrava : Technicka univerzita Ostrava : Vyzkumne energeticke centrum, 2010, 131 p., ISBN 978-80-248-2255-6.

[4] LYCKA, Z.: *Wood Pellet II : Combustion in Small Heat Source (in Czech),* 1st ed., Krnov: LING Vydavatelstvi, 2011, 71 p., ISBN 978-80-904914-1-0.

[5] KOPPEJAN, J., VAN LOO, S.: *The Handbook of Biomass Combustion and Co-firing.* London: Earthscan Publications, 2010, 442 p., ISBN 978-1-84971-104-3.

[6] JANDACKA, J. et al.: *Biomass Like Energy Source : Potential, Sorts, Balance and Fuel Properties* (in Slovak), 1st ed., Zilina : Juraj Stefun : GEORG, 2007, 241 p., ISBN 978-80-969161-3-9.

[7] GOMEZ, M. A., et al.: Simulation of the Effect of Water Temperature on Domestic Biomass Boiler Performance. *Energies*, 2012, vol. 5, No. 12, pp. 1044-1061.

[8] ION, I. V. et al.: A Biomass Pyrolysis Model for CFD Application. *J. of Thermal Analysis and Calorimetry*, 2013, vol. 111, No. 3, pp. 1811-1815.
[9] THUNMAN, H.: *Principles and Models of Solid Fuel Combustion*. Goteborg : Chalmers University of Technology, 2001.
[10] SHARMA, A. K. et al.: Modelling Product Composition in Slow Pyrolysis of Wood. *SESI Journal*, 2006, vol. 1, No. 16, pp. 1-11.
[11] PORTEIRO, J. et al.: Numerical Modeling of a Biomass Pellet Domestic Boiler. *Energy & Fuels,* 2009, No. 23, pp. 1067-1075.
[12] KLASON, T. et al.: Investigation of Radiative Heat Transfer in Fixed Bed Biomass Furnaces. *Fuel,* 2008, vol. 87, No. 10-11, pp. 2141-2153.
[13] ZAHIROVIC, S. et al.: *Advanced Gas Phase Combustion Models: Validation for Biogases by Means of LES and Experiments as well as Application to Biomass Furnaces*. 7th European Conference on Industrial Furnaces and Boilers, Porto: CENERTEC, 2006.
[14] ERGUN, S., ORNING, A. A.: Fluid Flow through Randomly Packed Columns and Fluidized Beds. *Industrial & Engineering Chemistry,* 1949, vol. 41, No. 6, pp. 1179-1184.
[15] SAS IP, INC. *ANSYS Fluent User's Guide,* U.S.A., 2013, 2692 p.

Miroslaw Luft - Daniel Pietruszczak - Elzbieta Szychta *

ANALYSIS OF DYNAMIC PROPERTIES OF ACCELEROMETER USING FRACTIONAL DERIVATIVES

The paper outlines the use of fractional derivatives for dynamic measurements while developing a method of improved description of dynamic properties of accelerometer, which the authors consider to be the original and unique achievement of their work. The main objective of the work is an implementation of a fractional calculus-based method which allows for a description of dynamic properties of signal processing of measuring transducers with fractional orders. A dynamics of transducer is identified by the ARX method (AutoRegressive with EXternal input identification method). Identification of accelerometer was accomplished with the use of the MATLAB&Simulink package.

Keywords: *Accelerometer, ARX method, fractional calculus, fractional derivatives, MATLAB&Simulink, measuring transducer.*

1. Introduction

The problem of describing dynamic properties of objects by means of fractional calculus although well known since the times of Gottfried Wilhelm Leibniz [1], and [2], yet due to restrictions resulting from lack of appropriate calculation methods and possibilities of their verification has always been ignored.

At present technical and calculation possibilities cause that the problems related to these limitations have, to a large extent, been solved. There are more and more publications dealing with the topic of fractional order differential equations.

Majority of them, however, deal with theoretical aspects of the problem. There are no publications which put strong emphasis on the practical application of fractional calculus and combine theory with real applications. The paper outlines the use of fractional calculus for dynamic measurements while developing a method of improved description of dynamic properties of measuring transducers which the authors considers to be the original and unique achievement of this work. Proposed by the authors of this paper method of description of the dynamic properties of measuring transducer in terms of signal processing, based on fractional calculus, allows for a description of dynamic properties of broader class of measuring transducers, i.e. integer-order and fractional-order accelerometers. The aim of this paper is to investigate how models of accelerometers based on the fractional calculus ([3], [4], [5], [6], [1], [7] and [2]) description convey their dynamic behaviour in comparison to models represented by differential equations of integer orders and in comparison to processing characteristics of their real counterparts.

2. Model of the second order accelerometer

Simulation and laboratory testing of the second order accelerometer is shown in Fig. 1.

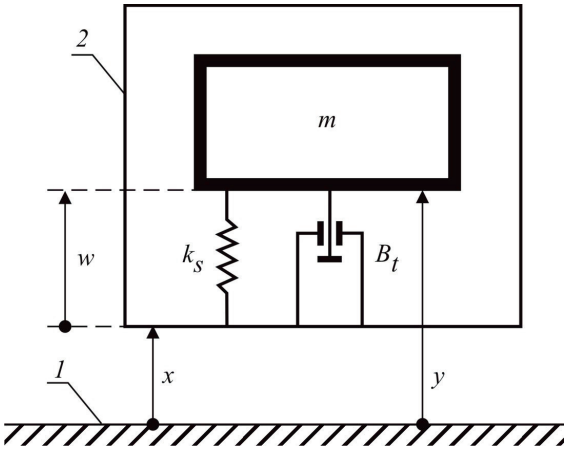

Fig. 1 Kinetic diagram of an accelerometer: m- vibrating mass, k_s - spring constant, B_t - damping coefficient, x - object motion relative to a fixed system of coordinates, y - motion of a vibrating mass relative to a fixed system of coordinates, w - motion of a vibrating mass relative to a vibrating object [4] and [7]

* **Miroslaw Luft, Daniel Pietruszczak, Elzbieta Szychta**
Faculty of Transport and Electrical Engineering, Kazimierz Pulaski University of Technology and Humanities in Radom, Poland
E-mail: m.luft@uthrad.pl; d.pietruszczak@uthrad.pl; e.szychta@uthrad.pl

A differential equation describing the absolute motion of the second order measuring vibrating mass of transducer can be expressed as [7]:

$$\frac{d^2}{dt^2}y(t)+2\zeta\omega_0\frac{d}{dt}y(t)+\omega_0^2y(t)=\omega_0^2x(t)+2\zeta\omega_0\frac{d}{dt}x(t) \quad (1)$$

where:

$$\omega_0=\sqrt{\frac{k_s}{m}} \quad (2a)$$

$$\zeta=\frac{B_t}{2\sqrt{k_s m}}. \quad (2b)$$

Considering the motion of the vibrating mass relative to the vibrating object (Fig. 1):

$$\frac{d^2}{dt^2}w(t)+2\zeta\omega_0\frac{d}{dt}w(t)+\omega_0^2w(t)=-\frac{d^2}{dt^2}x(t). \quad (3)$$

Depending on the selection of k_s, m and B_t, a transducer can serve to measure acceleration as an accelerometer [7] assuming a high k_s, a low m and B_t. In practical vibration measurements, acceleration-measuring transducers, the so-called accelerometers, are employed. For purposes of simulation testing, a measuring transducer was assumed of the frequency f = 350 Hz, that is, circular frequency of free vibrations $\omega_0 = 2200\frac{rad}{s}$ and degree of damping $\zeta = 0.2$. Dynamics of such a transducer, characterized by means of the second order differential equation (3), is described by operator transmittance:

$$G(s)=\frac{1}{s^2+880s+4.84\cdot10^6}. \quad (4)$$

Figure 2 illustrates amplitude and phase frequency characteristics of a measuring transducer with operator transmittance (4).

3. Quasi-fractional model of accelerometer

There are many definitions of fractional derivative. Three most commonly used definitions are those by Riemann-Liouville, Grünwald-Letnikov and Caputo ([8], [1], [7] and [2]). The Grünwald-Letnikov derivative is:

$${}_{t_0}D_t^{(v)}f(t)=\lim_{\substack{h\to0\\ t-t_0=kh}}\left[\frac{1}{h^v}\sum_{i=0}^{k}a_i^{(v)}f(t-hi)\right] \quad (5)$$

with:

$$a_i^{(v)}=\begin{cases}1 & i=0\\ (-1)^i\dfrac{v(v-1)(v-2)...(v-i+1)}{i!} & i=1,2,3,...\end{cases} \quad (6)$$

where (6) is defined as the reverse difference of the discrete function and h is the increment of $f(t)$ defined in the range $[t_0,t]$:

$$h=\frac{t-t_0}{k}. \quad (7)$$

Introducing a non-integral order to the measuring transducer's equation (1) converts it into:

$$\frac{d^2}{dt^2}w(t)+2\zeta\omega_0\frac{d}{dt^{(v_1)}}{}^{(v_1)}w(t)+\omega_0^2w(t)=-\frac{d}{dt}x(t) \quad (8)$$

where v is order of a fractional derivative.

The concept of this work is based on a comparison of different models of an accelerometer's dynamic behaviour (based on differential equations of integer and fractional orders) with the processing characteristics of a real accelerometer so as to obtain answer to the question about which method of modelling is more accurate and whether there are any criteria for which a certain model is better at reproducing the dynamic behaviour of the real accelerometer. The research results has included algorithms of determining models describing an accelerometer's dynamic behaviour based on differential equations of integer and fractional orders for the definitions by Grünwald-Letnikov (5). The results were presented in works [2], [3], [4], [7] and [8].

On comparing responses of the measuring transducer to the input sinusoid signal, it was described by means of three models using the Grünwald-Letnikov derivative (5): *Classic model* described with operator transmittance (9) – the same as formula (4). The operation of a transducer described with the equation was simulated for appropriately selected parameters: natural angular frequency and degree of damping:

$$G(s)=\frac{1}{s^2+880s+4.84\cdot10^6}. \quad (9)$$

Classic discrete mode, derived from the operator transmittance model (9), described by means of discrete transmittance (10):

$$G(z)=\frac{1.667\cdot10^{-15}z^2+6.666\cdot10^{-15}z+1.667\cdot10^{-15}}{z^2-2z+0.999}. \quad (10)$$

Response of a continuous object to a discrete input depends not only on values of this signal at discrete moments of time but also on sampling time and the extrapolator used.

The quasi-fractional discrete model described by discrete transmittance (11):

$$G(z)=\frac{z^2}{1\cdot10^{14}z^2-2\cdot10^{14}z+1\cdot10^{14}}. \quad (11)$$

Discrete transmittance (11) is produced by implementation of the method of determining quasi-fractional expression of the measuring transducer in MATLAB&Simulink programme [3], [5], [7] and [9]. It can be noted that the model described by means of the discrete transmittance (11) correctly reproduces values of the input signal amplitude – the same as the model of

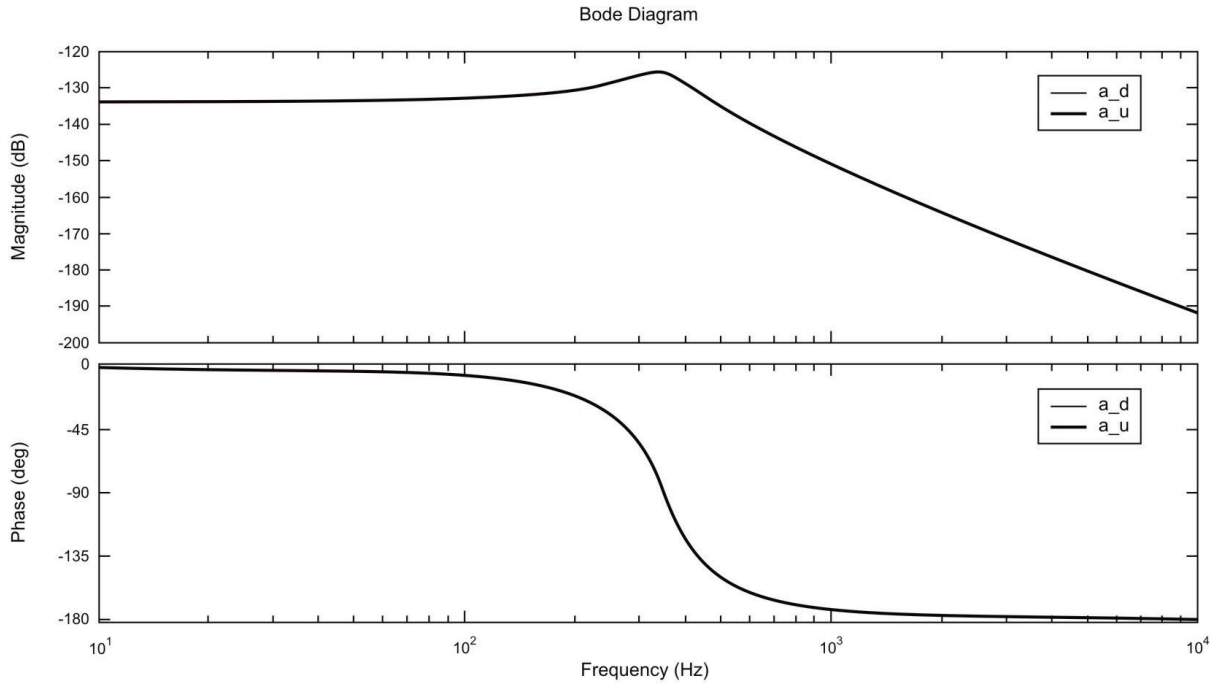

*Fig. 2 Comparison of Bode diagrams of measuring transducer models (10) and (11) (**diagrams of the models overlap**) [4]*

transmittance (10). It can be noted in Bode frequency diagrams [6] (Fig. 2) that the measuring transducer model determined by the derivative-integral method presents the dynamics of the classically determined model (the diagrams of the models coincide). This confirms that integral-order differential-integral calculus is a special case of differential-integral calculus of non-integral orders.

Measuring transducer models (10) and (11) have only been subject to simulation testing and do not fully represent real models but the simulations indicate that the quasi-fractional model (11) exhibits the same dynamics as the classic model. The 'apparent' time of stabilization of time diagrams – the time after which description of a model is independent from time – for the quasi-fractional model is the same as for the classic model.

4. Model of a laboratory system with accelerometer

An overview of the measurement system is shown in Fig. 3. In order to determine measuring transducer's operator transmittance, we built a system with two accelerometers *A1* and *A2*. Accelerometer *A1*- DeltaTron by Bruel&Kjaer type 4507, which sensitivity 10.18mV/ms^{-2} and the range of frequency measurements from 0.4 Hz to 6 kHz was tested. The operating ranges of conditioner was between 1Hz and 20 kHz. The transducer was mounted on an electrodynamic inductor. A model accelerometer *A2* - by VEB Metra, type KB12, which sensitivity 317 mV/ms^{-2} was aligned with the tested transducer *A1*.

The operator transmittance (12) describing dynamics of the measurement system was determined by identification with an

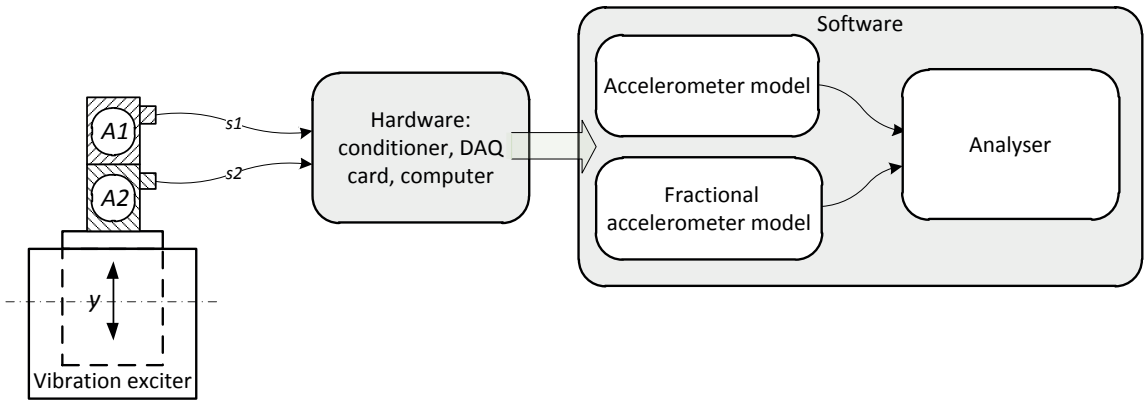

Fig. 3 Laboratory measurement system for testing of mechanical vibration transducers: A1, A2 – model and tested measuring transducers [9]

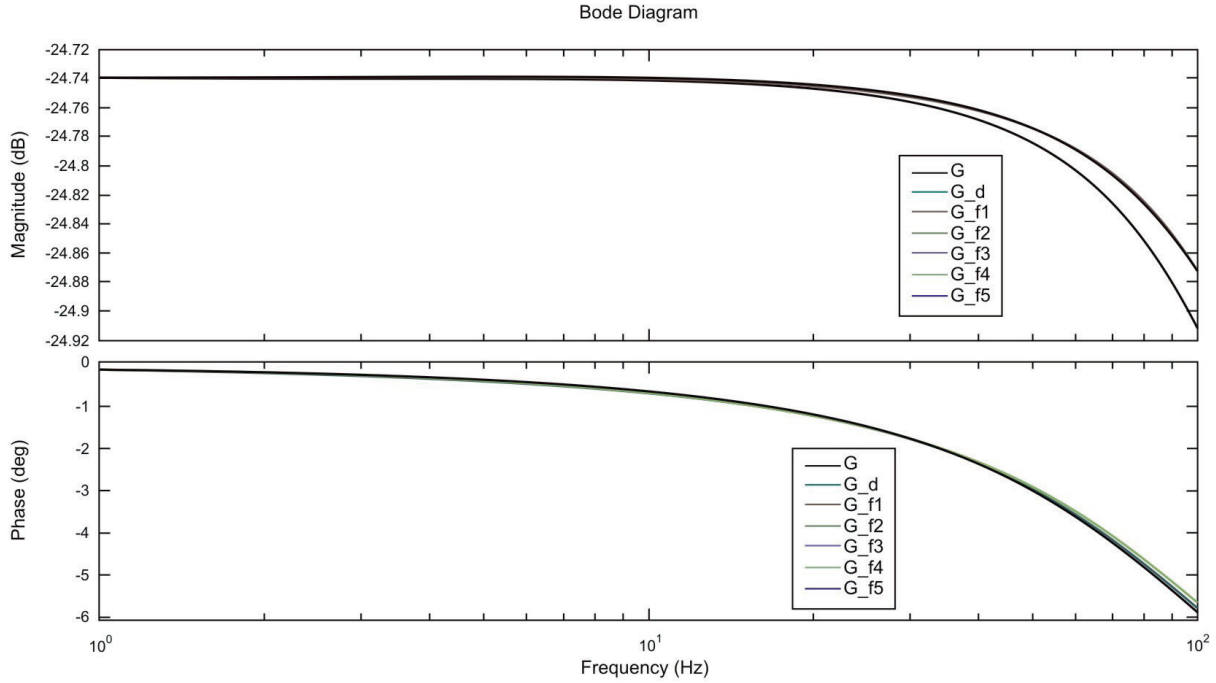

Fig. 4 Bode frequency diagrams of measuring transducer models of transmittance (models from the Table 1) [4]

external ARX (AutoRegressive with EXternal input) [7]. The voltage signal from the end of the tested measurement track is the identified signal, and the signal from the model accelerometer in response to the sinusoidal function of the generator of 100 Hz is the comparative signal.

The ARX identification method produced the operator transmittance $G(s)$ describing the dynamics of the system:

1. *Classic model*:

$$G(s) = \frac{0.03215s^2 + 1319.6s + 1.338 \cdot 10^6}{s^2 + 4.678 \cdot 10^4 s + 2.309 \cdot 10^7}. \qquad (12)$$

2. *Discrete transfer function* of the model was determined on the basis of the operator transmittance (12):

$$G(z) = \frac{0.03215z^2 + 0.05368z + 0,02163}{z^2 + 1.625z + 0.6264}. \qquad (13)$$

The discrete model (13) was produced by discretizing the classic model (20) by means of the 'Zero-Order-Hold' method [7] with the sampling time $T_p = 10^{-4}$s.

3. *Discrete transfer function of fractional models* was determined with a method implemented in MATLAB&Simulink. For varying increment of h, quasi-fractional transducer models become discrete transmittances which is presented in the Table 1 [4]:

Discrete transmittances of measuring transducer models for varying increment — Table 1

Increment variation h	Discrete transmittance $G(z)$
10^{-7}	$G_{f_1}(z) = \frac{3.228z^2 - 6.443z + 3.215}{100.5z^2 - 200.5z + 100}$
10^{-6}	$G_{f_2}(z) = \frac{3.347z^2 - 6.562z + 3.215}{104.7z^2 - 204.7z + 100}$
10^{-5}	$G_{f_3}(z) = \frac{4.548z^2 - 7.75z + 3.215}{104.7z^2 - 246.8z + 100}$
10^{-4}	$G_{f_4}(z) = \frac{1.775z^2 - 1.963z + 0.322}{59.09z^2 - 66.78z + 10}$
10^{-3}	$G_{f_5}(z) = \frac{2.69z^2 - 1.384z + 0.032}{70.87z^2 - 48.78z + 1}$

The model of the real measurement system in the form of discrete transmittance and models expressed by means of a differential-integral equation were then compared. Both types of the models were based on the classic model derived by ARX identification method.

Figure 4 shows logarithm frequency amplitude and phase diagrams of the measurement system models. It can be observed that for the adopted increment of h, the diagrams clearly diverge. This means that other increments h far lower than the sampling frequency, must be adopted.

5. Conclusion

Dynamic development of recent research into the use of fractional calculus for the dynamic system analysis encouraged the authors of this paper to attempt the use fractional derivatives for the analysis and modelling of measuring transducers and measurement systems [3], [4], [5], [7] and [9]. The main objective of the work is an implementation of a fractional calculus-based method for a description of dynamic properties of signal processing of measuring transducers with integer-order and quasi-fractional-order. Fractional calculus is a generalisation of integral-order differential calculus – this is confirmed by laboratory testing of dynamic systems.

The effect of h on fractional measuring amplitude of fractional measuring transducer and phase diagrams was also shown in this paper. In this case increments h, far lower than the sampling frequency, must be adopted [4].

Application of the quasi-fractional method of describing dynamic properties of measuring transducers discussed in this paper, based on fractional calculus, will help to undertake analyses of simulated dynamics of various objects and processes which, due to their complexity, must be described by means of differential equations of any orders.

References

[1] OSTALCZYK, P.: *Epitome of the Fractional Calculus. Theory and its Applications in Automatics (in Polish)*, Wydawnictwo Politechniki Lodzkiej, 430 p., ISBN 978-83-7283-245-0, Lodz, 2008.

[2] PODLUBNY, I.: *Fractional Differential Equations*. *An Introduction to Fractional Derivatives, Fractional Differential Equations, Some Methods of Their Solution and Some of Their Applications*. Academic Press, 368 p., ISBN 0125588402, San Diego: Boston: New York: London: Tokyo: Toronto, 1999.

[3] LUFT, M., CIOC, R., PIETRUSZCZAK, D.: *Fractional Calculus in Modelling of Measuring Transducers*. *Electronics and Electrical Engineering*, No. 4(110), ISSN 1392-1215, Kaunas, 2011.

[4] LUFT, M., SZYCHTA, E., PIETRUSZCZAK, D.: *Some Applications of Fractional Calculus to the Analysis of Dynamic Properties of Selected Measuring Transducer*. Proc. of 11th European conference of young scientists and postgraduate students Transcom 2015, section 4, Electric Power System, Electrical and Electronic Engineering, ISBN 978-80-554-1046-3, pp. 29-34, June 2015, Zilina, 2015.

[5] LUFT, M., SZYCHTA, E., CIOC, R., PIETRUSZCZAK, D.: *Application of Fractional Calculus in Identification of the Measuring System*. Transport Systems and Processes, CRC Press Balkema, Taylor & Francis Group, pp. 63-68, ISBN 978-0-415-69120-8, London, 2011.

[6] LUFT, M., SZYCHTA, L., NOWOCIEN, A., CIOC, R., PIETRUSZCZAK, D.: *Bode Plots of the Pressure Sensor Modelled by Fractional Calculus* (in Polish), *Logistyka,* 4/2015, ISSN 1231-5478, pp. 4539-4545, Poznan, 2015.

[7] PIETRUSZCZAK, D.: *Application of Fractional Calculus to the Analysis of Dynamic Properties of the Measurement Systems (in Polish)*, Doctoral dissertation, The Main Library of Kazimierz Pulaski University of Technology and Humanities, Radom, 2012.

[8] KACZOREK, T.: *Selected Problems of Fractional Systems Theory*. Springer-Verlag GmbH, 344 p., ISBN 978-3-642-20501-9, Berlin, 2011.

[9] PIETRUSZCZAK, D., SZYCHTA, E.: *Analysis of Selected Dynamic Properties of Fractional Order Accelerometers for Application in Telematics Equipment*. Communications in Computer and Information Science, ISSN 1865-0929, pp. 321-329 Springer-Verlag Berlin Heidelberg, 2013.

Andrzej Chudzikiewicz - Magdalena Sowinska *

MODELLING AND SIMULATIONS OF DYNAMICS OF THE LOW-FLOOR TRAMCAR WITH INDEPENDENTLY ROTATING WHEELS

The article is devoted to the analysis of numerical simulation results of the tramcar dynamics. It presents the mathematical model of the one section of the low-floor tram with the bogie with independently rotating wheels. The simulations were performed according to different scenarios, connected with the track geometry, which seem to be dangerous for the tram behaviour e.g.: curving, gauge narrowing, track buckling, etc. Special attention was paid to wheel lateral displacement and forces occurring in wheel-rail contact. The simulation results reveal characteristic features of such an unconventional system of the tram, which can often demonstrate dynamics considered worse than in the conventional case of the tramcar.

Keywords: *Low-floor tramcar, independently rotating wheels.*

1. Introduction

Currently, the demand of the urban transport providers on the modern tramcars leads designers to the new point of view of the tramcar construction. However, the realisation of the goal which is a constant improvement of the passengers comfort cannot be fulfilled further. The reason is a construction of the bogies, which makes the introduction of 100% low floor impossible. The researchers adjust to new design requirements and analyse the unconventional wheelsets with independently rotating wheels.

Present research paper aims at development of the model of unconventional bogie in the tramcar section. As the characteristic features of the dynamics of such wheelsets are still not well known, several simulations were performed in order to recognize the behaviour of the system. The results of simulations were analysed and general conclusions derived.

Studies on the concepts of wheelsets with independently rotating wheels have started in the half of the last century. These studies have concentrated generally on the steering strategies of running gear that could overcome the drawbacks of IRW bogie design. Positions [1 - 3] deal with the active control of the wheelsets and survey various possibilities of its control. Goodall in [4] presents experimental approach to torque control of IRW wheelsets. Paper [5] deals with the comparison of mathematical modelling of both conventional and unconventional bogies. The earlier works as [6] which concern mathematical modelling of unconventional bogies is also worth mentioning. Self-steering ability of wheelsets with independently rotating wheels, known as Einzelrad - Einzelfahrwerk, which uses gravity stiffness was proposed in [7] and [8]. Papers [9] and [10] concern the subject of dynamics of tramway with wheelsets equipped with IRW. Paper [9] deals with the linear model of a bogie with independently rotating wheels and paper [10] uses commercial software package to solve equations of motion. The problem of low floor tram dynamics was also the subject of authors' papers [11] and [12]. These articles discussed problem of stability of different types of low floor tram bogies.

2. Model

The three dimensional model of tramcar dynamics was considered in all cases of simulations. One section of the tramcar has 20 degrees of freedom and consists of four rigid bodies which are

- car body, which has 6 degrees of freedom,
- bogie frame body, which has 6 degrees of freedom,
- two wheelsets with independently rotating wheels which have 4 degrees of freedom each.

The section of the tramcar with marked degrees of freedom of car body is presented in Fig. 1.

* **Andrzej Chudzikiewicz, Magdalena Sowinska**
Warsaw University of Technology, Faculty of Transport, Warsaw, Poland
E-mail: ach1@wt.pw.edu.pl

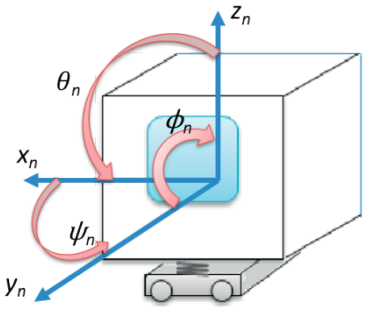

Fig. 1 Tramcar section scheme with degrees of freedom of the car body

Degrees of freedom of the bogie frame are analogical to the car body degrees of freedom. The unconventional wheelset with independently rotating wheels has a cranked axle which allows lowering the floor in the whole tramcar inner space. Such a wheelset has the wheels mounted on the common axle with the use of bearing system which enables independent rotation of wheels. In this case, the wheelset has 4 degrees of freedom as it is visible in Fig. 2a. The analysis of dynamics of the wheelset is limited to the motion in a horizontal plane. The whole model of the bogie has 14 degrees of freedom and it is symmetric with respect to x axis as captured in Fig. 2b.

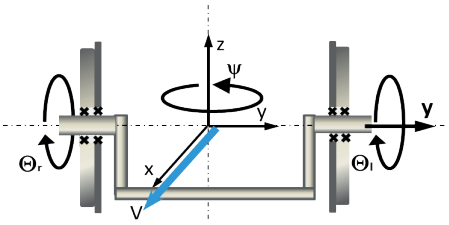

a)

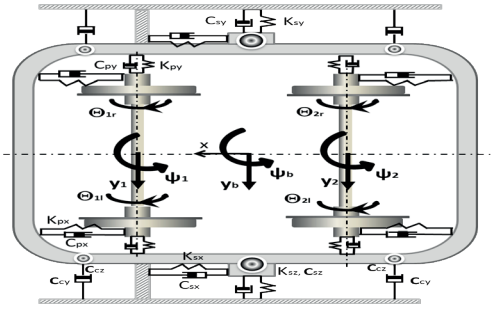

b)

Fig. 2 a) the wheelset model
b) the bogie model with elastic-damping elements marked

Bodies are connected with the elastic and damping elements which have linear characteristics. Inertial parameters as well as stiffness and damping correspond to the construction of the low floor tramcar which has been introduced lately to the exploitation in the Warsaw city transport. During simulation studies we assume that the tramcar is moderately loaded with passengers.

The vehicle's motion is investigated in the non-inertial frame connected with the centreline of a track. The Fastsim procedure was involved in the numerical calculations. However, the procedure had to be modified in terms of creepages formulas, because of the free rolling of the wheels. For that reason, the longitudinal creepage was assumed zero. Material parameters taken to the procedure match parameters of steel 900A according to PN – EN 13674-1. Rail profiles were typical grooved tramway track rails Ri60.

3. Simulation study

The track's sections where the simulation research was conducted were considered potentially dangerous for railways traffic according to [13].

Figure 3 presents three different track geometries assumed for the simulations.

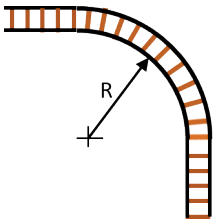

a)

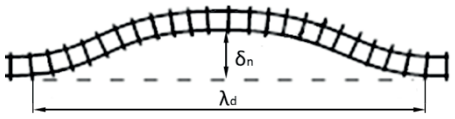

b)

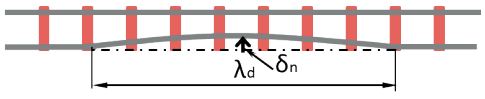

c)

Fig. 3 Tracks taken for the simulations:
a) steady curving b) buckled track
c) track with lateral misalignment

Figure 3a presents track in the steady curving case and it is modelled as a quarter of the circle with straight entrance and exit, Fig. 3b pictures buckled track modelled as half of the sinusoid of 50 cm amplitude and long 10 m, and Fig. 3c a track with lateral sinusoidal misalignment of 1 cm and 2 cm amplitude of right rail long 5 m. Simulations were performed according to different velocities and track parameters.

Figure 4 presents lateral displacement of the wheelset's centre of mass during the ride on the curve (Fig. 3a) with velocity equal

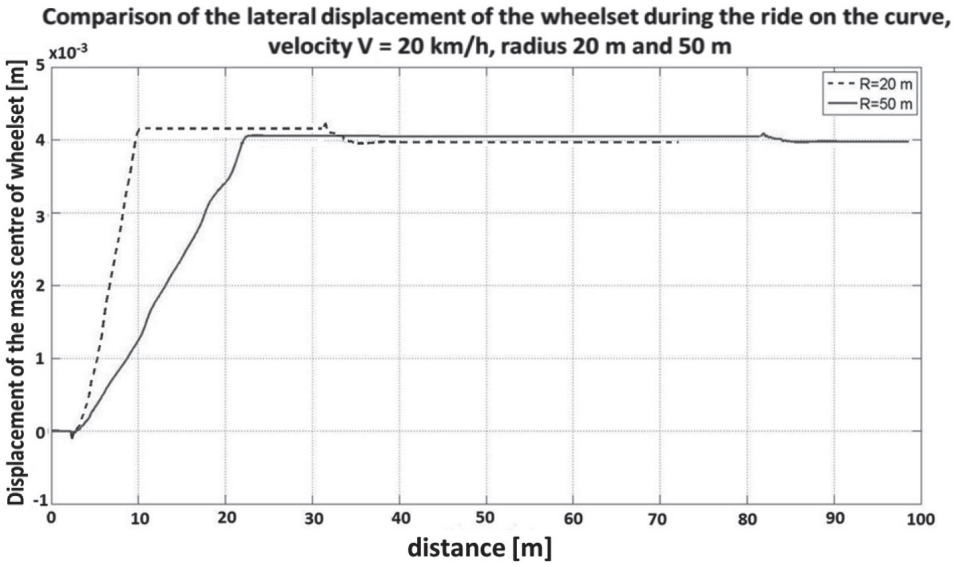

Fig. 4 Lateral displacement of the wheelset during the steady curving; 20 and 50 m radius, 20 km/h

to 20 km/h. It compares two curves of different radii: 20 and 50 m.

The wheelset displaces faster to the maximal position on the tighter curve than on the curve of 50 m radius. The maximal position means the position when the wheel flange is in contact with the rail. In both cases such situation occurs. After exiting the curve the wheelsets remain displaced. The centre of the wheelset mass does not return to the central position on the track. Figure 5 shows the yaw angle of the wheelset in the same case of the track scenario.

It is shown that wheelsets with independently rotating wheels have the ability of radial positioning, because the yaw angle stabilizes on the zero value during the ride on the curve. The comparison of wheelset lateral displacement on the curve of 50 m radius in two cases of velocity is shown in Fig. 6. It reveals features which are: slow climbing up to the flange, remaining of the flange in the constant contact with the rail and no self-centring ability.

Figure 7 presents the lateral forces in the area of the wheel-rail contact and rail during the ride with the velocity of 40 km/h on

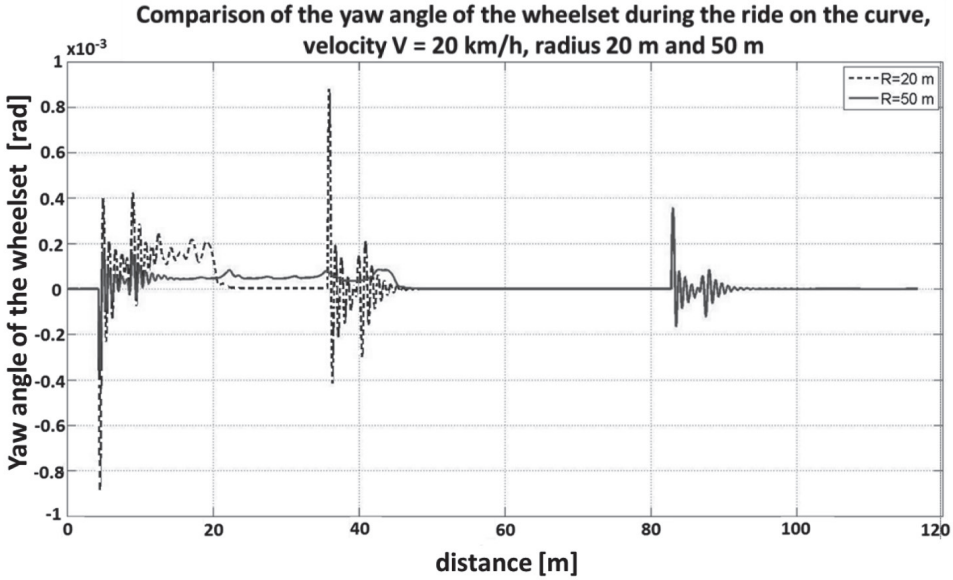

Fig. 5 Yaw angle of the wheelset during the steady curving; 20 and 50 m radius, 20 km/h

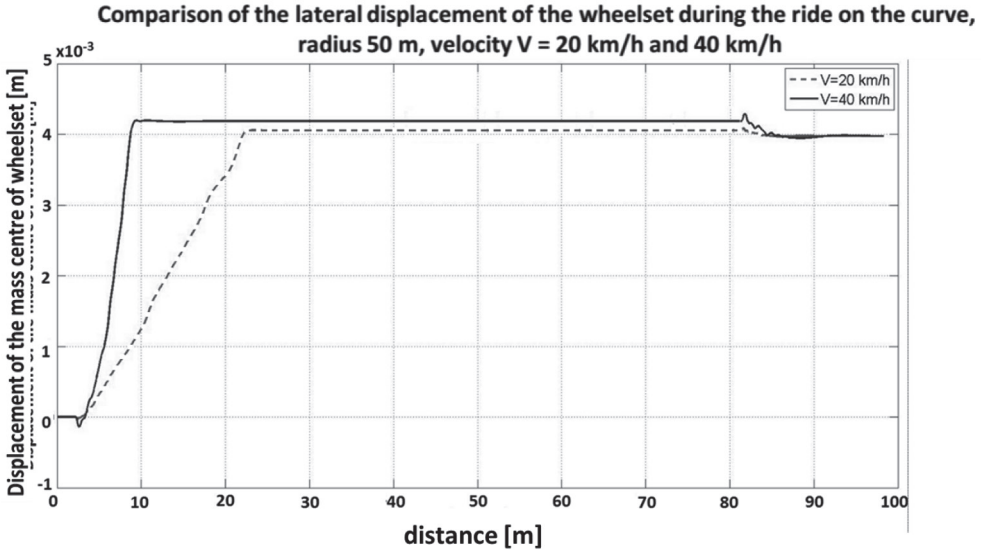

Fig. 6 Lateral displacement of the wheelset during the steady curving; 50 m radius, 20 and 40 km/h

the curve of 50 m radius. The graph compares the forces on the left and right side of the wheelset.

When the tramcar turns right on the curve, the lateral forces in the outer wheel area of contact are about 1.4 kN and in the inner wheel area of contact are about 15 kN. The forces have an oscillating character around these values because of the flange-rail contact on the curve.

Next interesting features of such a wheelset appear in the simulation results of the ride on the buckled track. As it is visible in Fig. 8, the wheelsets perform distinctly different motion in the case of velocities equal to 40 km/h and 60 km/h. When the velocity is 40 km/h, the wheelset has smaller displacements on the buckled section of the track than in 60 km/h case. After exiting to the straight track the wheelset which rides with the velocity equal to 40 km/h approaches shortly the centreline of the track and then returns to the previous position. When the velocity of ride is 60 km/h, the wheelset after exiting the buckled section passes the centreline and takes the maximum position on the other side of the track and does not return to the centre.

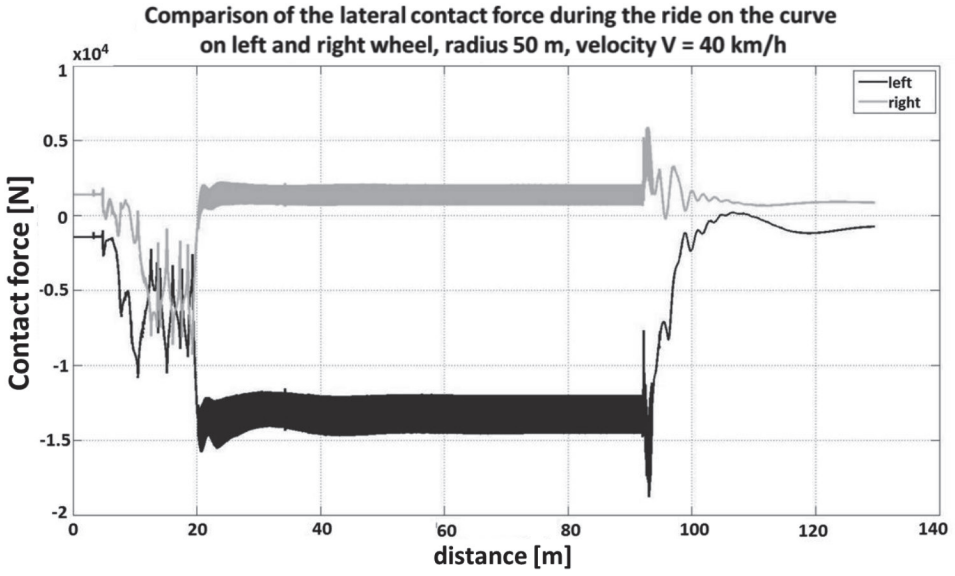

Fig. 7 Lateral contact forces on the left and right wheel during the steady curving; 50 m radius, 40 km/h

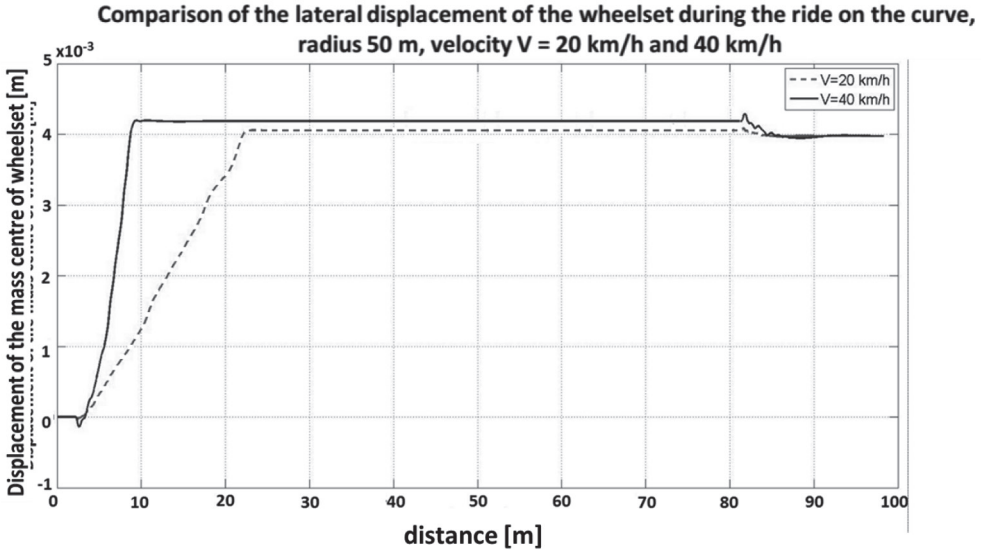

Fig. 8 Lateral displacement of the wheelset during the ride on the buckling; 40 and 60 km/h

Figures 9 and 10 present the lateral forces in the area of left and right wheel contact with the rail during the ride on the buckled track. When the velocity is equal to 40 km/h, the forces are approximately equal to 12 kN on the entrance and exit from the buckled section.

Figure 10 pictures lateral forces in the area of wheel/rail contact in the case when the ride velocity is equal to 60 km/h.

The simulation results have shown that when the velocity increases to 60 km/h, the lateral forces values are about 5 times bigger than in the case when ride velocity is equal to 40 km/h.

Figure 11 presents lateral displacement of the wheelset on the last type of the track, which is a track with the lateral misalignment of one of the rails. This graph compares the response of the IRW wheelsets on the misalignment of different amplitude - 1 cm and 2 cm. The ride velocity is constant and equal to 20 km/h. This scenario shows strong influence of misalignment on lateral motion of the wheelset. It seems that the bogie system nearly does not react on the 1 cm amplitude misalignment, which cannot be observed in the case of 2 cm amplitude. In this case, the lateral

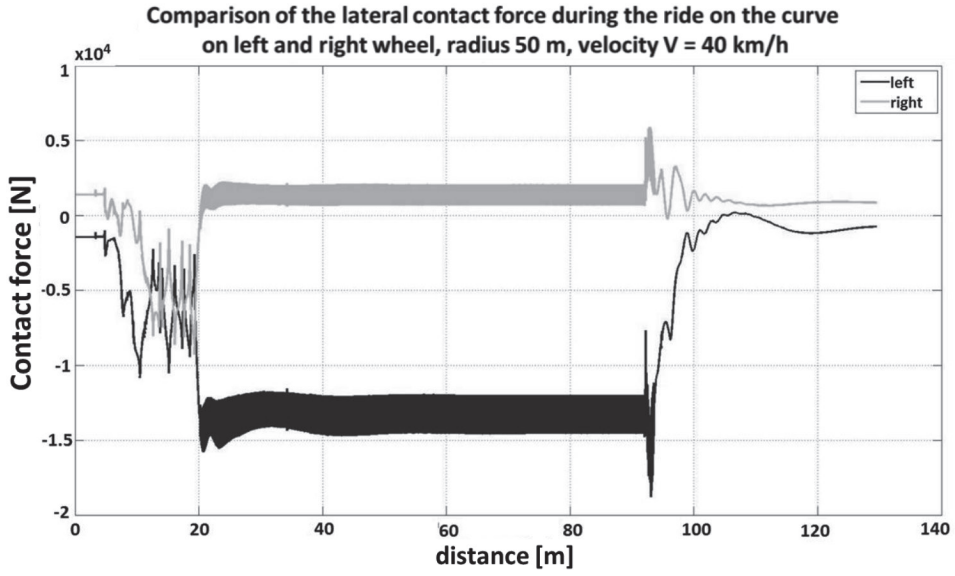

Fig. 9 Lateral contact forces on the left and right wheel during the ride on the buckling; 40 km/h

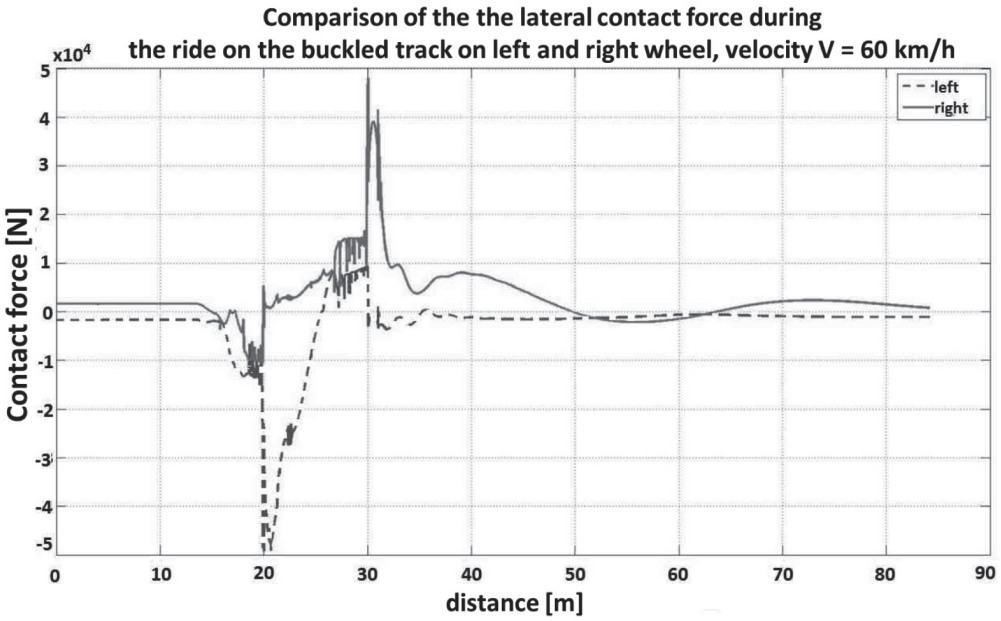

Fig. 10 Lateral contact forces on the left and right wheel during the ride on the buckling; 60 km/h

displacement of the wheelset increases till the flange-rail contact and afterwards decreases towards the centreline of the track.

Figure 12 depicts lateral forces in the area of wheel/rail contact in the case of 2 cm amplitude misalignment on the track.

Lateral forces in the case of 2 cm amplitude misalignment are equal to 47 kN which is nearly the same value as in the case of 1 cm misalignment, however this force acts on the longer distance.

4. Conclusion

The paper presents examples of simulation results of the low floor tramcar motion performed according to different scenarios. Analysis of the results focuses on the lateral displacements of the wheelset's centre of mass, yaw angle of the wheelsets and lateral forces in the area of wheel and rail contact. The numerical model has shown that the new wheelset type requires a modified

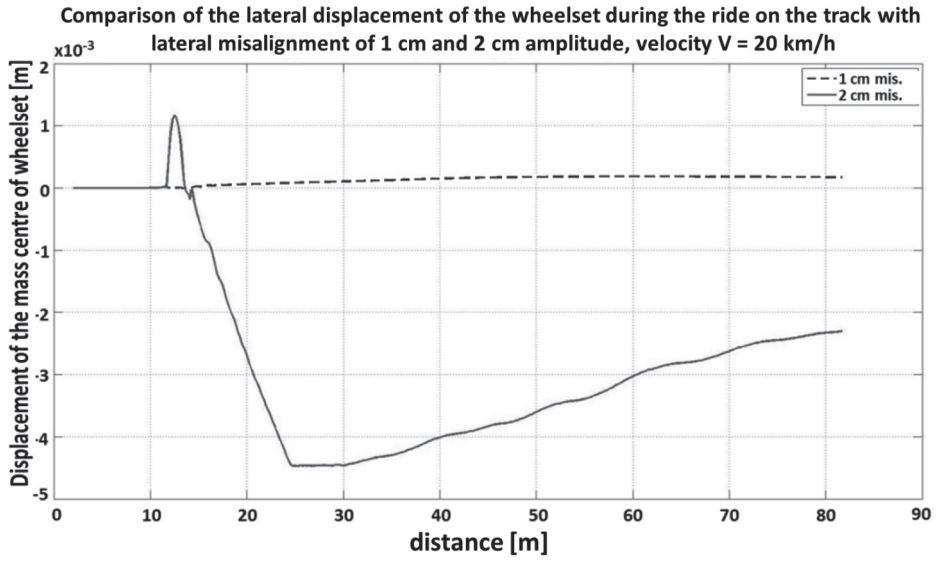

Fig. 11 Lateral displacement of the wheelset during the ride on the track with lateral misalignment; 1 and 2 cm amp., 20 km/h

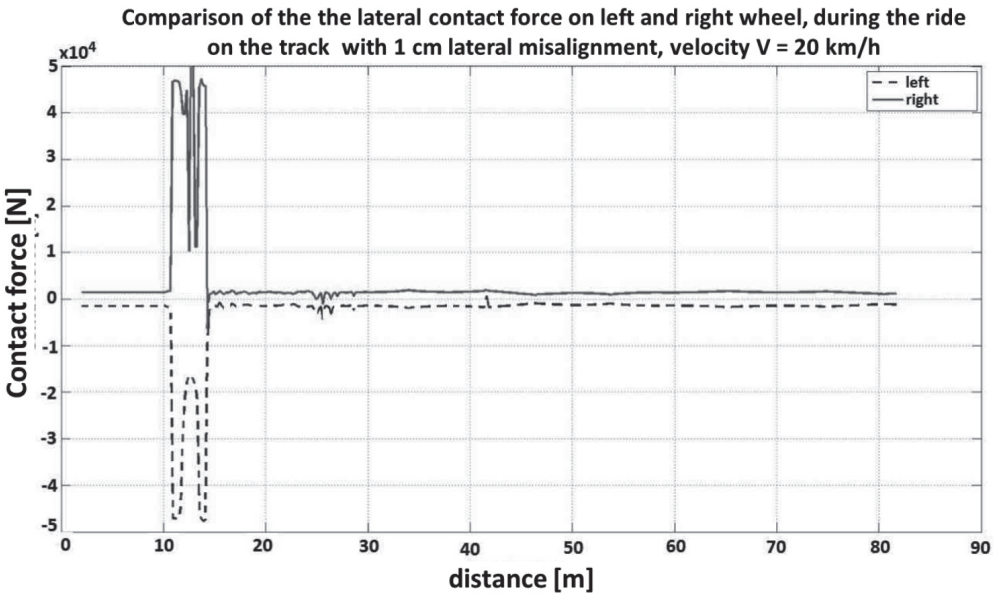

Fig. 12 Lateral contact forces on the left and right wheel during the ride on the on the track with 2 cm lateral misalignment; 20 km/h

mathematical model of contact what mainly expresses in formulas of the creepages. Various simulations were performed for real wheel and rail profiles and different track geometries. They revealed the characteristic features of bogie with independently rotating wheels, which are: no self-centring ability, easy radial positioning, long contact of the flange with the rail. The scenarios of the ride on the buckled track and track with lateral misalignment give an insight on how strong influence has the ride velocity and size of the irregularity on the bogie motion. The responses of the system are hardly predictable.

Acknowledgement

The work was done as a part of the research project WND-DEM-1-493/000, "Support for scientific research and development on a demonstration scale DEMONSTRATOR+".

References

[1] GOODALL, R. M., HONG, L.: Solid Axle and Independently Rotating Wheelsets - A Control Engineering Assessment of Stability, *Vehicle System Dynamics*, vol. 33, 2000, pp. 57-67.

[2] MIYAMOTO, M., SATO, T.: Study on the Stabilization of Railway Vehicles with Independently Rotating Wheels by Control of Steering on Wheelset (1 Axle trailer bogie), JSME, *10th Conf. Transportation 01-36*, 2001, pp. 149-152.

[3] OBATA, R., TANIFUJI, K., SOMA, H., MASUDA, T.: Curving Performance of a Rail Vehicle with Independently Rotating Wheels by Torque Difference Control, *Transaction of the Japan Society of Mechanical Engineers Series C*, vol. 72, No. 716, 2006, pp. 1064-1070.

[4] MEI, T. X., GOODALL, R. M.: Practical Strategies for Controlling Railway Wheelsets Independently Rotating Wheels, *ASME*, vol. 125, 2003, pp. 354-360.

[5] JAWAHAR, P. M., GUPTA, K. N.: Mathematical Modelling for Lateral Dynamic Simulation of a Railway Vehicle with Conventional and Unconventional Wheelset, *Mathematical and Computer Modelling*, vol. 14, 1990, pp. 989-994.

[6] DUKKIPATTI, R. V., OSMAN, M. O. M., NARAYANA SWAMY, S.: Independently Rotating Wheel Systems for Railway Vehicles - A State of the Art Review, *Vehicle System Dynamics*, vol. 21, 1989, pp. 297-330.

[7] FREDERICH, F.: Dynamics of a Bogie with Independent Wheels, *Vehicle System Dynamics: Intern. J. of Vehicle Mechanics and Mobility*, vol. 19, 1989, pp. 271-232.

[8] FREDERICH F.: A bogie concept for the 1990s, *Railway Gazette International*, vol. 9, 1988. pp. 583-585.

[6] CHO, Y., KWAK, J.: Development of a New Analytical Model for a Railway Vehicle Equipped with Independently Rotating Wheels, *Intern. J. of Automotive Technology*, vol. 13, No. 7, 2012, pp. 1047-1056.

[10] KUBA, T., LUGNER. P.: Dynamic Behaviour of Tramways with Different Kinds of Bogies, *Vehicle System Dynamics: Intern. J. of Vehicle Mechanics and Mobility*, vol. 50, 2012, pp. 277-289.

[11] CHUDZIKIEWICZ, A., SOWINSKA, M.: A Comparative Simulation Studies of a Conventional Bogie and Bogie with Independently Rotating Wheels (in Polish), *Pojazdy Szynowe*, vol. 2, 2014.

[12] CHUDZIKIEWICZ, A., SOWINSKA, M.: Low Floor Trams Running Gear - A Comparative Simulation Studies, *14th Mini Conference on Vehicle System Dynamics, Identification and Anomalies 2014*, Book of Abstracts, p. 11.

[13] Safety of Railroad Passenger Vehicle Dynamics - Final Summary Report, U.S. Department of Transportation, Office of Research and Development, 2002.

Josef Vodak - Jakub Soviar - Viliam Lendel - Michal Varmus *

PROPOSAL OF MODEL FOR EFFECTIVE MANAGEMENT OF COOPERATION ACTIVITIES IN SLOVAK COMPANIES

Aim of this article is to offer a proposal for effective planning and organization of cooperation activities in a company, based on a comprehensive analysis of scientific literature and performed empirical research in Slovak republic. The article thus provides a tool for company managers for managing their cooperation activities. Use of this tool is meant to help minimize occurrence of conflict situations and to support smooth progress of cooperation activities from the organizational and planning perspective.

Keywords: *Cooperation, cooperation activities, cooperation management, planning, organization.*

1. Introduction

The topic of managing cooperation activities is currently highly up-to-date. In present, cooperation as such represents for a company an important tool for increasing its competitiveness. The topic of managing cooperation activities is highly up-to- date in Slovak enterprises. Managers in Slovak companies strive to build in their enterprises a functioning cooperation process, which would help with establishing of successful partnerships and cooperations. In order for this initiative to be successful, it is necessary to apply elements of process management and to create an environment that would support establishing of partnerships, enable communication and efficient work with information related to cooperations. In this respect managers may find useful the model that we propose in this article for effective management of cooperation activities in a company.

2. Objective and methodology

The purpose of the article is to offer, in a comprehensible form, a coherent overview of managing cooperation activities in a company. This includes a methodology of planning and organizing company cooperation activities, which is based on a detailed mapping of theoretical and practical knowledge in the area of cooperation management and a performed research of the level at which it is used in Slovak enterprises.

In order to address the points in question, as set by this article, it was necessary to use several methods, depending on and fitting to the character of the individual parts of the solution. In order to accumulate necessary data, we used the method of document analysis (for analysis of current as well as historical data about the topic), a questionnaire method and a method of semi-structured interview (gathering data in an empirical research) and a method of observation (used during visits of selected companies).

For processing the data, we mainly used a method of quantitative evaluation (statistical methods and tools were applied) and a method of comparison (for comparing data gathered by empirical research and data from the analysis of secondary information sources).

The performed research focused on medium and large enterprises active in the Slovak Republic. The actual respondents were company managers on the mid to top management level within the managerial hierarchy of companies. In total, 221 respondents took part in the research focused on diagnostics of the level of use of cooperation management.

Research included companies active in multiple sectors of the Slovak economy. Companies included were categorized by the Statistical Office of the Slovak Republic as medium or large enterprises. Size of the sample was 345 respondents, with the required 95% interval of reliability and the maximum allowable error of 5%. Since 221 respondents actually took part in the research, the maximum allowable error reached 6.37%. Data was gathered exclusively via personal interview.

* **Josef Vodak, Jakub Soviar, Viliam Lendel, Michal Varmus**
Department of Management Theories, Faculty of Management Science and Informatics, University of Zilina, Slovakia
E-mail: josef.vodak@fri.uniza.sk

The following methods were used for approaching and solving the research goals: induction, deduction, synthesis, abstraction and model building.

3. The current state of dealing with the issue

Scientific literature offers several theories that try to explain to managers how they could manage cooperation activities more efficiently and what factors influence the outcomes. Even though these theories look at the management of cooperation activities from various points of view, they all mention the need to create a complex illustration of company's cooperation activities. However, this effort often leads to excessive complexity and in the end may appear even confusing, thus failing to properly support the decision making processes in a company. It is often the case that the realized cooperation initiatives of a company fail to produce the expected outcomes.

Several authors ([1], [2], [3], [4] and [5]) point out that even though there is ongoing research in various areas of management of cooperation activities, the results are still not consistent. Creation of a unified view on the management of cooperation activities is largely blocked by the following factors:

- Cooperation management stems from several scientific branches (social sciences, economics, management, psychology...) and continues to interact with them.
- Research in cooperation management is oriented towards various industries and markets that have specific characteristics.
- Theoretical and practical researchers are mainly interested in different types and forms of cooperations.

Even companies sometimes misinterpret the term cooperation management and the management of cooperation activities. While these companies emphasize the need to create new cooperations, many of them lack functional cooperation process that would

Summary of the contributions of individual approaches to managing company cooperation activities — Table 1

Author(s)	Emphasis	Contribution
Sahut a Peris-Ortiz [6]	Role of innovations in planning cooperation activities	Basis = favourable environment for entrepreneurship and innovations
Ritala a Sainio [7]	Determination and close collaboration between cooperating parties	Application of the business model
Mutak [8], Kultti [9]	Creation of cooperation networks	Application to the area of innovation of services
Felzensztein et al. [10]	Portfolio of the areas of collaboration and its gradual expansion	Application to marketing activities and innovations
Weck and Ivanova [11]	Trust between cooperating parties	Gradual adaptation of business cultures of partner organizations
Wicks et al. [12]	Company performance	Cooperation process based on trust
Fawcett et al. [13]	Correct understanding of trust	Dynamics of trust building in cooperation
Monczka et al. [14]	Information background of cooperation processes	Quality of information and their sharing
Jassawalla a Sashittal [15]	Organizational factors	Organizational structure that supports cooperation
Schmoltzi a Wallenburg [16]	Organizational and strategic complexity in building cooperation management	Efficient planning of cooperation activities

Key elements of the management of cooperation activities — Table 2

Key element	Attributes
Innovations	A suitable environment should be established in a company that would support entrepreneurship and innovations, characterized by determination and close collaboration between the cooperating parties.
Trust	This aspect is an important part of strategic decision making. Managers who use optimal trust in the relations with the involved parties improve performance of the company. For this reason it is necessary to correctly understand the character of trust and the dynamics of building trust within cooperation, and to pursue gradual adaption of the business cultures of the cooperation partners.
Information background	It is necessary to ensure the quality of information in the company, as well as its sharing for the needs of managerial decision making. Effective work with information within a collaboration can help prevent conflicts and aid with solving complex cooperation tasks.
Organizational factors	This aspect involves change of organizational structures to support cooperation, interest and support from top management of the partners, openness to changes while maintaining mutual goals of the partner companies.

generate new partnerships. We noticed that in some companies there is a significant effort to build a functional cooperation. However, in many cases the cooperation does not bring the expected benefits (not only the financial ones), particularly because it does not have clear rules, metrics and methodology of evaluation, limited communication and cooperation between the sections of the company (logistics, manufacturing, marketing, research and development...) in relation to cooperations. Managers are often not familiar with the methodical toolbox for effective management of cooperation activities in a company.

The listed problems are interconnected and affect each other. It is therefore necessary to deal with them one by one. The first step is to analyze current theoretical models related to cooperation (Table 1) and to identify key elements of the management of cooperation activities (Table 2). The second step is to create complex model of efficient management of cooperation activities.

4. Situation in Slovak enterprises – results of the empirical research

Between September 2012 and February 2013 we conducted a research, with the primary goal to gather and interpret information about the level of use of cooperations in the environment of Slovak enterprises. The main goal of the research was to identify the key aspects of efficient management and functioning of cooperations, related issues, degree of satisfaction of companies within cooperation and the opportunities for improvement of already functioning cooperations. Data that was gathered provided complete picture about readiness of Slovak enterprises to use (implement) cooperation management. In total, 273 managers of small, medium and large enterprises took part in the research, from companies active in the Slovak Republic. Data from the respondents was gathered via personal interviews.

It could be considered positive that almost half of the respondents (47.62 %) plans in the near future (within one year) to establish a more intense cooperation with a company or an organization. When selecting partners for cooperation, companies make decisions based on the following factors: costs (8.12), insolvency (8.03), market position (7.25), profitability (7.18) and certificates (7.05). In contrast, the lowest importance was assigned to the factors such as the legal form (4.16) and company seat.

The main challenges and problems that were listed by respondents to occur in the process of cooperating with companies and organizations were mainly insufficient adherence to the agreed contractual terms (58.39%), financially demanding (35.04%), distortion of information (34.41%), low effectiveness of cooperation (29.56%), unwillingness to provide internal information by a cooperating company, i.e. concerns about providing internal information to a company (28.83%).

5. Proposal of Model for Effective Management of Cooperation Activities in a Company

Management of cooperation activities in a company is a real challenge faced by company managers. A number of elements play a role in establishing the management of cooperation activities, including theoretical concepts, modeled solutions and practical applications. Probably the most significant challenge is the lack of unified, complex, comprehensive yet understandable and clear model for management of cooperation activities in a company. Based on the results of the performed research we can conclude that at present many companies try to manage their cooperation activities and processes intuitively. Oftentimes they face multiple challenges while doing this, which arise mainly from the lack of readiness of a company to manage cooperation activities. During the interviews with representatives of companies that we conducted during the realized research, we identified the need for complex and at the same time clear and understandable model for the management of cooperation activities in a company. Such model would be very helpful to the managers.

In relation to the viewpoints of other authors who are working on models for management of cooperation activities and after thorough analysis of these approaches we proposed a model for management of cooperation activities in a company (Fig. 1).

The proposed model is related to the existence of a competitive environment as well as a cooperative environment. Organizations that are active in the competitive environment generally have an objective to remain competitive and to achieve their goals through effective processes. This objective creates the initial need. Organizations that are active in the competitive environment often have common goals as well as problems. In case a reciprocity of a coordinated approach is sufficiently attractive, organizations may agree on a cooperative solution. Cooperative solution starts with the process of facilitation, i.e. facilitation of a cooperation. The goal of this process is to establish a real cooperation. The result of the process of facilitation is a mutual agreement. In case the agreement is not reached, organizations continue to be active as mutual competitors. In case the agreement is reached, organizations start to act in the mutual cooperative environment. This environment is made of individual subjects for the purpose of achieving set goals. This environment is cooperative only towards the participating entities, while it is competitive towards other subjects.

Facilitation of a cooperation and management of a cooperation are processes that are directly influenced by the basic company processes – functions of management (decision making, organization, leadership, planning, and control). These functions are ongoing and determine effectiveness of these processes.

A key element in the model is feedback. It makes it possible to overcome arising problems in the individual phases of the cooperative process. The model also takes into account the element of learning, which contributes to continuous improvements within

cooperation. Thus, organizations are able to learn based on the ongoing cooperative activities and are able to improve the way they manage these activities.

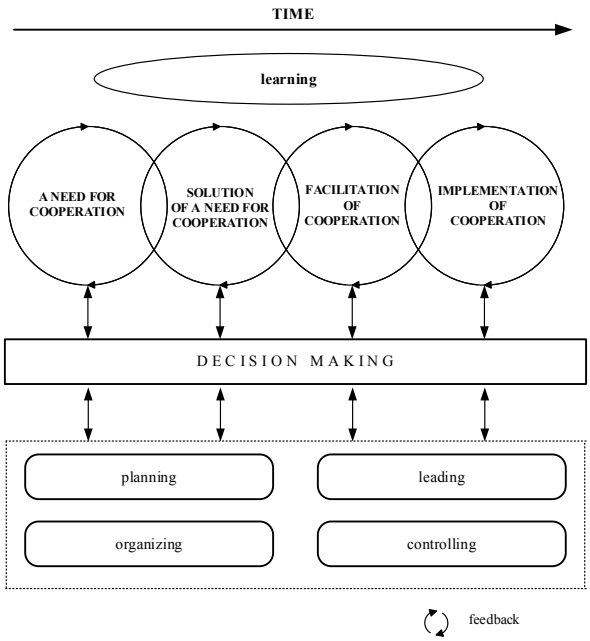

Fig. 1 Model for Effective Management of Cooperation Activities in a Company
Source: Own elaboration

Effective Planning of Cooperation Activities in a Company

Existence and justifiability of cooperation management is strongly influenced by the *dynamic development* of the market environment. For this reason *planning* represents a crucial part of all important processes here. Planning is ongoing on all levels of the goals – long-term (strategic goals, ca. 3 – 5 years), mid-term (tactical goals, ca. 1 – 3 years) as well as short-term (operational goals, ca. less than 1 year) (see [17]). In case of the planning within already existing cooperation connection, this is in the theoretical sense the case of standard methods. *Specific situations arise in two cases:*

- *Planning as part of facilitation:* Start and establishment of cooperation is a separate and specialized managerial process called labelled facilitation. Here is planning focused on the activities needed for start and successful launch of cooperation (analyses, agreements, negotiations...). This specialized managerial activity then ends.
- *Planning in dynamic environment:* Decline or significant change of a cooperation bond is a frequent occurrence. Planning then becomes specific to the situation such as successful termination of the cooperation (division of shares, settlements etc.) or a transformation in relation to the set goals.

Strategic planning relates to the start of cooperation and to setting parameters of its existence. The term "existence" here means that on the strategic level exact parameters of competitiveness of the cooperation bond are specified. If it happens that these cease to be achievable in a given situation, termination or modification of the cooperation follows. *Tactical planning* relates to specific cases of facilitating cooperation and its termination or transformation. *Operational planning* is used in the standard meaning as well as in the case of the mentioned specific cases.

Competitiveness and efficiency (power and reciprocity) are in general the long-term strategic goals of cooperation groups. In concrete cases – strategic goals adjusted to fit given situation. Other goals (tactical and operational) are managed by mutual agreement of the cooperating parties and are primarily dependent on the market situation.

Efficient Organization of Cooperation Activities in a Company

Organization, whether commercial or not, is a social group. Its goal is to fulfill the set goals. Cooperating organization have certain categories in common. Most often these are common goals that can be reached more effectively via cooperation. Organizations assume culture of the society from which they stem and at the same time they create their own (organizational or company culture). Success represents an important aspect – this is represented in a way by company survival, market success, profit etc. If organization is not in the long-term successful in fulfilling its goals or it is not competitive, one of the solutions is to connect with other organization or organizations.

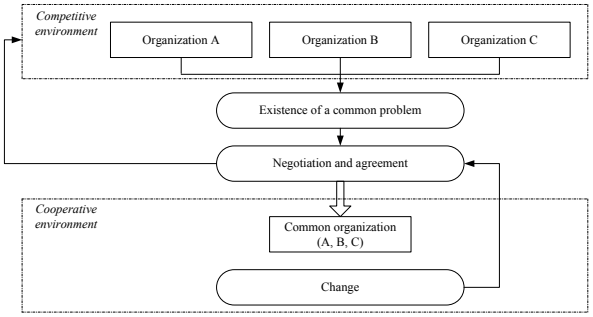

Fig. 2 Process of creating cooperation organization
Source: [18]

Figure 2 represents basic steps necessary for creating cooperating organization. Organizations exist in a state of mutual competition. In case a certain problem turns out to be significant

enough, it may represent a potential stimulus for establishing mutual cooperation. Mutual discussion and agreement leads to cooperation. Organizations exist in a dynamic environment that creates further changes that in turn create need for another discussion (planning and decision making). This may result in a decision to continue the cooperation, to modify it or to terminate it and to return to mutual competition.

The described aspects form dynamic cooperation organizational structures, that are created, modified and terminated, depending on current goals and tasks. One organization could participate in multiple dynamic organizational structures. It could also be the case that only a part of organization participates. This arrangement enables individual structures and employees to work on tasks from multiple projects, depending on the current needs. The cooperation organization itself takes on standard organizational structures.

Frequently we encounter matrix organizational structure, which suitably addresses the needs created by the environment dynamics. This type of organizational structure is also partially defined by the management literature: "Virtual organization or organization with virtual organizational structure is a special type of organization. It differs significantly from the hierarchical organizations. It is a temporary connection of companies, based on information technologies. Its purpose is to rapidly and efficiently use available entrepreneurial opportunities. Subjects connected within the virtual organization are not connected via ownership, and do not form formal organizational structures. Rather, they are independent and each of them contributes to taking advantages of the opportunity by its specific skill and obtains that what could not be obtained in being isolated" [19].

Work with people in managing cooperative activities

Within the context of cooperative activities, communication needs to be open, transparent and informal, enabling easy exchange of strategic information between internal and external parties.

In terms of personnel active in the management of cooperation activities, it would be preferable that one person would bear responsibility for the cooperation – a *manager of cooperation*. Such person would be responsible for smooth progress of the cooperation activities. The following Table 3 lists requirements and job description of this work position.

Manager of cooperation should also take the *leadership role*. This means s/he needs to be able to set a vision of future company success and clearly define cooperative opportunities that will lead to achieving this success. S/he needs to be able to transform this vision into cooperative programs and to win support of top management for their realization. S/he should be able to motivate her/his team members for realization of cooperative activities and to create effective cooperative team.

Related to the theme of leadership, it is suitable to strengthen motivation of employees by a company remuneration scheme. The process of employee motivation should mainly include basic needs of employees [20]. Company should particularly pay attention to defining of the evaluation, criteria based on which will the outcomes of cooperation activities be evaluated.

Control in the management of cooperation activities

In general, control is used to monitor the level of fulfilling of cooperation goals. It involves the process of tracking, analysis, evaluation, and making conclusions about the deviations between the goal (plan) and its realization. It is necessary to set control points within the process of realization of cooperation activities so that correct measures can be taken in case of deviations. Ideally, control should be performed after conclusion of every phase in the proposed model.

6. Discussion

The elementary prerequisite for successful functioning of the proposed model of management of cooperation activities is a detailed analysis of cooperation activities within the company. For this purpose a variety of analyses can be used (SWOT, SPACE, STEEP, PORTER, etc.) that will help to identify partial problems of a company in the field of realizing its cooperation activities.

In most cases, these analyses confirm weak utilization of cooperation opportunities in a company. Another problem is

Requirements and job description for the position manager of cooperation — Table 3

Requirements	Job description
- Creativity - Teamwork and communication - Managerial skills - Experience, track record	- Evaluate and process all real needs within cooperation - Create cooperation team - Coordinate tasks of the cooperation team - Evaluate effects of the realized cooperation activity - Organization and chairing of the mutual meetings - Responsibility for cooperative ideas (record keeping, identification of the best ideas, prioritization, decision making)

insufficient utilization of cooperation potential, which results in low rate of utilization of already existing partnerships.

Another necessary prerequisite for success is a suitable *information background for managing cooperation activities in a company*. A system should be in place to ensure and enable suitable information background. It should also take into consideration the requirements of the people involved in the newly created cooperation.

Top management of the company should also support *nurturing of creative human potential*. This means that the employees should be able to fully utilize their skills and abilities during their work on cooperation activities. Specifically, during the first and second phase of the model presented above, a need for cooperation arises and cooperation ideas are created. In these stages employees apply their ability to identify opportunities, structure and plan changes and come up with ideas and solutions. In the consequent phases of the model employees need to apply their ability to realize cooperation activities, manage the cooperation process and to continuously learn based on the development of the cooperation. By practicing their ability to cooperate, employees can identify new sources of ideas, e.g. potential shared use of research and development facilities etc.

In order for the cooperation activities to be managed efficiently, it is necessary that the company demonstrates certain results in the areas that influence its management of cooperation. Every company has a different level of management of cooperation activities. It is therefore needed, as the first step, to ascertain the current level of management of cooperation activities in a company. This is followed by identification of weaknesses and by formulation of recommendations for improvement. For this to work, it is necessary to have in place a suitable *methodology for evaluation of the management of cooperation activities in a company*.

7. Conclusions

Ideas about complexity of managing cooperation activities in a company are justified. The topic of managing cooperation activities is currently very relevant among Slovak enterprises. Managers in Slovak enterprises strive to build cooperation management in their companies, aiming to enable creation of successful cooperation and fulfillment of set cooperation tasks. In order for this initiative to be successful, it is needed to use elements of project management and to establish such environment that will support new cooperation, enable communication and effective work with information within created partner relationships [21].

The general belief that managing cooperation activities in a company is a complex undertaking is indeed justified. The search for one effective concept of the management of cooperation activities that would be applicable to all companies is a strenuous task. This is because each company has at its disposal different amount of cooperation resources and each company realizes different types of cooperation on a different level. The proposed model aims to contribute to better clarity and understanding in this area of research.

Acknowledgement

This paper was partially supported by the Slovak scientific grant VEGA 1/0621/14 Marketing management in cooperative environment – Proposal of strategic cooperation management implementation model.

References

[1] RAY, P. K.: *Cooperative Management of Enterprise Networks*. Kluwer Academic Publishers, 2002.

[2] VALENZUELA, J. L. D., VILLACORTA, F. S.: The Relationship between the Companies and their Suppliers. *J. of Business Ethics* 22(3): 273-280, 1999.

[3] VEERAKUMARAN, G.: *COCM 511 - Management of Cooperatives and Legal Systems*, Faculty of Dryland Agriculture and Natural Resources: Mekelle University, 2006.

[4] ZHANG, W.: *Cooperation System Constructing and Model of its Operation Mechanism,* Proc. of the Intern. Conference on Business Management and Electronic Information (BMEI), vol. 3, 2011, 784-787, 2011.

[5] SOVIAR, J., VODAK, J.: Value Network as Part of New Trends in Communication. *Communications - Scientific Letters of the University of Zilina*, vol. 14, No. 2, 2012. ISSN 1335-4205.

[6] SAHUT, J.-M., PERIS-ORTIZ, M.: Small Business, Innovation, and Entrepreneurship. *Small Business Economics,* 42(4): 663-668, 2014.

[7] RITALA, P., SAINIO, L.M. Coopetition for Radical Innovation: Technology, Market and Business-model Perspectives. *Technology Analysis & Strategic Management* 26(2): 155-169, 2014.

[8] MUTAK, M.: Service Innovation in Networks: A Systematic Review and Implications for Business-to-business Service Innovation Research. *J. of Business & Industrial Marketing* 29(2): 151-163, 2014.

[9] KULTTI, K.: Sellers like Clusters. *J. of Theoretical Economics* 11(1), 2011.
[10] FELZENSZTEIN, C., GIMMON, E., AQUEVEQUE, C.: Cluster or Un-clustered Industries? Where inter-firm marketing cooperation matters. *J. of Business & Industrial Marketing,* 27(5): 392-402, 2012.
[11] WECK, M., IVANOVA, M.: The Importance of Cultural Adaptation for the Trust Development within Business Relationships. *J. of Business & Industrial Marketing* 28(3): 210-220, 2013.
[12] WICKS, A. C., BERMAN, S. L., JONES, T. M.: The Structure of Optimal Trust: Moral and Strategic Implications. *Academy of Management Review,* 24(1): 99-116, 1999.
[13] FAWCETT, S. E., JONES S. L., FAWCETT A. M.: Supply Chain Trust: The Catalyst for Collaborative Innovation. *Business Horizons,* 55(2): 163-178, 2012.
[14] MONCZKA, R. M., PETERSEN, K. J., HANDFIELD, R. B., RAGATZ, G. L.: Success Factors in Strategic Supplier Alliances: The Buying Company Perspective. *Decision Sciences,* 29(3): 553-577, 1998.
[15] JASSAWALLA, A. R., SASHITTAL, H. C.: An Examination of Collaboration in High-Technology New Product Development Processes. *J. of Product Innovation Management,* 15(3): 237-254, 1998.
[16] SCHMOLTZI, C., WALLENBURG, C. M.: Operational Governance in Horizontal Cooperations of Logistics Service Providers: Performance Effects and the Moderating Role of Cooperation Complexity. *J. of Supply Chain Management,* 48(2): 53-74, 2012.
[17] ROBBINS, P. S., COULTER, M.: *Management (in Czech),* Grada : Praha. ISBN 80-247-0495-1, 2004.
[18] SOVIAR, J.: *From Cooperation to Management - Cooperative Management (in Slovak).* Habilitation thesis. University of Zilina: Faculty of Management Science and Informatics, 2012.
[19] VEBER, J. et al.: *Management. Foundations, Prosperity, Globalization (in Czech),* Management Press: Prague, 2006.
[20] KAMPF, R., HITKA, M., POTKANY, M.: Interannual Differences in Employee Motivation in Manufacturing Enterprises in Slovakia. *Communications - Scientific Letters of the University of Zilina*, vol. 16, No. 4, 2014, ISSN 1335-4205.
[21] VODAK, J., SOVIAR, J., LENDEL, V.: Identification of the Main Problems in Using Cooperative Management in Slovak Enterprises and the Proposal of Convenient Recommendations, *Communications - Scientific Letters of the University of Zilina*, 15(4): 63-67, 2013.

Pawel Olszowiec - Miroslaw Luft *

METHOD OF IDENTIFYING THE REAL STATE OF THE COUNTER VEHICLE BASED ON THE INTERPRETATION OF ELECTRICAL SIGNALS

The article presents the analysis of electrical signals and system reports of motor vehicles in which the mileage counter indication has been questioned under service conditions as compared to the vehicles mechanical wear and tear. The essence of the aforementioned deliberations is an attempt at determining the universal procedures allowing for obtaining data concerning the actual vehicle mileage. Search for the intended method results from many factors functioning on the used motor vehicle market. The major factor is the uncontrolled safety level on the roads among the road users and, equally important, financial frauds in the area of motor vehicle sales, as well as vehicle cost estimation by the insurance companies.

Keywords: *Vehicle mileage, technical condition, mechanical wear and tear.*

1. Introduction

According to the data collected by the company 'Motoraporter', involved in the technical expertise of the used motor vehicles all over the territory of Poland, the 2014 summary presents the proportions described below [1]. During the year about 1000000 transactions were registered on the used motor vehicle market, among which 23% constituted domestic origin vehicles and 77% were the imported vehicles. The relation of transactions between private persons and dealers was 32% and 68% for second-hand car dealers and dealer's markets. The percentage of Poles purchasing motor vehicles from car dealers is minor, nevertheless, it is worthwhile to state that majority of the cars purchased by Polish people is 4 - 8 years old (53% of all inspected vehicles). For the purpose of comparing, the percentage of inspected vehicles dated 1990 - 1995 was only 3%. Cars dated 2011 and newer constituted 15% of all inspected motor vehicles. Last year the station wagon type of vehicles prevailed, and the most popular engine was Diesel (increase from 60% to 72%). The mileage of the inspected vehicle is a curiosity. The greatest number of vehicles, among the inspected ones, constitute those dated 2006 - 2010. We also know that imported vehicles constitute the majority. According to the statistics, a European annually drives about 30,000.00 km. Relatively, it means the mileage between 120,000.00 and 240,000.00 km. Among the inspected vehicles the declared mileage usually was between 101000 and 150000 km. The mileage exceeding 200000 km was very rare (6% of the inspected cars), and if we would like to follow the statistics, it should possibly occur regularly. It has been also confirmed by the reports prepared by the company experts, informing that over 35% of the inspected vehicles had 'fraudulent' indications of the mileage counter. The data above present that the procedure of lowering the mileage counter indication, in spite of being illegal, is commonly employed, which in turn means the overestimation of the vehicle value and drastic decline of the safety level.

2. Interpretation of signal drive system

The implementation of the continuously increasing ecological requirements has forced the motor vehicle manufacturers to exceptionally develop as regards the internal combustion unit metering and the permanent supervision over its operating parameters. The technological advancement and the toxic substance emission limits have also caused the complete alteration of the diagnostic procedures applied for the contemporary vehicles. The necessity of applying modern diagnostic tools such as diagnoscopes dedicated to car brands, or universal tools, allow for the real-time viewing of the unit operation parameters, by means of the serial diagnostics method, with the application of the CAN bus. The limited life span of particular combustion unit components resulting from their precisely calculated number of work cycles in order to maintain the correct ecological parameters is a perfect tool to make an attempt at deducing the actual vehicle

* **Pawel Olszowiec, Miroslaw Luft**
Faculty of Transport and Electrotechnik, University of Technology and Humanities in Radom, Poland
E-mail: p.olszowiec@urhrad.pl

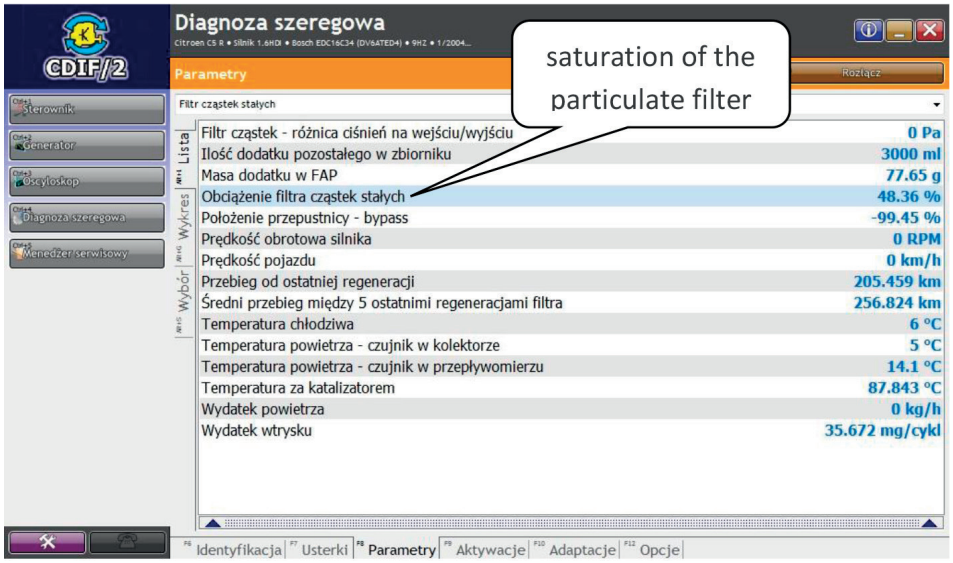

Fig. 1 CDIF2 Diagnostic Program window – diesel particulate filter saturation and the regeneration process regularity of the PSA Group vehicle readout [2]

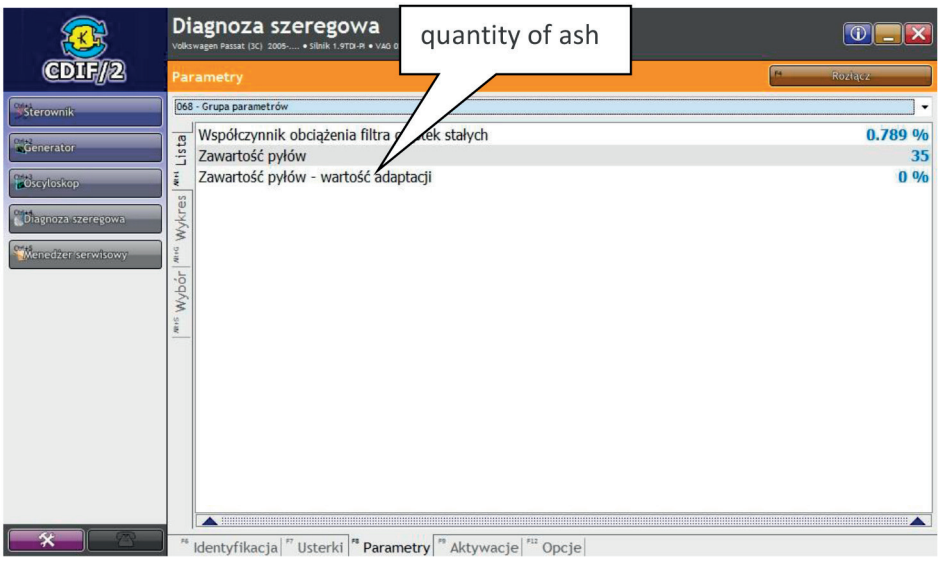

Fig. 2 - CDIF2 Diagnostic Program window – dust content parameter for the PSA Group vehicle readout [2]

mileage. It is applicable to the spark-ignition engines as well as to the compression-ignition engines. One of the elements which is directly connected to the mileage is the dust saturation of the diesel particulate filter in compression ignition engines (Fig. 1).

This parameter informs the diagnostician not only about the environment in which the vehicle was driving, but also about the number of successful regeneration processes, therefore, what the approximate vehicle mileage is. Nominal DPF/FAP type filter is prepared for the maintenance-free mileage of about 350,000.00 km. For example, for the 1.9 TDI unit, engine code BLS, power 105 km, VW Group, the foregoing mileage means the dust content at the level of 35 g (Fig. 2).

Which is more, the significant element indicating the condition of the system for cleaning fumes from the carbon particles is the regeneration frequency and regeneration interval factor. In case of an attempt at the mechanical disposal of dust, there will remain information in the control concerning the interval between burning. Another element, which directly influences the vehicle mileage, is determination of the vehicle injection system condition - compression-ignition engine. The

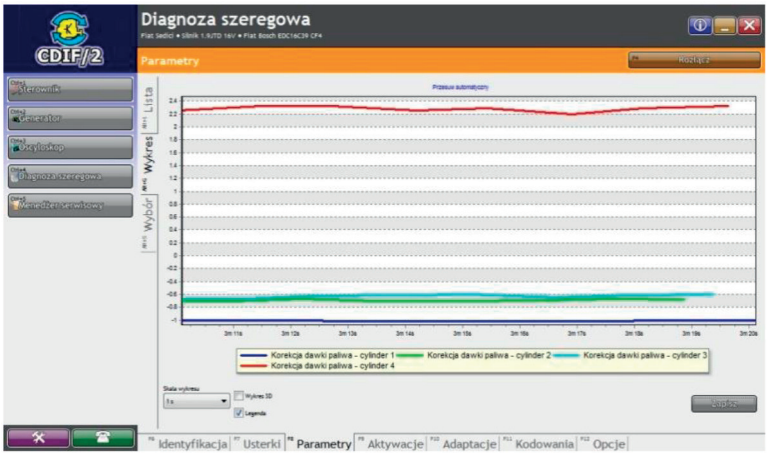

Fig. 3 CDIF2 Diagnostic Program window – graphic visualisation of the fuel injection correction for vehicle Fiat 1.9 JTD [2]

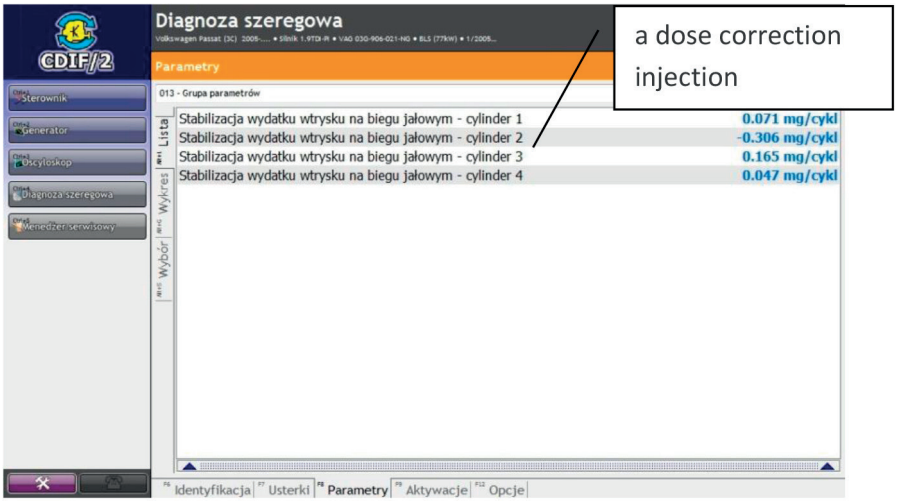

Fig. 4 CDIF2 Diagnostic Program window – fuel injection dose stabilisation parameters readout [2]

example of such a case is the fuel injection correction parameters readout on the particular fuel injection valve. At the moment the parameters, as in Fig. 3 are obtained, which means the significant discrepancy on the single injection, such state means the system damage and breakdown.

Another case is to identify the state of even balance of the significant injection dose corrections (value of about +/- 1 mg). Such a state means the even wear and tear of the fuel injection valves, which in turn means the significant vehicle mileage. The example of the balanced readout of the injection dose correction parameters is presented in Fig. 4, which shows the data of VW Group vehicle, 1.9TDI unit, BXE code with the mileage of 165,000.00 km.

In case of the attempt at the mileage identification of the spark-ignition engine vehicle, it is crucial to try to determine the catalyst system wear and tear and inertia condition of the oxygen controlling sensors (lambda probes). Similarly to the diesel particulate filter, the three-way catalyst system efficiency is scheduled for a particular number of cycles equal to the mileage of about 180,000.00 - 250,000.00 km. The voltage or current signal (Fig. 5) is the parameter indicating the catalyst wear and tear, depending on the oxygen sensor type - lambda probe.

The window above constitutes the presentation of the current scale of broad band oxygen sensors in the VW Group car with the spark-ignition engine with the direct injection of the TFSI type fuel. It is worth to note that the value of the actual vehicle mileage is among the parameters connected with the fume cleaning system. It corroborates the rule concerning the dispersion of data concerning mileage in various system modules. However, this issue is going to be analysed in more detail in the subsequent

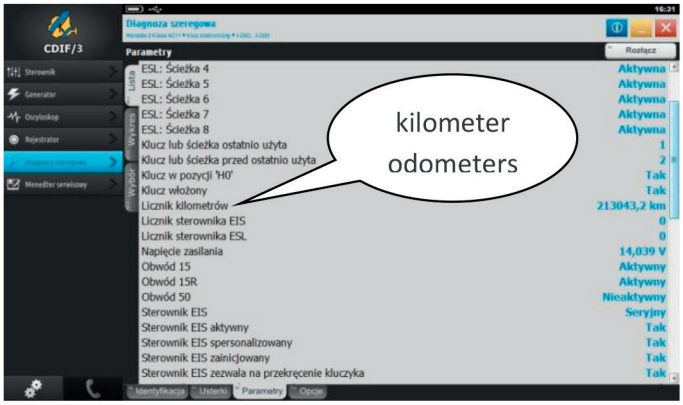

Fig. 7 CDIF3 Diagnostic Program window – Actual parameters of the key module readout vehicle MB W211 [2]

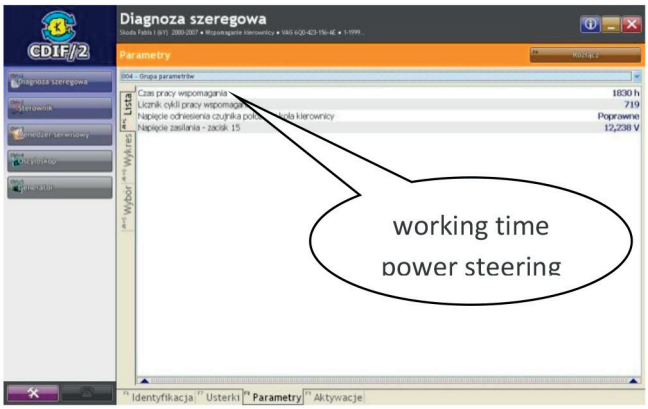

Fig. 8 CDIF3 Diagnostic Program window -- hours of operation in the power steering system readout VW Group vehicle [2]

chapter. Figure 6 constitutes the presentation of the registered breakdowns connected with functioning of the catalyst system and lambda probes.

The exceeding of the probe voltage maximum may be the sign of the fuel injection system damage as well as the wear and tear resulting from the exceeded operation cycles. The complementing inspection is the visualisation of the probe voltage signal on the diagnoscope. If the obtained chart does not reach the time amplitude below 1 second with 2000 revolutions per minute of the internal combustion unit, it will mean the lost inertia of the oxygen sensor, resulting from its wear and tear.

3. The compatibility meter state between the different vehicle systems

The already mentioned in the first chapter mileage dispersal system ensures the possibility of obtaining access to the vehicle mileage readout in various electronic modules. Apart from the mileage indication in the vehicle mileage counter, it is placed in the following components: key (Fig. 7), engine driver, power steering module, air conditioning, or xenon light driver.

Such dispersal of the mileage information has two objectives. First of all, the vehicle mileage parameter is, indeed, an important information for the module functioning, e.g. in the key, since it registers precise date and course of the damage occurring in the vehicle to be data carrier for the service purposes. Functioning information concerning the vehicle mileage in the light module allows for the active control over the light source wear in order to maintain the optimum safety level. Registration of the mileage parameter in the power steering module is done by means of the hours of operation registration. That is why, for example in the vehicle where the operation of the electric and hydraulic power steering amounted to 1830 hours (Fig. 8), in order to obtain the approximate vehicle mileage, you have to multiply the hours of operation by average local roads driving speed. In Poland this value is assumed to be at the level of 45 km/h.

The obtained value should be close +/- 5% to the mileage counter indications. Of course the extent of the problem, not only in Poland but also in Europe, is so high that there are first diagnoscopes available on the market with the function of

the mileage readout from the engine module, e.g. EDC16 and comparing it to the mileage counter indication. Even though many discrepancies could be seen only on the basis of this example, the comparison of two modules is still not enough. The proper certainty level as to the mileage could be ensured by the tester allowing for the comparison of the mileage data taken from all available in the vehicle modules and the tester assessing the consistency of such indications.

4. Summary

In this work, the main sources of readout of the electrical data directly connected with the vehicle mileage have been indicated on the basis of many car manufacturers. The analysis of the aforementioned data allows for proposing a thesis that there is a possibility of defining quite precisely the actual vehicle wear level on the basis of the interpretation of the actual parameters connected with the driving unit and the remaining system modules functioning within the vehicle. It seems to be reasonable to make an attempt at defining common directions and procedures allowing for straightforward and consistent description of the vehicle mileage, in order to reduce the wheedling of money from the insurance companies and to increase the Polish roads safety.

Reference

[1] http://motoraporter.com/uploads/pressroom/pod_2014/podsumowanie_2014_roku_na_rynku_samochodow_uzywanych.pdf
[2] OLSZOWIEC, P.: *Training Materials - Diagnoscopes,* Radom, 2013.

Marek Patek - Augustin Sladek - Milos Mician *

DESTRUCTIVE TESTING OF THE WELD JOINTS ON SPLIT SLEEVE FOR BRANCH CONNECTIONS REPAIRS

New type of repairing technology for branch connection defects on gas pipelines has been designed recently. Repairing technique is based on manufacturing of split sleeve and welding of its parts together and to the repaired pipes by manual metal arc welding technology. Appropriate testing has to be performed to ensure practical and permanent use of such kind of sleeve in commercial area. Destructive testing was performed to confirm quality of the welds on the prototype sleeve repair. Macrostructural and hardness evaluation showed inhomogeneity present in some welds. According to that, microstructure observations, spectral analysis and mechanical tests were performed on the base metal of the sleeve. It has been showed that even when some problems may be present, repairing technique by split sleeve can be still suitable for permanent repairs of the defects of the branch connections.

Keywords: *Destructive testing, macrostructural analysis, split sleeve, Vickers hardness, weld joint.*

1. Introduction

Quality of weld joints is very important factor to ensure safety and long term lifetime of the gas transport pipelines. According to European Gas Pipeline Incident Data Group (EGIG) are construction defects (where weld joint defects also belongs) and material failures the third most frequent cause of the pipeline incidents [1]. Welding quality control is thus important and every new type of weld joint has to be analyzed by non-destructive evaluation and it also should be tested by destructive testing methods.

Numerous kinds of repair techniques are now available including the cut out and replace of the pipeline, construction of the bypass along the damaged area, grinding, weld deposition, metallic or composite sleeves [2]. Although the repairing techniques for straight parts of pipelines are well established, only a few of them are applicable for branch connections defects (e.g. defects in the area of fillet weld between header and branch pipe). Recently a new kind of split sleeve for such defects repairs has been designed [3 and 4]. Relatively complicated construction together with different manufacturing processes of sleeve parts might cause weld joint problems and precise weld examination is necessary. Non-destructive examination of weld joints has been proposed by ultrasonic technique TOFD [5] but destructive testing of such welds has not been proposed yet.

The aim of presented article is to perform the destructive testing of weld joints on split sleeve for branch connection repairing. Macrostructural analysis and hardness evaluation is presented together with selected base metal examinations.

2. Experimental measures and results

Weld joint analysis has been performed on the split sleeve for branch connections repairs (Fig. 1). Split sleeve consists of cylinder part and sphere-like part, which has to ensure safe installation of the sleeve to the repaired branch connection. Such type of split sleeve is joined together by butt welds and to the repaired pipes it is connected by circumferential fillet welds.

Different manufacture processes and also semi-finished products were applied to parts of the sleeve. Cylindrical part was prepared by welding of end plates to thick-walled pipe (thickness of 16 mm for each part). Both end plates are made of S355J2+N steel and material of the thick-walled pipe is S355J2H steel. Segments of the sphere-like part were made by machining of S355JR steel block to required shape and size. Machined part was after that split to two segments. Materials used in this type of construction ensured weldability without additional conditioning. Weld joints were prepared by manual metal arc (MMA) welding technique.

* **Marek Patek, Augustin Sladek, Milos Mician**
Department of Technological Engineering, Faculty of Mechanical Engineering, University of Zilina, Slovakia
E-mail: marek.patek@fstroj.uniza.sk

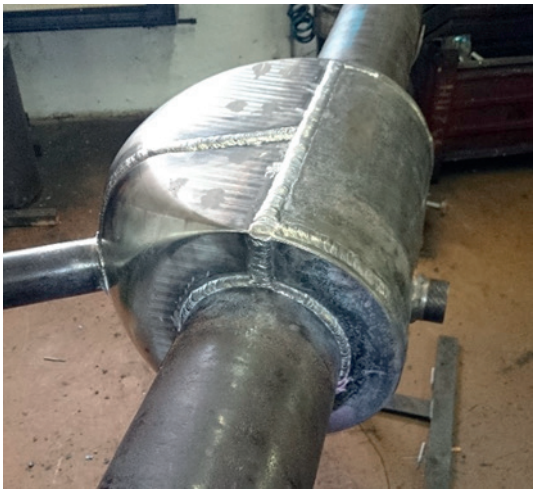

Fig. 1 Split sleeve for branch connection repairs

2.1. Macrostructural analysis of weld joints

Macrostructural analysis of the split sleeve weld joints was performed in terms of the EN ISO 17639 standard. Four characteristic welds were selected to analysis. Macrographs of the butt weld joints are shown in Fig. 2 and 3. Unacceptable defects were not detected neither on the macrographs of the butt joint between cylindrical and sphere-like part (Fig. 2) nor in the macrograph of weld joint between sphere-like segments of the sleeve (Fig. 3). Some imperfections might be observed such as linear misalignment or excessive penetration. Dimensions of these imperfections are within the allowed range according to standards (ISO 5817-B). In the lower part of the Fig. 2 and 3 the sealant carriers can be seen, which serve to carry a sealants that isolates the places of welding from places where leaking gas is present. Large size of the root opening can be seen between the sealant carrier and wall of the sleeve in macrograph shown in Fig. 3. Weld joint between the sealant carrier and split sleeve wall are only supplementary and after the sleeve is welded onto the pipeline, it has no function. Such kind of defect might be consider as acceptable for the functionality of the split sleeve. Macrostructural evaluation of the weld between the cylindrical and sphere-like part (Fig. 2) shows significant heterogeneity of the joint, which might be a sign of inappropriate microstructure and also mechanical properties of the base metal.

Typical macrographs of the girth fillet welds are shown in Fig. 4 and 5. Fillet welds do not show the presence of unacceptable defects similarly to the butt welds. Base metal and heat affected zone on the side of the sphere-like part also pointed out different character of macrostructure (Fig. 4) that confirms weld joint heterogeneity.

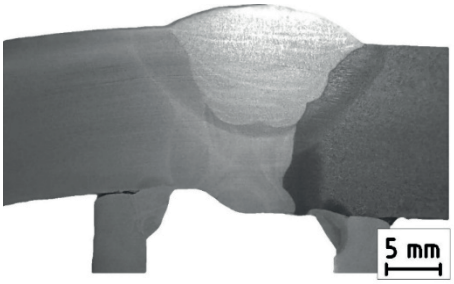

Fig. 2 Macrograph of butt weld joint between cylindrical (left) and sphere-like (right) part of the sleeve

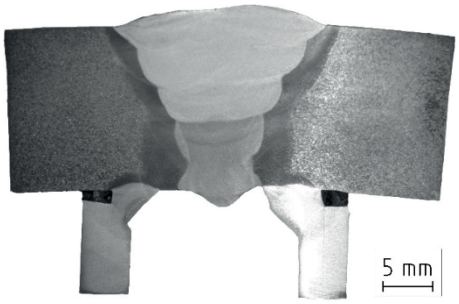

Fig. 3 Macrograph of butt weld joint between sphere-like parts of the sleeve

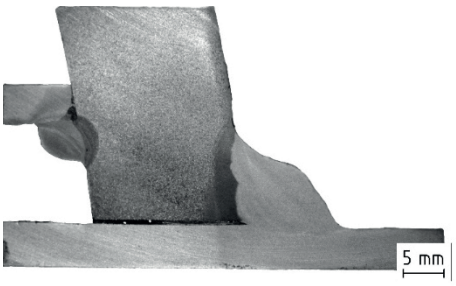

Fig. 4 Macrograph of fillet weld joint between sphere-like part of the sleeve and pipe

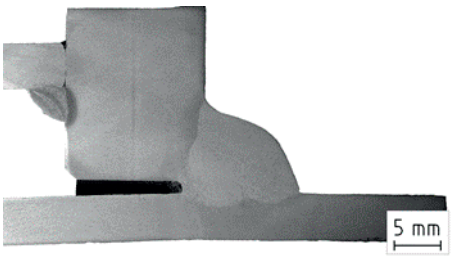

Fig. 5 Macrograph of fillet weld joint between cylindrical part of the sleeve and pipe

2.1. Hardness measuring

Vickers hardness method (HV10) was used to evaluate the weld joints hardness. Measuring was performed in terms of EN

ISO 9015-1 standard. Significant increase of Vickers hardness can be seen in heat affected zone (HAZ) of the weld on the sphere-like side of weld joint (Fig. 6 - 8). In these areas hardness reaches values higher than 300 HV and in some cases it almost reached maximal allowed value for this type of material (380 HV without heat treatment according to EN ISO 15614-1 standard). Hardness of weld joint on the side of cylindrical part of the sleeve did not significantly increase in HAZ (Fig. 6, 8 and 9).

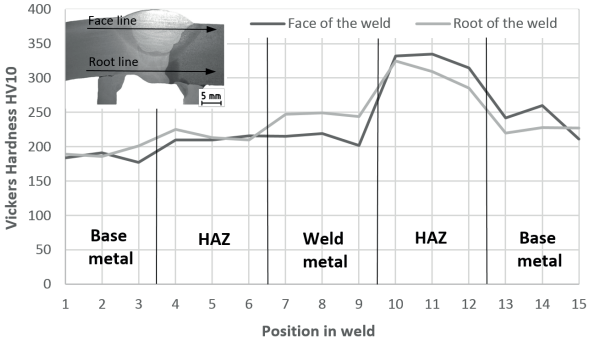

Fig. 6 Hardness of butt weld joint between cylindrical and sphere-like part of the sleeve

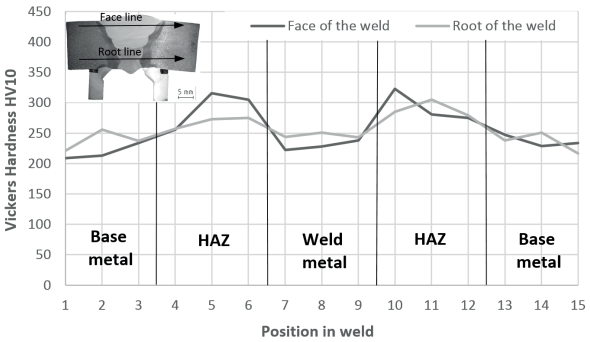

Fig. 7 Hardness of butt weld joint between sphere-like parts of the sleeve

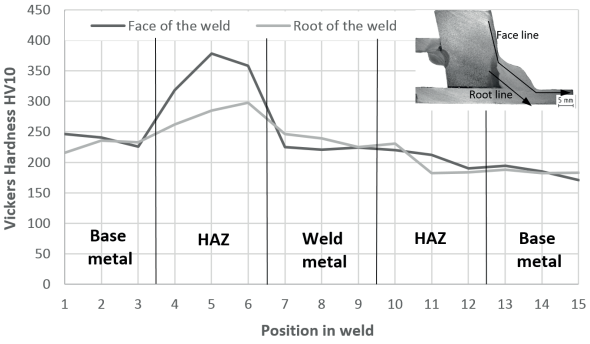

Fig. 8 Hardness of fillet weld joint between sphere-like part of the sleeve and pipe

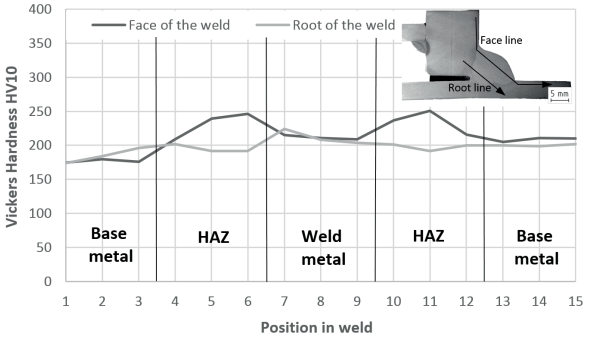

Fig. 9 Hardness of fillet weld joint between cylindrical part of the sleeve and pipe

2.2. Approval of the sphere-like part base metal chemical composition and mechanical properties

Macrostructural analysis and hardness measuring pointed out to possibility of insufficient base metal quality or to material interchange of sphere-like part of the split sleeve. Chemical composition, tensile properties and impact toughness of base metal were thus analyzed to prove material quality.

Comparison of the spectral analysis results, attest values and standardized chemical composition according to data sheet are shown in Table 1. Measured values show higher carbon level

Results of spectral analysis compared to semi-product attest and material data sheet (wt. %) Table 1

Chemical element	C	Mn	Si	P	S	N	Cr	Ni	Cu
Spectral analysis	0.415	0.797	0.236	0.018	<0.01	-	0.088	0.095	0.019
Semi-product attest	0.14	0.68	0.35	0.013	0.009	-	0.5	0.09	0.1
Data sheet	max. 0.27	max. 1.70	max. 0.60	max. 0.055	max. 0.055	max. 0.011	-	-	-

Comparison of tensile properties after measuring and values from material data sheet Table 2

	Yield strength R_{eH} [MPa]	Tensile strength R_m [MPa]	Elongation A_5 [MPa]
Tensile test	332	516	3
Data sheet values	275	450-630	17

detected by spectral analysis compared to semi-product attest, which exceeds maximal allowable value defined in material data sheet of S355JR steel.

Ultimate tensile strength, Yield strength and elongation were measured by tensile testing procedure according to directions of EN ISO 6892-1 standard. Three tensile specimens with diameter of 10 mm were prepared and loaded to fracture at the ambient temperature of 20 °C. Comparison of average value after measuring and values from material data sheet of S355JR steel is shown in Table 2.

Tensile strength and Yield strength correspond with data sheet requirements but elongation obtained from tensile test is evidently lower.

Charpy pendulum impact test was used to determine impact toughness of the sphere-like part of the sleeve material. Conditions of the testing method are defined in the international standard EN ISO 148-1. Experimental samples with V-notch, cross-section size of 10 x 10 mm and 55 mm length were used to testing. Measuring of impact energy was performed at ambient temperature -20 °C. Average value of impact energy KV obtained by three measures is 6.7 J while required value is minimum 27 J. Material thus does not satisfy impact toughness.

2.3. Evaluation of the base metals microstructure

Microstructure analysis was performed in order to verify microstructure of the sphere-like part of the split sleeve. Characteristic microstructure of sphere-like part of the sleeve is shown in Fig. 10. Microstructure is formed by large perlite grains surrounded by ferritic envelopes. Base metal microstructure of the cylindrical part of the split sleeve (Fig. 11) is fine-grained ferritic-pearlitic and corresponds with S355 grade steel quality.

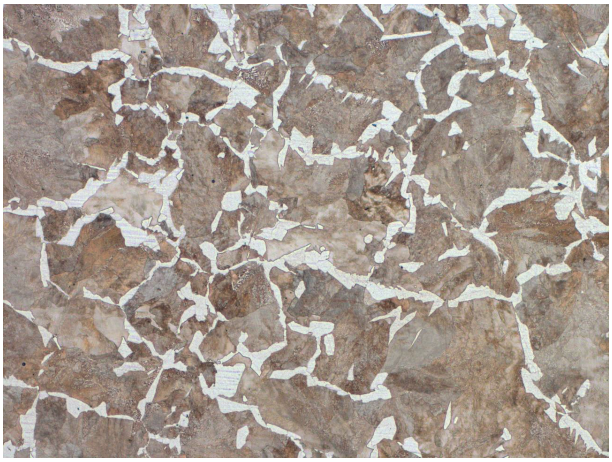

Fig. 10 Microstructure of the sphere-like part of the sleeve, etch. 5 % Nital

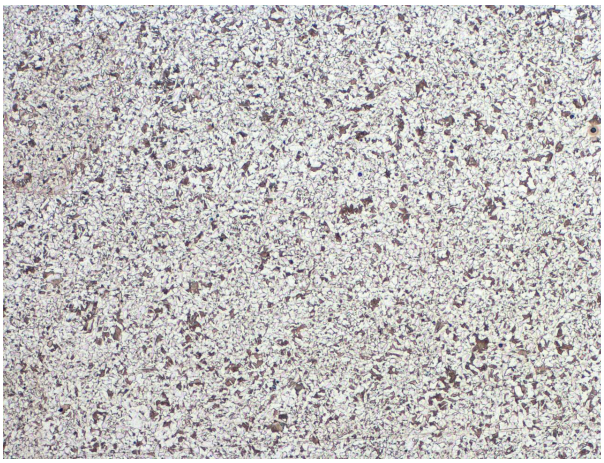

Fig. 11 Microstructure of the cylindrical part of the sleeve, etch. 5 % Nital

3. Discussion

Macrostructural analysis and hardness evaluation of the weld joints of split sleeve for branch connection repairs was performed on four characteristic welds. Significant inhomogeneity of the base metal and HAZ on cylindrical and sphere-like side of the weld was observed during macrostructural analysis. This fact was approved by followed microstructural evaluation (coarse-grained pearlitic structure of sphere-like part base metal).

As the microstructure of the sphere-like part of the sleeve does not correspond with assumed structure of applied material, chemical composition and selected mechanical properties were analyzed. Spectral analysis revealed higher carbon level (0.47 wt. %), which exceeded limit value given by material data sheet. However, amount of carbon corresponded with material structure. Measured values of tensile and yield strength were between the standardized value interval for S355JR steel but ductile properties (elongation and impact toughness) were below the limits.

Higher carbon level leads to significant increase of the hardness (up to 378 HV), especially in fillet welds with increased heat transfer to the wall of the sphere-like part of the sleeve. Welding and cooling conditions then lead to increased cooling rate in HAZ of the fillet weld on the sleeve side and increasing of the Vickers hardness. This effect together with material structure sensitive to hard and brittle phase formation may cause exceeding of the hardness tolerance.

4. Conclusions

Results of the presented analysis pointed to low quality of base metal used to sphere-like part of the sleeve manufacturing. Two possible reasons might be taken into account as follows:

(1) Interchange of the material for steel with higher carbon level in the whole volume of the semi-product.
(2) Material inhomogeneity of semi-product after manufacturing. Steel block with dimensions of 400x800x400 mm was used to manufacturing. Such kind of semi-product is commonly used to forming operation. As cast microstructure of the block can be very inhomogeneous and uneven chemical distribution may be also present.

To prevent similar behavior of the weld joints, there should be performed measurement of chemical composition before machining of the semi-product and/or full annealing of steel block or manufactured part should be applied. Even when some insufficient material properties can be present, repairing technique by split sleeve can be still suitable for commercial application as there were not exceeded hardness limits, no unacceptable defects of weld joint were present and material properties are still sufficient to carry the loading during the operational time of the sleeve.

Acknowledgement

This work has been supported by Scientific Grant Agency of Ministry of Education of the Slovak Republic, grants VEGA 1/0610/12 and KEGA 034ŽU-4/2015. Authors acknowledge the grant agency for support.

References

[1] EUROPEAN GAS PIPELINE INCIDENT DATA GROUP (EGIG): *Gas pipeline Incidents. 9th Report of the European Gas Pipeline Incident Data Group (period 1970 – 2013)*, 2014.
[2] BATISSE, R.: *Review of Gas Transmission Pipeline Repair Methods.* Safety, Reliability and Risks Associated with Water, Oil and Gas Pipelines. Dordrecht: Springer, 2007.
[3] MICIAN, M., PATEK, M., SLADEK, A.: Concept of Repairing Branch Pipes on High-pressure Pipelines by Using Split Sleeve. *Manufacturing Technology*, vol. 14, No. 1, 2014.
[4] MESKO, J., FABIAN, P., HOPKO, A., KONAR, R.: Shape of Heat Source in Simulation Program SYSWELD Using Different Types of Gases and Welding Methods. *Strojirenska technologie*, No. 5, 2011.
[5] PATEK, M., KONAR, R., SLADEK, A., RADEK, R.: Non-destructive Testing of Split Sleeve Welds by the Ultrasonic TOFD Method. *Manufacturing Technology*, vol. 14, No. 3, 2014.

Zuzana Florkova *

USAGE OF 3-D BASED METHODS FOR THE DETECTION OF AGGREGATE MICROTEXTURE

Some of the available advanced three-dimensional based methods for measurement of microtexture have been described. These methods are generally divided into three categories, namely image analysis based methods, laser based methods and photogrammetry methods. Moreover, a particle of aggregate can be captured using a stereomicroscope and using the appropriate software to obtain a 3-D image of investigated aggregate. Software also includes an interactive measurement tool that allows to obtain a profile of aggregate particle. The stereomicroscope method is also presented in the paper. The usage of the microscope for the detection of aggregate microtexture allows to eliminate some of the disadvantages of described methods and provides additional opportunities for microtexture evaluation.

Keywords: *Microtexture, aggregate, 3-D based methods, microscope method.*

1. Introduction

Microtexture is defined as configuration of particular peaks on the surface of aggregate particles. Microtexture is very considerable parameter in term of skid resistance and mainly influence friction at low speeds on dry pavement surface [1]. Microtexture is also necessary to assure high friction value between a tire and pavement [2]. Microtexture is characterized by wavelengths and amplitudes in the range between 1μm - 0.5 mm [3].

In [4], the microtexture is defined as the angularity of the aggregate particle, which represents geometric attribute of the aggregate to have sharp edges (Fig. 1). The more shaped surface of the aggregate, firmer and also sharper material of surface means that better and more lasting friction is expected.

It is clear that the possibilities of measuring microtexture and the knowledge of the roughness of aggregate particles are particularly important for road traffic safety.

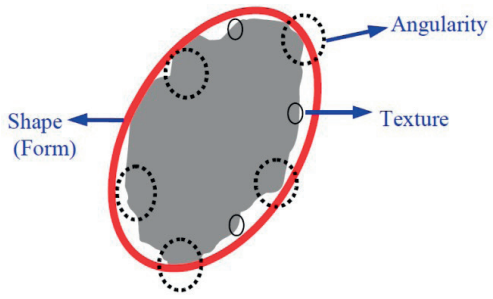

Fig. 1 Geometry of aggregate [5]

Variety of methods has been developed for detection of microtexture. These methods can be generally divided into manual measurements, detection of microtexture based on comparison and digital image analysis methods. The manual methods and the methods on basis of comparison are easy to realize, but are considered as subjective and time consuming. The current development of technique provides enhancement of microtexture detection methods by the methods obtaining outputs in the form of three-dimensional image of investigated particle.

2. Methods based on an image analysis

Determination of microtexture using digital image analysis methods (DIAM methods) generally consists of image acquisition, the image processing (image editing) and subsequent evaluation of the image by various methods. The image analysis means conversion of image to data. Because the digital image is used, all transformations and calculations are implemented in pixels. In most cases, the evaluation is carried out by various mathematical algorithms in different computing programs. Many of used algorithms are complicated and very difficult to programming. Therefore, this method requires considerable computer knowledge and longer processing time.

A wide range of complex systems based on digital image analysis which allow obtaining a 3D view of the particle and then evaluation of aggregate microtexture have been developed. These systems generally consist of mechanisms for obtaining high-quality images of aggregates and evaluation software. These

* **Zuzana Florkova**
Department of Highway Engineering, Faculty of Civil Engineering, University of Zilina, Slovakia
E-mail: zuzana.florkova@fstav.uniza.sk

systems include, for example, the system UIAIA (University of Illinois Aggregate Image Analyzer - Fig. 2).

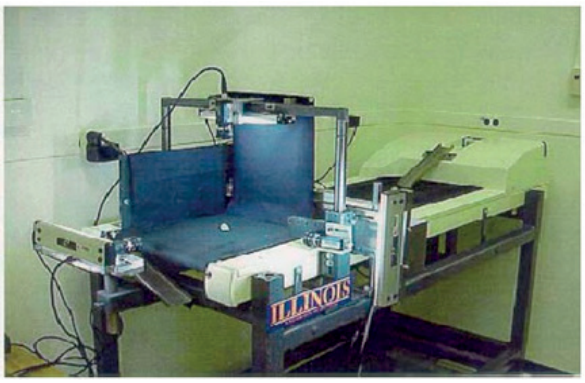

Fig. 2 UIAIA system [5]

The UIAIA uses three cameras to capture projections of a particle from three orthogonal directions. The UIAIA features a moving conveyor belt that carries the individual aggregate particle into the view of a sensor, which detects the particle and immediately triggers the cameras. The use of three images for each particle allows creating the 3-D view of each particle. This system uses for microtexture evaluation the outline slope angularity index. The outline slope angularity index measures the angularity of a particle as change in the slope of the particle polygon outline (Fig. 3).

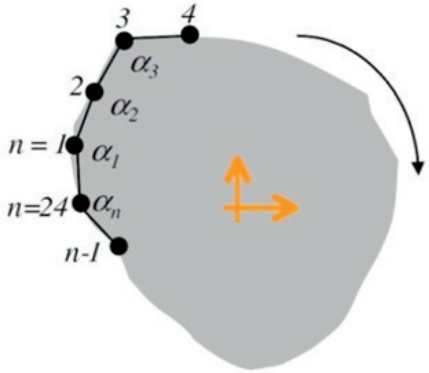

Fig. 3 The polygon outline of particle [6]

The main disadvantage of these systems is that the available parameters for angularity characteristics of aggregate particles by these methods are based on analysis of 2-D images. Despite of this disadvantage complex systems provide outputs in the form of 3-D view of the particle, the appropriate evaluation software of these systems allows microtexture evaluation of individual particles only by 2-D parameters. Then, the resultant value is assessed as the average value of the parameters obtained from the evaluation of 2-D images of many projected sides of an aggregate particle.

In general, disadvantage of 2-D parameters based on digital image analysis is that these parameters allow to capture only the larger peaks on the surface of aggregate particles. As the result of this, only the upper part of microtexture range is included into the evaluation. Used microtexture parameters are described in the [6].

3. 3D laser scanning device

This laser-based method is intended for simple three-dimensional (3-D) reconstruction of aggregate particles (Fig. 5). The 3-D laser scanning device in Fig. 4 uses advanced non-contact laser sensors to scan an object in three dimensions. Aggregate particles are scanned on rotating plate using a laser beam, which travels vertically up the rotating object to generate three dimensional digital scan file. Data processing software is an integral part of the 3-D laser device [7].

Fig. 4 3D laser scanning device [8]

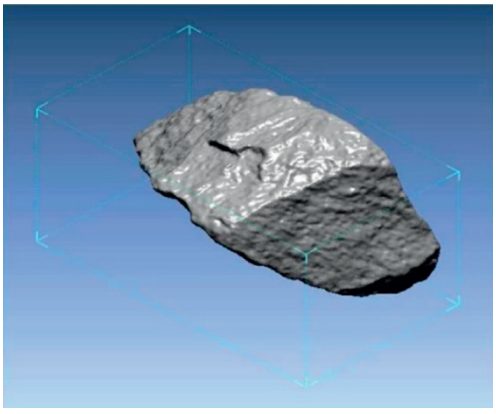

Fig. 5 3D image of aggregate particle obtained by 3D laser scanning device [8]

This method has the same disadvantage as in the case of the above presented methods of digital image analysis. The entire evaluation is carried out automatically, but by the 2D parameters. The capture of the entire field of microtexture values is also

problematic, because of the laser device software, which scans objects with a 0.1 mm scanning resolution.

4. Photogrammetry method

The photogrammetry method is another method for the detection of microtexture, which allows obtaining the outputs in the 3-D form (Fig. 7). Photogrammetry is a set of methods for obtaining the coordinates of prepared aggregate sample (Fig. 6) from analogue or digital photography. The principle of this method is in obtaining photographs, getting the coordinates of the surface using the appropriate software and the further transformation of the coordinates in the 3-D model.

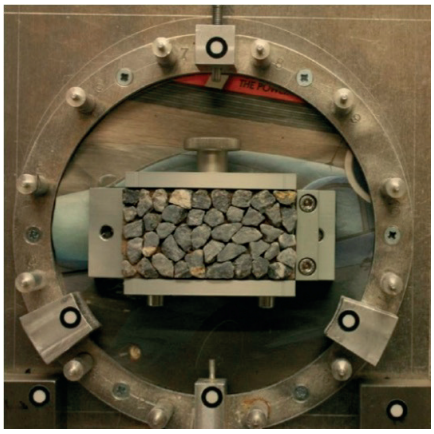

Fig. 6 Sample of aggregates used for obtaining the 3D aggregate image by photogrammetry method [9]

This method uses software Mountain Map for microtexture evaluation. The advantage of this software is that it enables to include into evaluation the entire particle surface by volume characteristics. One of the possibilities is to use the material ratio curve so-called the Abbott-Firestone curve.

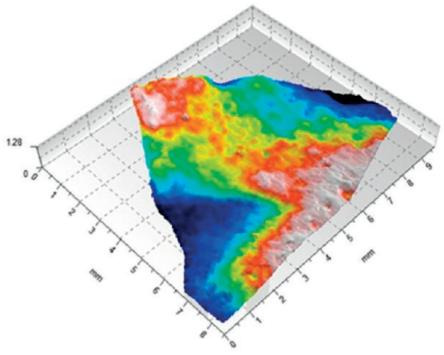

Fig. 7 The photogrammetry method used for obtaining the 3D aggregate image [9]

Using the Abbott curve, a graphical analysis can be performed in order to retrieve volume parameters characterizing the roughness of aggregate particle. According to Fig. 8, the curve distributes the surface texture into four volume parameters: Vmp (peak material volume), Vmc (core material volume), Vvc (core void volume) and Vvv (valley of the void volume) [9]. Then, the resultant characteristic of microtexture represents the volume parameter Vmp (peak material volume) (Fig. 9). The downside is that this method requires considerable computer knowledge and longer processing time.

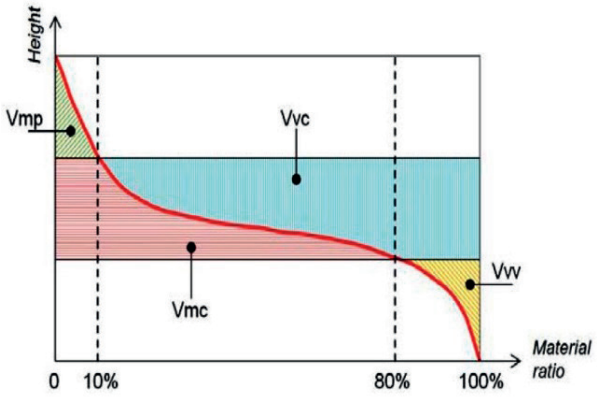

Fig. 8 Principle of Abbott-Firestone [10]

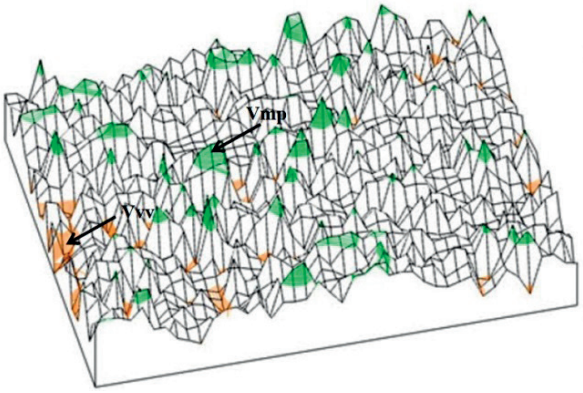

Fig. 9 Characteristic of microtexture represented by the volume parameter Vmp (peak material volume) [10]

5. Usage of microscope method for the detection of microtexture

It is possible to scan a particle of aggregate by a microscope (e.g. NIKON AZ 100). On the basis of the software Nis Elements D it is possible to achieve a 3-D view of investigated aggregate (Fig. 10). This view can be exported into the wrml (Virtual Reality Modelling Language) format. It makes possible to image the aggregate in 3-D also apart from the software Nis Elements D in the workspaceof different programs (e.g. in the workspace of

Matlab program - Fig. 11). The appropriate software also includes an interactive measurement toll EDF profile. Usage of this one allows obtaining the coordinates of singular profiles of aggregate. The acquired profile of aggregate is then expressed by x (y) and z coordinates. This data file can be also exported to various formats.

The principle of 3-D view acquirement by microscope rests in scanning of aggregate particle by cameras at different height levels. Aggregate particle is scanned on the microscope stage, which is vertically moved in micro steps by rotary knob. Then, the software creates the resultant 3-D image from the images obtained by scanning. The accuracy of the obtained output depends on the before selected range of scanning, of the number of steps and the required zoom level.

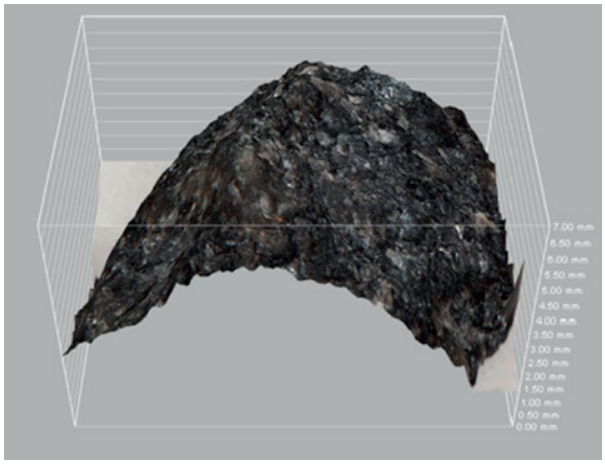

Fig. 10 Three-dimensional view of aggregate particle obtained by microscope

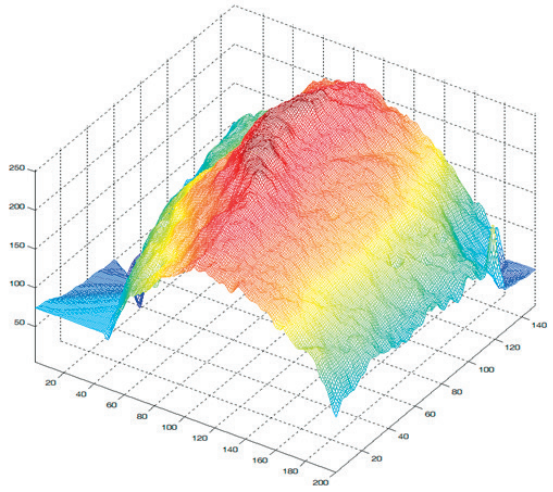

Fig. 11 Image of aggregate in the Matlab program workspace

The main advantage of this method is the possibility to image aggregate particle in 3-D apart from the software Nis Elements D in the workspace of different programs. Then, a program can be used for following evaluation. The program allows microtexture evaluation by 3-D parameters and eventually deals with creation of new parameters, which provide new possibilities of microtexture evaluation using the surface areas and volumes.

An aggregate particle can be captured by microscope in different zoom levels. It provides the capturing of the entire field of microtexture values and it gives more accuracy and better representativeness of results (compared to other detection methods of microtexture).

In all, the process of measuring by microscope is not time-consuming and it is quite simple.

6. Conclusion

The possibility that microtexture information can be obtained from three-dimensional data by the 3-D image methods involves the series of advantages in monitoring the aggregate microtexture. By these outputs, it is possible to detect aggregate microtexture in a more realistic way. In particular, it allows determination of microtexture characteristics with high accuracy and reliability of the results when compared to other used microtexture detection methods.

Despite of these advantages, these methods have still some limitations. The main limitation of these systems is that the systems provide outputs in the form of a 3-D view of the particle and the appropriate evaluation software of these systems allows microtexture evaluation of individual particles only by 2-D parameters.

Generally, the approach to quantification of aggregate microtexture based on the microscope methods is not commonly used as compared to other 3-D based methods. The usage of the microscope method for the detection of aggregate microtexture allows eliminating some of the disadvantages of described methods and mainly the limitation in the form of resultant 2-D image analysis.

Using these outputs in the tree-dimensional form obtained by microscope method gives possibility to include into the evaluation the entire surface of the investigation particle of the aggregate and also deals with microtexture evaluation based on volume characteristics.

The previous considerations can be used as a starting point for further studies of aggregate microtexture by the microscope method. Working with a 3-D surface, it is possible to go one step further and move to evolution of new parameters, with the main aim to find the most suitable parameter as the best characterization of microtexture. Possible further applications of these indicators can be very useful for more complex evaluation of pavement microtexture.

Acknowledgement

The paper is an output of the project VEGA 1/0804/12 Influence of material composition of asphalt on characteristics of pavement surface texture, noise emission and air pollution supported by funds of Scientific Grant Agency of the Ministry of Education, science, research and sport of the Slovak Republic.

References

[1] HIBBS, B., LARSON, R.: *Tire Pavement Noise and Safety Performance: PCC Surface texture Technical Working Group.* Report No. FHWA-SA-96-068. Federal Highway administration. Washington, D.C., May 1996 [cit. 2015-29-03]. Available on: http://isddc.dot.gov/OLPFiles/FHWA/013169.pdf

[2] KOVAC, M. et al.: *Diagnostics of Serviceability Parameters of Pavements,* EDIS: University of Zilina, 2012, ISBN 978-80-554-0568-1.

[3] STN EN ISO 13473-5. *Characterization of Pavement Texture by Use of Surface Profiles. Part 5: Determination of Megatexture,* ISO 13473-5:2009

[4] KIM, Y., SOUZA, L.: *Effects of Aggregate Angularity on Mix Design Characteristics and Pavement Performance*. December 2009 [cit. 2014-08-05]. Available on: http://neltap.unl.edu/Documents/NDOR/Aggregate_Angularity_on% 20Mix_Design.pdf

[5] MASAD, E. et al.: *Appendixes to NCHRP Report 555: Test Methods for Characterizing Aggregate Shape, Texture, and Angularity*. May 2005 [cit. 2014-25-04]. Available on: http://onlinepubs.trb.org/onlinepubs/nchrp/nchrp_w80.pdf

[6] TAFESSE, S. et al.: *A New Image Analysis Technique to Quantify Particle Angularity*. [cit.2014-30-04]. Available on: http://kth.divaportal.org/smash/get/diva2:499535/FULLTE XT01

[7] KOMBA, J.: *Analytical and Laser Scanning Techniques to Determine Shape of Aggregates Used in Pavements*. June3. [cit. 2015-13-03]. Available on: https://www.google.sk/search?client=opera&q=Analytical+and+laser+scanninf+technuques+to+dtermine+shape+properties+of+aggregates+used+in+pavements&sourceid=opera&ie=UTF-8&oe=UTF-8&gws_rd=cr&ei=xW4SVY7lDcXyUvvYggL

[8] ANOCHIE-BOATENG, J. et al.: *Evaluation of 3D Laser Device for Characterizing Shape and Surface Properties of Aggregates Used in Pavements*. [cit. 2015-13-03] Available on: https://www.google.sk/search?client=opera&q=+Evaluation+of+3D+laser+device+for+characterizing+shape+and+surface+properties+of+aggregates+used+in+pavements&sourceid=opera&ie=UTF8&oe=UTF8&gws_rd=cr&ei=_3ASVaTFNsbfUdWcgsgF#q=3d+laser+scanning+device+aggregate

[9] MCQUAID, G. et al.: Use of Close Range Photogrammetry to Assess the Micro-texture of Asphalt Surfacing Aggregate. *Intern. J. of Pavements Conference*, Sao Paulo, 2013.

[10] BITELLI, G. et al.: Laser Scanning on Road Pavements: A New Approach for Characterizing Surface Texture. *Sensors,* July 2012, ISSN 1424-8220.

Veronika Orieskova - Jan Havko *

SANCTIONS AND EMBARGOES AS A CRISIS RESPONSE INSTRUMENT IN THE CONTEXT OF THE UKRAINIAN CRISIS

The paper analyzes the importance of sanctions and embargoes as a tool used by organizations of international crisis management to resolve large-scale crisis events in a peaceful way. The attention is paid to one of these crisis events, the Ukrainian crisis. On the basis of value selected parameters, which are the change of exchange rates and inflation growth in particular countries, it reviews their impact on both stakeholders, namely the countries of the European Union and the Russian Federation.

Keywords: *Crisis, sanctions, embargoes, inflation, change of exchange rates.*

1. Introduction

International organizations use the whole spectrum of crisis management instruments to prevent and solve existing crisis events. Deployment of armed forces is the last resort. The focus is on a peaceful resolution of the crisis. Sanctions and embargoes are one part of them. Through economic and political measures, international organizations try to affect and force the target country to change its behavior. The content of actions varies depending on the specific situation, the nature of the crisis event and other important factors.

2. Theoretical background and importance of sanctions and embargoes

Sanctions and embargoes are political and trade restrictions, they are imposed on target countries to maintain or restore peace and security in the region. According to Filip, sanctions are economic instruments used in international crisis management. They keep on influencing the state of a crisis development through the prosperity of another country [1]. They are divided into economic rewards and economic sanctions, the sanctions are a particular form of economic punishment against the target country.

Sanctions and embargoes are put in place by international organizations, namely the United Nations (hereinafter "UN"), the Organization for Security and Cooperation in Europe (hereinafter "OSCE"), but also the European Union (hereinafter "EU"). The main aim is to maintain or restore peace in the affected area. The basis for the use of these instruments is Chapter VII. Article 41 of the UN Charter, which stated: "The Security Council may decide what measures not involving the use of armed force are to be employed to give effect to its decisions, and it may call upon the Members of the UN to apply such measures. These may include complete or partial interruption of economic relations and of rail, sea, air, postal, telegraphic, radio, and other means of communication, and the severance of diplomatic relations" [2].

The EU uses sanctions and embargoes as a tool of the Common Foreign and Security Policy. Through economic and diplomatic sanctions the EU tries to influence the policy of countries, where international law, human rights and freedoms or democratic principles are violated. Their application is in accordance with Article 215 of the EU Treaty [3]. Specific sanctions are applied after approval by the UN Security Council in accordance with the accepted resolution. If necessary, however, the EU can also decide to apply further restrictions. It must always choose the kind which will effectively deal with the situation from a range of possible measures. Types of sanctions are shown in Fig. 1.

Sanctions and embargoes are imposed to stabilize and improve situation in affected area by changing the behavior of main leaders of the country, but also high profile individuals or groups. Of course, the main objective depends on particular circumstances e.g. an arms embargo, a ban on the export of certain goods and other restrictive measures are aimed at limiting the inflow of financial resources to terrorist groups or other destabilizing groups. Imposition of sanctions and embargoes

* **Veronika Orieskova, Jan Havko**
Department of Crisis Management, Faculty of Security Engineering, University of Zilina, Slovakia
E-mail: Veronika.Orieskova@fbi.uniza.sk

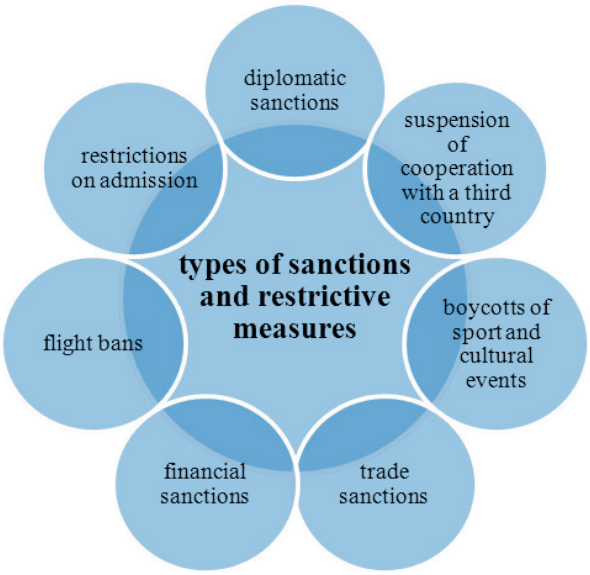

Fig. 1 Types of sanctions and restriction measures imposed by EU [4]

affect mainly the most vulnerable population groups in negative way, so the UN Security Council adopted a more sophisticated approach for planning and imposing sanctions. It is possible to direct them to specific individuals or groups, for example frozen assets, blocked financial accounts and transactions. These sanctions are called smart sanctions [5].

3. Ukrainian conflict solution through sanctions and embargoes between the EU and Russia

The conflict between pro-Russian separatists and Ukrainian armed forces threatens peace and security in Europe. It is difficult to clearly identify what launched a chain of events which resulted in the current situation. We can only assume that it is caused by dissatisfaction of Ukrainian people associated with the results of the elections in 2004 or suspension of negotiations about the EU Association Agreement. Organizations of international crisis management take initiative to end the conflict in a peaceful way and as soon as possible. The EU decided to solve the situation in February 2014 by imposing sanctions (for example freezing Ukrainian National Accounts), then the sanctions were imposed direct towards the Russian Federation, which supports, according to the media information, activities of pro-Russian separatists.

Mentioned sanctions imposed against the Russian Federation include:

- an asset freeze for certain individuals (total of 151) and entities (total of 37) and a travel ban for certain individuals because of their direct involvement in the situation development in Ukraine [6];
- the sectorial sanctions target Russia's oil industry, financial sector and the military or arms industry, which include following restrictions:
  - restrictions on financing some companies owned by the Russian government (banks, oil companies and companies and entities engaged in production, conception, sales or export of military equipment or services); this restriction includes a prohibition to deal in security and money market instruments, issued by the companies mentioned above, with a maturity above 30 days;
  - restrictions to provide, directly or indirectly, loans or credit to mentioned companies with a maturity exceeding 30 days;
  - restrictions on export of military and dual-use items to Russia and for use in Russia;
  - restrictions on the export and supply of certain oil-related goods and technologies to Russia and for use in Russia [7, 8 and 9];
- imposition of the strictest sanctions targeted towards trade with Crimea and Sevastopol in response to the illegal annexation of Crimea and Sevastopol.

General Assembly of the UN adopted resolution no. 68/262 about territorial integrity of Ukraine which recalls the obligations of all states under Article 2 of the Charter of the UN to refrain in their international relations from the threat or use of force against the territorial integrity or political independence of any State, and to settle their international disputes by peaceful means [10]. This resolution notes that the referendum held in the Autonomous Republic of Crimea and the city of Sevastopol in March 2014 was not authorized by Ukraine. In direct connection with the UN resolution, the EU Council adopted decision No. 2014/386/CFSP and EU Regulations No 692/2014 (June 2014) and No 825/2014 (July 2014), which were significantly extended by the EU Regulation No 1351/2014 in December 2014. Through this regulation any trade and investment in Crimea and Sevastopol was practically restricted.

The Russian Federation responded with sanctions against the EU through adoption of retaliatory measures in March 2014. At first, it was asset freeze and travel ban for people, also even government officials to Russia. In August, the Russian president V. V. Putin signed a decree on the application of specific economic measures, which imposed annual ban on import majority of agricultural products from countries, which had adopted sanctions. Next day, the Russian Federation government adopted a decree with list of countries and different products to which the embargo is targeted. It should be noted that before imposing an embargo, food export from the EU to Russia was approximately about 11.8 billion € which represents 10% of Russian consumption [11].

4. The consequences of sanctions on changes in exchange rates and inflation growth

The most apparent consequences of sanctions are in the economic field. It also includes changes of euro and ruble exchange rates in relation to US dollar. Imposition of sanctions also affects the inflation growth in selected countries. We perceive it as a direct consequence of adopting the restriction measures. Changes of several commodities prices, for example crude oil and gas, can be considered as an indirect consequence. Sanctions against Russia were adopted in March and December. Restriction measures adopted in December can be classified as more strict. In August, Russia responded by imposing an embargo on import of agricultural products from countries which had adopted restrictive measures against it. This paper pays attention mainly to the development of mentioned indicators, namely in short term after imposition of sanctions.

Progress of exchange rate reflects the confidence level of financial markets to a specific country. Figure 2 shows change of euro and ruble exchange rates against exchange rate of US dollar. Although euro is relatively stable, it has depreciated gradually since September 2014. That decrease can be caused by solving the Greek debt issue. It is influenced by embargo introduced in August 2014 only partially. On the other hand, ruble exchange

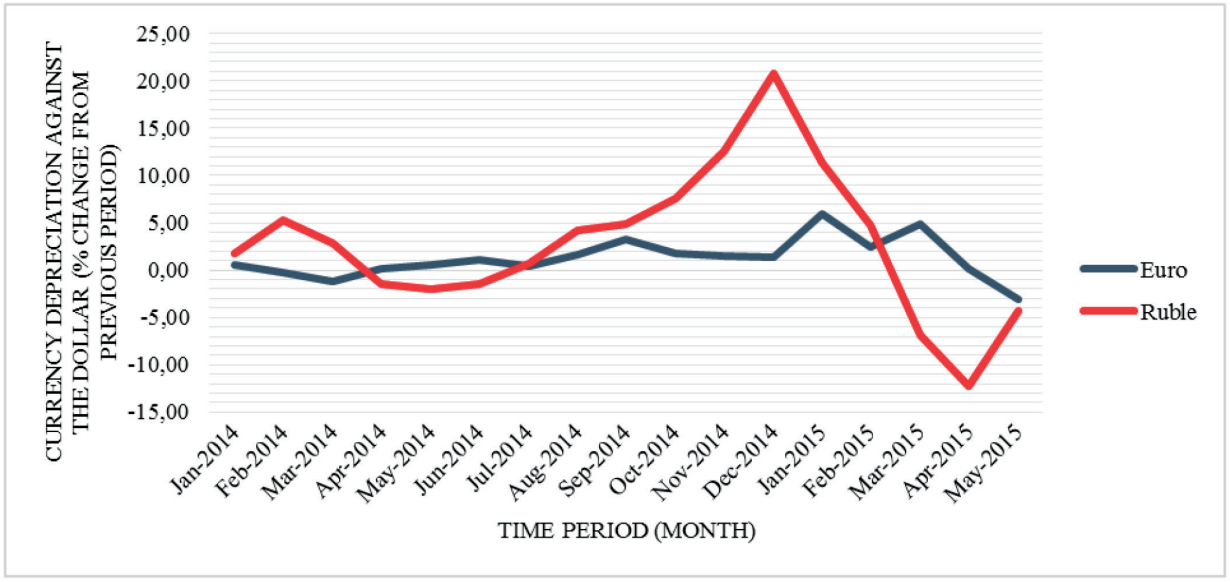

Fig. 2 Graph of the euro and ruble exchange rate development [12]

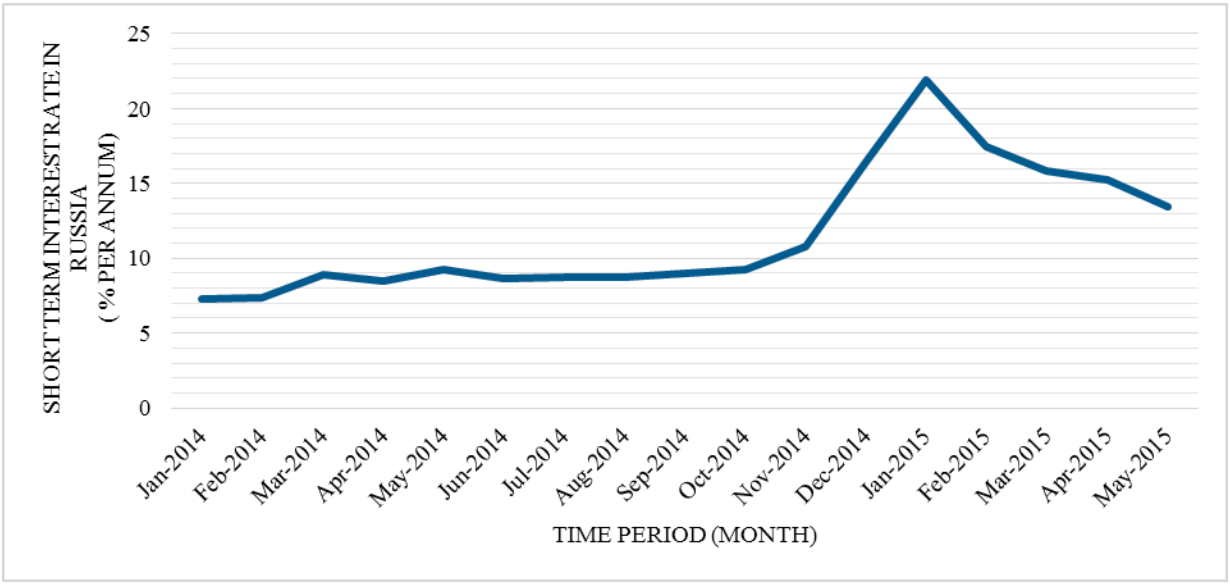

Fig. 3 Graph of the short term interest rate in Russian Federation [13]

rate is significantly influenced by EU sanctions. Due to the first sanctions introduced in March 2014, its exchange rate decreased. However, the decrease was not so significant, so the ruble remained relatively stable. After stricter sanctions imposed in December 2014, exchange rate of the ruble had already declined significantly, namely by over 10% per month. Russia has responded by adopting several monetary measures. Through them, the ruble exchange rate slightly appreciated in March 2015. It can be assumed that development of the ruble exchange rate will be influenced by Council Decision 2015/959 CFSP, which extended the sanctions until 23 June 2016.

The short-term interest rate was and still is one of the most important tools used to stabilize ruble exchange rate. Its development is shown in Fig. 3. After imposition of the sanctions in December 2014, the short-term interest rate in Russia increased above 20%. The main aim of this measure was to avoid mass cash withdrawal and thus subsequent loss of Russian banks liquidity. Currently, value of the short-term interest rate is still higher than it was before sanctions imposing. Totally it was more than 7%. The EU short-term interest rate did not exceed 0.3% during selected months [13].

The average value of long-term interest rate was 8% in the Russian Federation, but after imposition of the sanctions in December 2014 it increased to 10%. On the contrary, value of the long-term interest rate in the EU has been decreasing since January 2014. It decreased from 3.21% in January 2014 to 0.85% in April 2015 [13].

Inflation, as an indicator, expresses the increase of the price level. The embargo imposed in August 2014 connected with the import of agricultural products should cause, according to the economic theory, an increase of inflation in Russia and deflation in the EU. Figure 4 shows progress of inflation in the OECD (only Europe countries) and Russian Federation. Fig. 4 shows a slight progress of inflation in Russia after August 2014 due to the lack of goods, which were related to the embargo.

The highest inflation rate in Russia, since the sanctions imposition, was during December 2014 and January 2015. It was directly caused by the depreciation of ruble exchange rate and increase of the short-term and long-term interest rates. Although, inflation rate in Russia is still growing after February 2015, its growth is slower. An inflation development in OECD - Europe countries shows that the embargo imposed against European countries did not have such substantial impact [14].

Based on the selected indicators, we can conclude that the EU sanctions significantly influence economy of the Russian Federation. The European Commission estimates that gross domestic product (hereinafter "GDP") growth in Russia will decrease at least by 1.1 % in 2015 and it will be influenced by sanctions against Russia. Furthermore, ruble exchange rate decreased and significant outflow of capital from Russia began. Overall, capital value is in the amount of 130 billion dollars. According to estimates of the European Commission, the sanctions will also reduce GDP growth in the EU by 0.2-0.3 % in 2015. According to available information sources, decrease of export from the EU to Russian federation is in the amount of more than 60 % [15].

In addition to the changes in exchange rates and inflation rate caused directly by sanctions and embargoes, there are also other indicators which should be paid attention to. It can be, for example, price of strategic raw materials, where is inherently oil and natural gas. These commodities are among the most important sources of the Russian Federation income. The EU together with the United States has the political and economic instruments to reduce prices of these commodities, either by

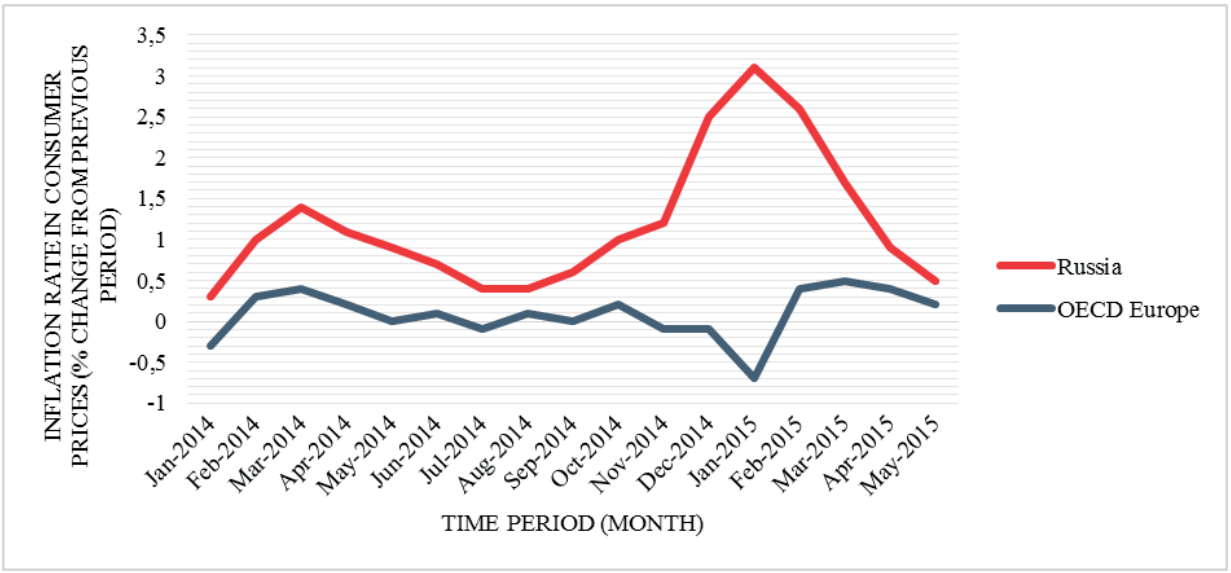

Fig. 4 Graph of the inflation rate development [14]

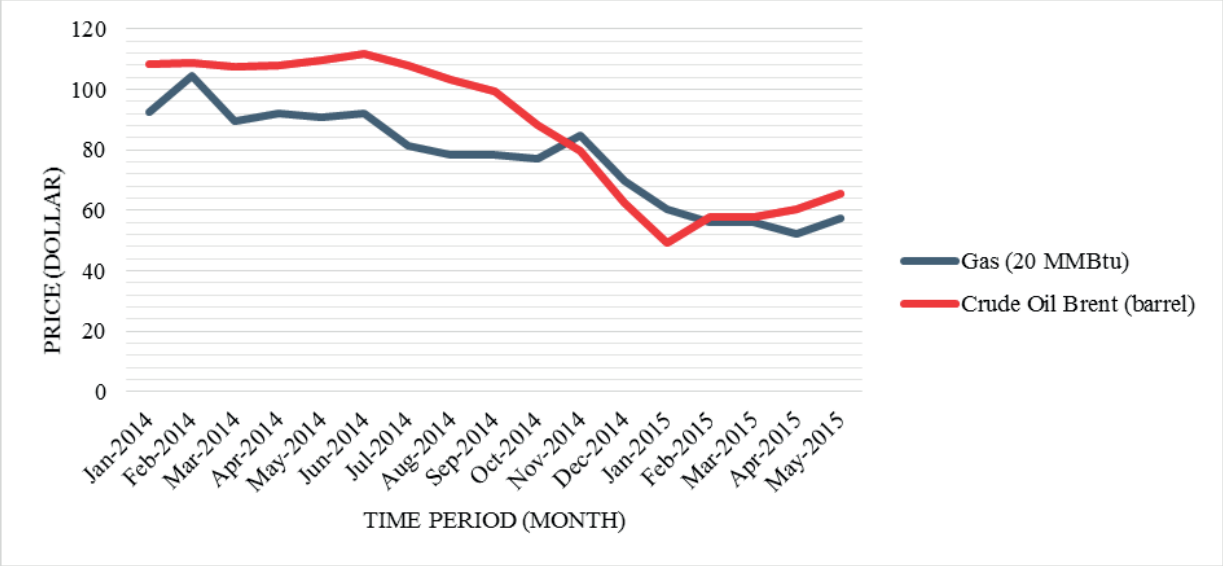

Fig. 5 Graph of the gas and oil stock market price development [16 and 17]

influencing the world stock exchanges, or pressure on OPEC members (OPEC means Organization of the Petroleum Exporting Countries). In Fig. 5 we can see a decline in oil prices, which is more than 50% in one year [16]. However, we can only assume that oil prices decline was an indirect revenge of the United States and other countries to which Russia imposed embargo on goods import. The price of gas did not fall as much as the oil price (Fig. 5). The gas price declined more than 25% in one year [17]. More significant decline was after imposing sanctions against Russia in December 2014.

Situation in Ukraine influences the global security environment. Changes in the security environment also reflect on the economic environment, for example by growth of strategic commodities prices, namely oil and gas. Mentioned strategic commodities are necessary for the sustainable economy of each country. Especially ensuring resources for future development of the country is considered as a strategic priority of security [18]. Sanctions raised concerns about the possible suspension of raw materials supply to Europe. Especially Eastern Europe countries are dependent on Russian gas. These countries rely on Russia for at least 60% of their gas [19]. Commodity prices did not increase, on the contrary, price decreased. Based on the current prices development, it can be stated that they will be regulated in some way by countries, which adopted sanctions against Russia. It could be meant, from one point of view, as another form of sanctions against Russia. However, this statement is not possible to substantiate by any official sources.

5. Conclusion

We can make some conclusions based on the description of sanctions and embargoes as such, but these conclusions are mainly based on characterization of specific measures imposed by the EU against the Russian Federation. Imposition of sanctions by the EU definitely disrupted economy of the Russian Federation. The exchange rate of ruble decreased and inflation rate in the country increased. Whether the adoption of specific restrictive measures fulfilled the primary purpose is already difficult to say with certainty. The main purpose of all these measures was the peaceful resolution of the conflict in Ukraine. Another purpose was to achieve that Russia ceased to support efforts of Crimea inhabitants to affiliate to the Russian Federation by its activities. Despite of the ceasefire, there are still a lot of attacks and fights, so the effectiveness of measures is questionable.

The consequence of sanctions imposed by the Russian Federation to the EU in the context of criteria selected by us does not seem so significant. However, we paid attention only to development of euro and ruble exchange rates, inflation growth and changes of oil and natural gas prices, this finding is not absolute. It is also necessary to take into consideration other factors to comprehensively assess the impact of the adopted measures. Because of the limited scope of the paper, it is not possible.

References

[1] NOVAK, L. et al.: *Resource Planning for Solution of Crisis Situations (in Slovak),* Bratislava: Vysoka skola ekonomie a manazmentu verejnej spravy, 2010.

[2] *Charter of the United Nations*. [on-line cit.: March, 04, 2015]. Available at: http://www.mzv.sk/servlet/newyorkosn?MT=/App/WCM/ZU/NewYorkOSN/main.nsf/vw_ByID/ID_621F5291AE4A5FD4C125715B004FFE51_SK&TG=BlankMaster&URL=/App/WCM/ZU/NewYorkOSN/main.nsf/vw_ByID/ID_14A4A60B573D8E62C12570DD0048A478_SK&OpenDocument=Y&LANG=SK&HM=25-Charta&OB=0.

[3] *Treaty on European Union. Treaty on the Functioning of the European Union. Consolidated texts in terms of the Lisbon Treaty.* Ministerstvo zahraničných vecí Slovenskej republiky: AVI TOBA PRESS, s.r.o., 2008.

[4] *European Commission - Restrictive measures.* [on-line cit.: March, 08, 2015]. Available at: http://eeas.europa.eu/cfsp/sanctions/docs/index_en.pdf.

[5] *Security Council Sanctions Committees: An Overview*. [on-line cit.: March, 08, 2015]. Available at: http://www.un.org/sc/committees/index.shtml.

[6] *Council Regulation (EU) No 269/2014 concerning restrictive measures in respect of actions undermining or threatening the territorial integrity, sovereignty and independence of Ukraine.* [on-line cit.: March, 16, 2015]. Available at: http://eur-lex.europa.eu/legal-content/SK/TXT/HTML/?uri=CELEX:32014R0269&from=SK.

[7] *Council Decision 2014/512/CFSP concerning restrictive measures in view of Russia's actions destabilising the situation in Ukraine.* [on-line cit.: March, 16, 2015]. Available at: http://eur-lex.europa.eu/legal-content/SK/TXT/HTML/?uri=CELEX:32014D0512&from=EN.

[8] *Council Regulation (EU) No 833/2014 concerning restrictive measures in view of Russia's actions destabilising the situation in Ukraine.* [on-line cit.: March, 16, 2015]. Available at: http://eur- lex.europa.eu/legal-content/SK/TXT/HTML/?uri=CELEX:32014R0833&from=EN.

[9] *Council Regulation (EU) No 960/2014 amending Regulation (EU) No 833/2014 concerning restrictive measures in view of Russia's actions destabilising the situation in Ukraine.* [on-line cit.: March, 16, 2015]. Available at: http://eur-lex.europa.eu/legal-content/SK/TXT/HTML/?uri=CELEX:32014R0960&from=EN.

[10] *Resolution Adopted by General Assembly No. 68/262 Territorial integrity of Ukraine*. [on-line cit.: March, 16, 2015]. Available at: http://www.un.org/en/ga/search/view_doc.asp?symbol=A/RES/68/262.

[11] *Russia Hits West with Food Import Ban in Sanctions Row*. [on-line cit.: March, 16, 2015]. Available at: http://www.bbc.com/news/world-europe-28687172.

[12] *Monthly Monetary and Financial Statistics (MEI): Exchange Rates (USD Monthly Averages).* [on-line cit.: July, 16, 2015]. Available at: http://stats.oecd.org/index.aspx?queryid=169.

[13] *Monthly Monetary and Financial Statistics (MEI): Interest Rates*. [on-line cit.: July, 16, 2015]. Available at: http://stats.oecd.org/index.aspx?queryid=86.

[14] *Consumer Prices (MEI): Consumer Prices.* [on-line cit.: July, 16, 2015]. Available at: http://stats.oecd.org/Index.aspx?DatasetCode=MEI_PRICES#.

[15] JANSEN, J.: *EU Sanctions Against Russia: New Targets and State of Play*. [on-line cit.: March, 16, 2015]. Available at: https://www.dlapiper.com/en/us/insights/publications/2015/02/eu-sanctions-against-russia/.

[16] *Brent crude - current and historical price of Brent crude oil (in Czech).* [on-line cit.: July, 16, 2015]. Available at: http://www.kurzy.cz/komodity/index.asp?A=5&idk=38&od=18.3.2014&do=17.3.2015&curr=USD.

[17] *Natural gas - current and historical gas prices (in Czech).* [on-line cit.: July, 16, 2015]. Available at: http://www.kurzy.cz/komodity/index.asp?A=5&idk=43&od=18.3.2013&do=17.3.2015&curr=USD.

[18] KELISEK, A. et al.: Economic Security - A Principal Component of Multilevel Security Cconcept in Global Economy. *Communications- Scientific Letters of the University of Zilina*, 13(2), 2011, pp. 44-48.

[19] SVENTEKOVA, E. et. al.: *Solution of Gas Crisis as a Task of Risk Management in Slovakia,* Proc. of WMSCI 2009 The 13th World Multi-Conference on Systemics, Cybernetics and Informatics, Jointly with the 15th Intern. Conference on Information Systems Analysis and Synthesis, ISAS 2009, 2009, pp. 384-388.

Jan Moravec *

EXTENDINGOF THE LIFE OF ACTIVE PARTS OF COLD-MOULDING TOOLS

Heat treatment of active components of cold-moulding tools is a necessary operation to guarantee their functionality. The tools made by this method lost required quality of durability and period of service and losses caused by their frequent exchange are high. One way we can stop it is by coating the active parts of pressing tools by thin, hard and abrasion resistant deposit that is suitable by definite method of the tool stress.

Keywords: *Cold-moulding tool, EDAX analysis, hardness, PVD coating, TiCN.*

1. Introduction

After Slovakia's accession to the EU, the opportunities for quality vacuum heat treatment of high alloy tool steels in heat treatment companies with precise direction and control of the upgrading process for the producers of the moulding tools have increased. Every year about one million tons of steel and 200 million tons of plastic are produced and processed. A big part of these materials is processed by moulding tools on which new and higher requirements are being placed:

- Accuracy, because of ever-increasing speeds of processing and loading there is a need to produce flawless details with ever tighter tolerances and thinner walls.
- Complete production on a single tool.
- Processing in dry and with minimal lubricating resulting in cost savings, reducing costs for cleaning of workpieces and machines and the reduction of environmental burden.
- Improved quality of product to minimise the need for additional work and the amount of scrap.

This forces us to seek more efficient methods that help eliminate losses. One possibility is the coating of dies by a thin, hard and abrasion-resistant layer, which is specific for the particular type of loading tool [1, 2 and 3].

2. Coatings and their properties

Processing technologies of depositions on surfaces of materials to improve their properties have been used for several decades. In the beginning, the chemical coating was used in the gas phase. This method is carried out under high temperature deposition (about 1000°C), when the heat is affecting surface structure of the coated material, and therefore, its use is limited primarily on sintered carbides. The development of physical and plasma chemical methods done at about 500°C allowed coating of conventional tool steels [4 and 5].

The functionality of the temperature of the deposition and the deposition thickness, for certain methods of deposition is shown in Fig. 1. The depositions that are most used in practice for the improvement of the properties of the active part of the tools are shown in Table 1 and examples for productions are presented in Table 2.

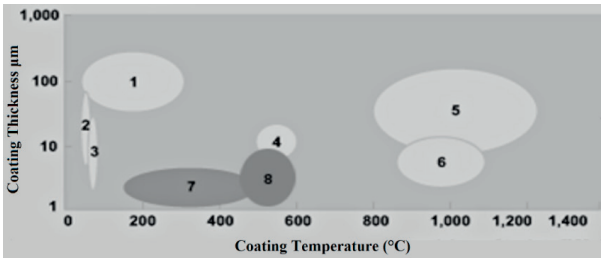

Fig. 1 Functionality of the temperature of the deposition and the deposition thickness [1]:
1. plasma spraying, 2. eElectrolytic and chemical deposition, 3. phosphating, 4. nitriding,
5. boronising, 6. CVD (CVD = Chemical Vapour Deposition),
7. PVD a PACVD (PVD = Physical Vapour Deposition), PACVD = Plasma Assisted Chemical Vapour Deposition),
8. P3e™ (P3e™ = Pulse Enhanced Electron Emission)

* **Jan Moravec**
Department of Technological Engineering, Faculty of Mechanical Engineering, University of Zilina, Slovakia
E-mail: jan.moravec@fstroj.uniza.sk

The selected parameters of the depositions Table 1

Deposition	Structure	Colour	Thickness / µm	Microhardness (0.05HV) / 1	Coefficient of friction	Process temperature	Max. service temperature
TiN	monolayer	gold	1-5	2300	0.4	<500	600
TiCN	gradient	grey	1-4	3000	0.4	<500	400
TiAlN	multilayer	purple	1-4	3000	0.4	<500	800
CrN	monolayer	metallic	1-4	1750	0.4	<500	700
PLC	gradient	grey	<1	1200-2000	0.15-0.2	<500	300

Examples for productions Table 2

Workpiece material	Punching	Forming
Steel< >1000N/mm^2	TiCN, TiN	TiCN, TiN
Steel 45-65 HRC	TiCN	TiCN
Stainless steel	AlTiN+PLC	AlTiN+PLC
Al, Al alloys	AlTiN (PLC), CrN	AlTiN+PLC, CrN
Cu, Cu alloys	CrN, CrC	CrN, C

Examples of tool steels for cold-mould working [3] Table 3

Brand of Steel	Metallurgical processing	The content of chemical elements (%)						
		%C	%Si	%Mn	%Cr	%Mo	%W	%V
1.2379	conventional	1.55	0.30	0.40	11.80	0.80	-	0.80
Caldie	ESR - Electroslag Remelting	0.60	0.35	0.80	5.30	-	-	0.20
Vanadis 4	PM - Powder Metallurgy	1.50	1.00	0.50	8.00	1.50	-	4.00

3. Choice of the appropriate brand of the cold-moulding tool steel

Quality of the steel is given predominantly by the origin, the primary and secondary metallurgy or the subsequent treatment in the solid state (forming, annealing). For materials of the same brand, but supplied by two different producers and supply companies, differences in hardenability can attain more than 10%, in wear resistance of the order of tens of percent and as for toughness these differences may vary up to several times.

Cleanliness of metallurgical processes for the production of steel and finishing surfaces of tools or tool design can have a major impact on performance of tools. The technology of metallurgical processing of steel is graded according to the quality and purity of the final product, from conventional metallurgy to powder metallurgy [6, 7 and 8]. Examples of cold-moulding tool steel by various methods of metallurgical processing are given in Table 3.

4. Experimental part

We examined the effect of using of TiCN deposition coated PVD method onto a substrate - tool steel Vanadis 4, hardened on secondary hardness 58-60HRC (Figs. 2. and 3.). Material for punching was used from sheets of material CuNi25 with strength 90HV30.

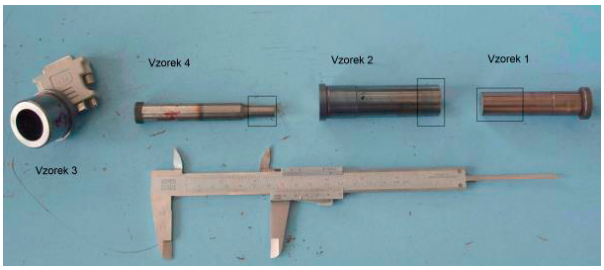

Fig. 2 Sample Nr. 1 - Cutting die

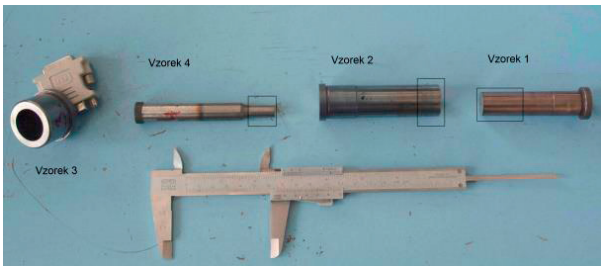

Fig. 3 Sample Nr. 2 - Cutting punch

4.1 Chemical analysis of the substrate

Chemical analysis of the substrate was done by the method GDOES. The choice of the analytical method was based on the dimensional and geometric options of evaluated material. The results of chemical analysis of the substrate are shown in Table 4.

Results of chemical analysis of the substrate — Table 4

Element	The content of chemical elements (%)	
	Sample Nr. 1	Sample Nr. 2
C	1,45	1,47
Mn	0,36	0,37
Si	0,61	0,56
P	0,023	0,023
S	0,016	0,019
Cr	6,85	6,91
Mo	1,50	1,45
V	3,64	3,60

4.2 Chemical analysis of the deposition

Chemical analysis of coating was done by the method EDAX. The choice of the analytical method was based on the dimensional and geometric options of evaluated material. EDAX analysis results of coating are reported in Figs. 4 and 5, and in Tables 5 and 6.

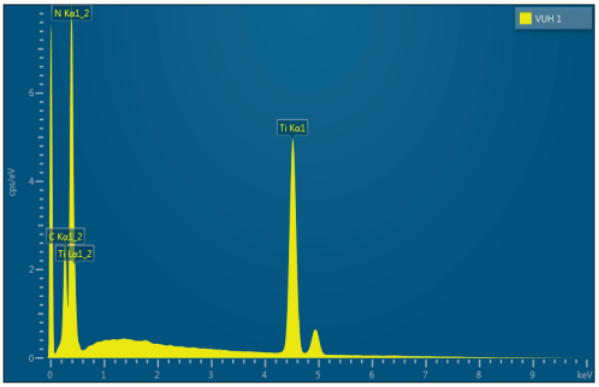

Fig. 4 Chart of EDAX analysis of sample No. 1

Table of EDAX analysis of sample No. 1 — Table 5

Element	Line Type	Wt. %	Wt. % Sigma	Atomic %
C	K series	7.13	0.14	18.08
N	K series	14.86	0.23	32.31
Ti	K series	78.01	0.25	49.61
Total:		100.00		100.00

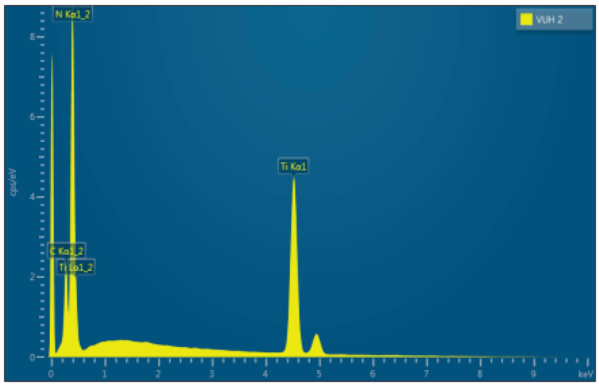

Fig. 5 Chart of EDAX analysis of sample No. 2

Table of EDAX analysis of sample No. 2 — Table 6

Element	Line Type	Wt%	Wt% Sigma	Atomic %
C	K series	6.60	0.14	15.99
N	K series	18.54	0.24	38.53
Ti	K series	74.86	0.26	45.48
Total:		100.00		100.00

4.3 Hardness of the substrate

Hardness of the substrate was done by methodology Vickers HV60, in accordance with ISO 6507-1. Measurement results are presented in Table 7. The results represent the arithmetic average of three individual measurements.

Hardness of substrate — Table 7

Marking of samples	Hardeness HV60
Sample 1	797
Sample 2	738

4.3 Microhardness of the deposition

Measurement of microhardness of the deposition in accordance with ISO 6507-1 - both on the surface and the cross-sectional view - could not be done due to the very small thickness of the coating, because there would be a complete penetration of the layer (from surface measurements), or overlapping of the measuring injection of the deposition to the substrate (measured in cross-section).

For this reason, it had to be done by the hardness measurement method known as “Nanoindentation” using the corresponding hardness testers CSM Instruments. All positions of performed measurements of microhardness of the depositon under nanoindentation were located in the working part of the samples. The measurement results are presented in Table 8. It

represents the mean value of the 15 indentations, which have been done, and the variability of the results is the coefficient of variation of the series of results.

Hardness measuring of deposition - nanoindentation Table 8

Marking of samples	Hardness HV
Sample 1	3210 ± 14 %
Sample 2	2992 ± 22 %

4.5 Experiment results

To produce the cutting punch and die we used the substrate - cold-moulding tool steel as the base material, known commonly as Vanadis 4 - the special tool steel produced by the method of PM from Uddeholm. Active parts were hardened and tempered to secondary hardness in vacuum hardening furnace. Chemical analysis of the substrate by the method GDOES is given in Table 4. The final hardness of the substrate is shown in Table 7.

In the first part of the experiment, we produced about 75 000 strokes with prepared active components without coating on the material CuNi25 of strength 90 HV30 until the end of life of the active parts. In the second part of the experiment, we used the active components using deposition of TiCN deposited by PVD on a substrate - the above-described tool steel hardened to secondary hardness 58-60HRC. Chemical analysis of deposition and the graphical representation of the percentage of the elements referred to in paragraph 4.2 and microhardness of the coating is shown in Table 8. With these modified components, we have reached 1.5 million strokes until the end of their operating life, which is a 20-fold increase in service life of active components of the tool.

5. Conclusion

We pointed out in the article that the appropriate choice of the coating method, layer and structure of the deposition for the mode of stress can significantly improve the properties of the active components of the cold-moulding tools, which is reflected in particular in a severalfold increase in durability of tools. The forming tools are characterized by the fact that their active components are usually produced of high alloy tool steels and their profile is complicated, with strict dimensional tolerances. PVD method has been successfully used in coating technology for this type of active components of cold-moulding tool because it retains all the desired properties. With DLC or PLC layers we are improving these properties. Currently mainly combinations of CVD and PVD or nanostructured coatings, which imply further improvement characteristics of cold-moulding tools, are gaining more and more importance.

References

[1] HOSFORD, W. F., CADDEL, R. M.: *Metal Forming, Mechanics and Metallurgy.* Cambridge University Press, 2011.
[2] KUMAR, S.: *Technology of Metal Forming Processes*. New Delhi, 2008.
[3] MARCINIAK, Z., DUNCAN, J. L., HU, S. J.: *Mechanics of Sheet Metal Forming.* Butterworth-Heinemann: Jordan Hill: Oxford, 2002.
[4] MIELNIK, M. E.: *Mechanical Metallurgy.* Mc Graw-Hill Book Company : New York, 1991.
[5] Metal Forming Handbook, Springer Verlag: Berlin, 2010.
[6] URL: www.oerlikobalzers.cz. (13.05.2015.).
[7] Uddeholm: Tooling Solutions for Advanced High Strength Steel. Uddeholm Tooling and SSAB Swedish Steel, 2004.
[8] Uddeholm: Brochure from Boehler – Uddeholm Slovakia, 2009.

Karol Hrudkay *

SELECTION OF SUITABLE URBAN TOLLING SYSTEM TECHNOLOGY

Article deals with the selection of suitableselection urban tolling system technology. In the paper, a lot of aspects, which have an influence on selection of particular technology in city conditions, were considered. For example: charging policy, user aspects, technical aspects and economic aspects. Although the analysis was not performed within specific conditions of a particular city, it was found out that in spite of general analysis, it is possible to form relevant and rather clear conclusions.

Keywords: *Urban tolling system, tolling technology, on-board unit.*

1. Introduction

Selection of technological solution is an important phase when deploying urban tolling system[1 - 4]. It is important to realise that selection of technology is not the first step of system deployment. In principle it applies that technology should not determine other aspects of objective system [5 - 7]. The reverse should be true. It means that technological solution should be a result of complex evaluation of many technical and non-technical requirements, objective and subjective requirements, aspects, parameters and criteria (often political ones, even at municipal level) [8 - 10].

Selection of technology itself should be preceded by the following phases (Table 1):

- identification of transport problems within city and its neighbourhood,
- selection of measures for solution of transport problems not only in context of city itself but within the whole agglomeration; one of these measures may be transport charging (maybe together with restriction) and then targets of charging (deployment of toll) have to be defined – the most frequent ones like traffic and environmental, or economic targets,
- defining pricing policy – especially setting the kind and form of charging, period of validity and so on,
- selection of organisational structure – mainly relates to selection of operation of urban tolling system (for example city itself, city organisation, commercial subject, PPP) and therefore indirectly with financial assurance of the project.

The selection of technological solution (in connection with the previous phases) is closely related to practical operation of system – with procedures and processes on the level of front office and back office levels as well.

Phases of tolling system deployment Table 1

Order	Phase
1	Identification of transport problems
2	Selection of measures for solution of transport problems Defining the objectives of charging
3	Defining the pricing policy
4	Selection of organisational structure
5	*Selection of technology* Elaboration of processes
6	System deployment Pilot (testing) operation Personnel training Marketing – info campaign
7	Regular system operation

From the above-mentioned steps, it is clear that several mentioned phases are interconnected.

2. Aspects affecting technology selection

Generally possible technological solutions for urban tolling system can be identified as follows [11]:

- non-technical solution (kiosks and terminals similar to ones for payment of parking fee),
- system with barriers,

* **Karol Hrudkay**
University Science Park, University of Zilina, Slovakia
E-mail: hrudkay@uniza.sk

- DRSC (Dedicated Short-Range Communications) – in principle here may be included solutions based on RFID (Radio Frequency Identification) as it is similar technology,
- GNSS/CN (Global Navigation Satellite System&Cellular Network),
- ANPR (Automatic Number Plate Recognition),
- odometer.

Aspects affecting selection of technological solution for urban tolling system Table 2

1	Object of charging
2	Principle of charging
3	Range of charging
4	Charged unit
5	Number of charged units per time unit
6	User identification
7	Toll payment means
8	Mode of individual types of participants
9	Number of individual types of participants
10	Enforcement intensity
11	Toll system deployment costs
12	Toll system operational costs
13	Effectiveness of toll collection
14	Toll system deployment time
15	Flexibility of tolling system
16	Initial costs for participant
17	Suitability/simplicity in term of participant
18	Compatibility/interoperability
19	Practical aspect – technology maturity, experience with deployment and operation
20	Perspective
21	Support of added value services
22	Affecting of traffic flow

The question is which solution is the most suitable for specific conditions of a particular city.

The aspects (Table 2) [11] which affect selection of technological solution for urban tolling system can be divided into following groups:

- aspects of charging policy,
- user aspects,
- technological aspects,
- economical aspects.

It is not possible to describe and evaluate individual aspects while details of intention for deployment of tolling system are not known (e.g. in Bratislava conditions). Although the following analysis is in principle general, it is possible to deduce such outputs which are relevant for small or middle-sized cities.

2.1 Aspects of charging policy and user aspects

Among aspects determining single framework of charging we can include:

- object of charging,
- principle of charging,
- range of charging,
- charged unit,
- mode of individual types of participants,

while these aspects are hardly known and we can possibly presume that even in case of political decision (though at municipal level) on deployment of urban tolling system, these aspects will be an object of serious discussions and will probably underlie relatively frequent and considerable changes.

In terms of user, there are especially important aspects directly connected with one´s duties and restrictions. From this point of view an essential aspect is:

- suitability/simplicity with respect to participant who primary evaluates requirements on the user from point of view of processes and their complexity and possible demands on operation of technical devices (OBU, user terminals, ...), while secondly this aspect includes even other aspects with relevant effect on participant.

From aspects of charging policy it is, for example:

- mode of particular types of users,

or from technical aspects the important ones are:

- user identification (especially obligatory OBU),
- payment means,
- affecting of traffic flow (especially if it is non-free flow system).

In terms of above mentioned aspects, the following elements as the most crucial ones were identified:

- *OBU*, i.e. if system is (not) based on use of vehicle unit,
- *detection of zone boundaries* because zone charging is typical for urban tolling systems,
- *detection of vehicle movement within the zone* enables to charge even the vehicles which are staying and realising its performance within the zone (such as an alternative to a possible charging based on time spent within zone),
- *affecting of user driving* (not affecting=”free flow”/lower speed/stopping/delaying).

The graph in Fig. 1 shows how individual solutions cope within four mentioned crucial elements.

From this graph, it is clear that ANPR is a suitable candidate for applied technology which meets the above mentioned elements (without OBU, detection of zone boundary and area, free flow). In case that solution based on OBU is acceptable, solutions based on DSRC or GNSS/CN are also suitable (GNSS/CN technology maturity has to be proven in the real urban environment).

Solution based on odometer is specific, it is not verified in conditions of the city – only Swiss national tolling system is based on odometer; in this case interconnection of OBU with vehicle is

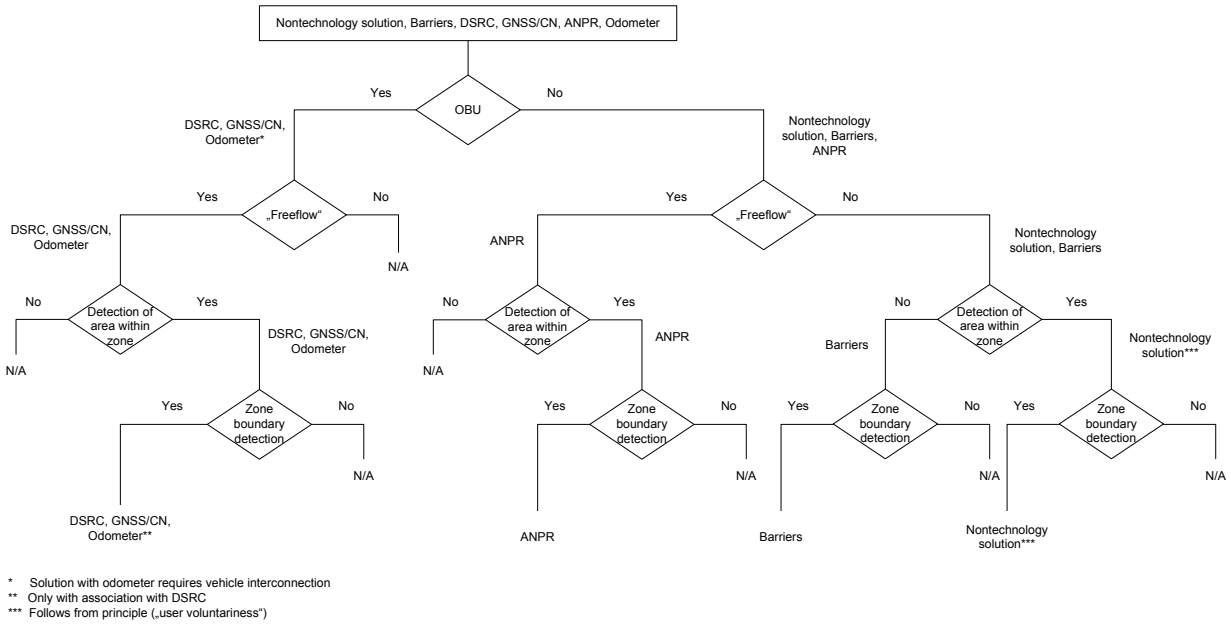

Fig. 1 Reviewing technological solutions in terms of essential aspects of charging policy and user aspects

necessary (except for connection to electricity supply) and such solution would be reasonable only in determination of tolling system according to performance of vehicle in the zone (distance travelled).

2.2 Technological and economic aspects

Technological and economic aspects affecting selection of technological solution are:

- identification of participant – defines the exactness of user identification, reliability of user determination or need to perform some additional steps on this determination,
- toll payment means – it is an aspect whether the solution enables/supports the broadest ways of toll payment including certain time freedom,
- intensity of enforcement – it is being evaluated if particular solution enables to reach required intensity of enforcement by adequate resources, or if some processes following from the basis of solution have essential effect on enforceability/ effectiveness of enforcement,
- costs on deployment of toll system reflect qualitative conception on investment demands,
- operational costs – it reflects qualitative conception on operational costs including expected future technology renewal,
- effectiveness of toll collection – typical standard for urban tolling systems is approximately within 90%-95% and in this case accessibility of this standard is evaluated or if implementation of a particular solution assumes processing aspects which can affect effectiveness of toll collection,
- time for deployment of tolling system – largely reflects the need of toll infrastructure establishment (so called technological part) within urban environment and related time requirements (including related bureaucracy),
- flexibility of tolling system – it reflects ability of solution to adapt to variable conditions (mainly to aspects of charging policy) in adequate time and with adequate costs,
- compatibility/interoperability – it reflects if solution with adequate costs is or may be compatible or interoperable with other tolling systems – in conditions of Slovakia only the national tolling system can be considered. However, in the future there may be also other urban tolling systems or city parking systems, even cross-border interoperability can be admitted, e.g. fictitiously Bratislava-Vienna (rem.: in terms of obligation to reach interoperability, Directive on interoperability 2004/52/EC [12] does not relate to systems which do not use OBU as well as urban systems where costs to achieve interoperability would be disproportionate to benefits),
- technology maturity, experience – it characterises experience with applied technology at least in the European context including estimation of possible future mid-term development,
- perspective – it evaluates technology in the framework of its expected deployment in defined time (in the framework of procurement procedure, such period is usually defined for 10-15 years) and its possible further use,
- support of value added services – it reflects possibilities of technology to provide wide variety of value added services (using technical means or obtained data),

Weight assigned to particular technical and economic aspects and their evaluation Table 3

Aspect	Weight [%]	Non-technical	Barriers	ANPR	DRSC	GNSS/CN	Odometer
User identification	9	-3	2	2	3	3	3
Toll payment means	8	-2	1	3	3	3	2
Enforcement intensity	10	-2	0	3	3	3	3
Costs on deployment of tolling system	9	3	2	1	-2	-1	-2
Tolling system operational costs	11	3	2	0	-1	-2	-1
Effectiveness of toll collecting	10	-3	2	1	2	2	2
Time for deployment of tolling system	4	3	2	1	-1	0	-1
Flexibility of tolling system	5	-2	1	0	-1	3	-1
Compatibility/interoperability	3	-3	-3	0	1	2	-1
Technology maturity, experience	7	-2	-1	3	2	0	0
Perspective	5	-3	-3	2	1	2	0
Support of value added services	4	-2	-2	1	0	3	0
Number of users, number of transactions per defined time period	5	0	-3	2	2	3	2
Affecting the traffic flow	10	-1	-3	3	3	3	3
Weighted average		-0.87	0.15	1.7	1.25	1.58	0.96
Overall ranking		6	5	1	3	2	4

Legend:			
-3	critical drawback	-3	critical drawback
-2	relevant drawback	-2	relevant drawback
-1	drawback	-1	drawback
0	neutral rating		

- number of users, number of transactions per defined time period – it characterises system dimensioning, possibilities or restrictions of system to completely serve certain absolute number of participants or in defined time period (for example in traffic jam), including further extension,
- affecting the traffic flow – it reflects to what extent tolling system affects fluency of traffic flow (need to slow down vehicle, stop vehicle, need to use particular entrance/transit and so on); ideal solution does not affect traffic flow (so called free flow solution).

From the above mentioned, it is clear that if aspects of charging policy are not defined specifically, it is not possible to assess individual aspects for particular solutions either in qualitative or in quantitative way.

From this reason, the relatively complex technical aspects affecting the selection of technological solution of urban tolling system qualitatively are assessed by the following procedure [13]:

1. method of ´survey among experts´ was used for qualitative assessment of individual aspects.
2. addressed experts assigned importance to individual aspects which characterises the seriousness of given aspect in complete interpretation.
3. the experts further evaluated individual aspects according to the fact whether a particular solution fulfils given criteria in a standard way, if it is for solution fundamental or relevant drawback or advantage.

Average weights and assessments of the individual aspects are shown in Table 3 (more accurate mentioned values are median ones).

With respect to meeting the requirements imposed by technical and economic aspects within the meaning of the following table, the most suitable solutions are offered by ANPR (as the only one without negative evaluation of any aspect) and GNSS/CN with similar evaluation. Following in the order is DSRC solution. As absolutely inappropriate solutions appear non-technical solutions and solutions based on the barriers.

3. Characteristics of technological solutions

Moreover, each of the mentioned options of urban tolling system is characterised by essential properties which can play an important role when selecting technological solution. In a nutshell, these features for all six solutions are mentioned in Table 4.

Essential typical features of technological solutions Table 4

Technological solution	Advantages	Disadvantages
Non-technological solution	Simplicity Relatively cheap solution (deployment and operation) Solution without OBU	Need to build network of terminals Low effectiveness of toll collecting ”Non-free flow“ solution (because of payment) Problematic enforcement
Barriers	Simplicity Relatively cheap solution (deployment and operation) Solution without OBU	”Non-free flow“ solution Low throughput Necessary construction changes Cash problem (if admitted)
ANPR	Solution without OBU The same technology either for charging or enforcement Proven (the most applied) technology ”Free flow“ solution	Need for infrastructure deployment (for charging and for enforcement as well) Possible lower effectiveness of toll collection
DRSC	Proven solution ”Free flow“ solution	Need of OBU Need for establishment of infrastructure (for charging as well as for enforcement)
GNSS/CN	”Free flow“ solution Advanced solution Multiplicative use (possibility to provide services with added value) The minimum infrastructure (only enforcement) Support of several ways of payment Flexibility	Non-verified solution (only pilot projects) Need of OBU Expensive OBU
Odometer	”Free flow“ solution Practical relevance only at charging according to distance travelled	Need of OBU and its connection with vehicle Solution without practical example within urban environment

4. Conclusions

From the above mentioned analysis of partial conclusions and foreign experience it can be concluded that main candidates for technological solution of up-to-date urban tolling system are ANPR, DSRC, GNSS/CN.

From these potential solutions of urban tolling system, ANPR solution does not require OBU what is an essential advantage . At the same time, this solution is the most extended solution in Europe and in the world and meets all placed requirements at least within standard level.

However, the other two solutions are based on the use of vehicle OBU which in case of charging of cities and thus mostly of passenger cars can be perceived as an obstacle and has many procedural, logistic and financial consequences on the side of charging organisation, or operator of such system as well.

DSRC is a well proven technology, especially on the level of national tolling systems. In case of urban tolling systems, in the past there were even cases when DSRC technology was replaced by ANPR technology.

Last solution which is appropriate, is the satellite - based solution whose basic disadvantage is its practical non-verification (except for realised pilot projects). Such solution still remains challenge and it can be expected that in close future such systems will not arise. They will probably get chance in medium-term horizon with EGNSS (Galileo) use and development of telematics within vehicles.

Acknowledgements

This paper is supported by the following project: University Science Park of the University of Zilina (ITMS: 26220220184) supported by the Research&Development Operational Program funded by the European Regional Development Fund.

References

[1] PICKFORD, A. T. W., BLYTHE, P. T: *Road User Charging and Electronic Toll Collection,* Artech House, 2006.

[2] NUMRICH, J., RUJA, S., VOSS, S.: Global Navigation Satellite System Based Tolling: State-of-the-art, *Netnomics,* 13:93-123, 2012, Springer.

[3] SANTOS, G., NEWBERY, D.: *Urban Congestion Charging: Theory, Practice and Environmental Consequences*, CESifo Workshop on Environmental Economics and the Economics of Congestion, Venice, June 2001, ISSN 1617-9595, pp. 20.

[4] HYMAN, G., MAYHEW, L.: Optimizing the Benefits of Urban Road User Charging, *Transport Policy,* 9, 2002, pp. 189-207, Elsevier.

[5] HRUDKAY, K.: *Technology and Interoperability of Electronic Toll Collection in Slovak Conditions* (in Slovak), PhD thesis, Department of Telecommunications: Faculty of Electrical Engineering: University of Zilina, 2010, 108 p.

[6] HERICKO, M., HERICKO, M., ZIVKOVIC, A.: *An Evaluation of Different Functional Solutions for Satellite-Based Tolling in Europe,* Proc. of the 44th Hawaii International Conference on System Sciences, 2011.

[7] HIURA, R., YAMAGUCHI, T., MABUCHI, Y., OKAZAKI, T., IEHARA, M., FUKASE, T.: System Evaluation Test of Global Navigation Satellite System-based Road Pricing System, *Mitsubishi Heavy Industries Technical Review*, vol. 50, No. 4, 2013.

[8] Transport Regulatory Uses of Telematics in Europe, vol. 2, Report prepared for Transport Certification Australia Limited, Rapp Trans Ltd, 2008.

[9] MADLENAK, R., MADLENAKOVA, L.: *The Proposal of Digital Advertising System,* TELECOM 2013 - Telecommunications in the context of globalization: 21st national conference with foreign participation, October 2013, Sofia: Publishing group of the Union of Scientists in Bulgaria, CD-ROM, pp. 11-20, ISSN 1314-2690.

[10] MIKULA, J., HRUDKAY, K., DZIMKOVA, R.: Utilisation of Toll Data (in Slovak), *Research Report*, 1/2013, Transport Research Institute Zilina, Slovakia.

[11] HRUDKAY, K.: Aspects Affecting the Selection of Urban Tolling Technology - Part 1 (in Slovak), *Svet dopravy* [electronic source]: science - reviewed online journal, 21 May, 2015, online, ISSN 1338-9629.

[12] Directive 2004/52/EC of the European Parliament and of the Council of 29 April 2004 on the interoperability of electronic road toll systems in the Community.

[13] MIKULA, J., HRUDKAY, K., DZIMKOVA, R., BADO, J., HRONSKY, P., ZUZIAK, L., GENZOR, P.: Urban Tolling Systems (in Slovak), *Research report,* 1, 2013, Transport Research Institute Zilina, Slovakia.

COMMUNICATIONS – Scientific Letters of the University of Zilina
Writer's Guidelines

1. Submitted papers must be unpublished and must not be currently under review for any other publication.
2. Submitted manuscripts should not exceed 8 pages including figures and graphs (in Microsoft WORD – format A4, Times Roman size 12, page margins 2.5 cm).
3. Manuscripts written in good English must include abstract and keywords also written in English. The abstract should not exceed 10 lines.
4. Submission should be sent by e-mail – as an attachment – to one of the following addresses: komunikacie@uniza.sk or holesa@uniza.sk (or on CD to the following address: Zilinska univerzita, OVaV – Komunikacie, Univerzitna 1, SK – 010 26 Zilina, Slovakia).
5. Uncommon abbreviations must be defined the first time they are used in the text.
6. Figures, graphs and diagrams, if not processed in Microsoft WORD, must be sent in electronic form (as JPG, GIF, TIF, TTF or BMP files) or drawn in high contrast on white paper. Photographs for publication must be either contrastive or on a slide.
7. The numbered reference citation within text should be enclosed in square brackets. The reference list should appear at the end of the article (in compliance with ISO 690).
8. The numbered references (in square brackets), figures, tables and graphs must be also included in text – in numerical order.
9. The author's exact mailing address, full names, E-mail address, telephone or fax number, the name and address of the organization and workplace (also written in English) must be enclosed.
10. The editorial board will assess the submitted paper in its following session. If the manuscript is accepted for publication, it will be sent to peer review and language correction. After reviewing and incorporating the editor's comments, the final draft (before printing) will be sent to authors for final review and minor adjustments
11. Submission deadlines are: September 30, December 31, March 31 and June 30.

COMMUNICATIONS

SCIENTIFIC LETTERS OF THE UNIVERSITY OF ZILINA
VOLUME 17

Address of the editorial office:
Zilinská univerzita
Office for Science and Research
(OVaV)
Univerzitna 1
SK 010 26 Zilina
Slovakia

E-mail: komunikacie@uniza.sk

Each paper was reviewed by two reviewers.

Journal is excerpted in Compendex and Scopus.

It is published by the University of Zilina in
EDIS – Publishing Institution of Zilina University
Registered No: EV 3672/09
ISSN 1335-4205

Published quarterly

Single issues of the journal can be found on:
http://www.uniza.sk/komunikacie

ICO 00397 563
December 2015